North–south Holocene seasonal contrast on the Italian peninsula: Clarification of the latitudinal transition zone based on the multi-proxy study of Lago Grande di Monticchio

Léa D'oliveira, Adrien Maignan, Odile Peyron, Sébastien Joannin, Nathalie Combourieu-Nebout, Marion Genet, Marion Lestienne, Lucas Dugerdil, Giada Fernandez, Biagio Giaccio, et al.

Quaternary Science Reviews 380 (2026) 109873

Contents lists available at ScienceDirect

Quaternary Science Reviews

journal homepage: www.elsevier.com/locate/quascirev

North–south Holocene seasonal contrast on the Italian peninsula: Clarification of the latitudinal transition zone based on the multi-proxy study of Lago Grande di Monticchio

Léa d'Oliveira [a,*], Adrien Maignan [b], Odile Peyron [a], Sébastien Joannin [a], Nathalie Combourieu-Nebout [c], Marion Genet [d], Marion Lestienne [e,f], Lucas Dugerdil [a,g], Giada Fernandez [h,i], Biagio Giaccio [i], Lorenzo Monaco [i,j], Sébastien Nomade [b], Alison Pereira [k], Vincent Scao [b], Edouard Regnier [b], Marie Balasse [l], Guillemette Ménot [g]

[a] ISEM, UMR 5554, Univ Montpellier, CNRS, IRD, Montpellier, 34090, France
[b] LSCE, UMR 8212, CEA, CNRS, UVSQ et Université Paris-Saclay, Gif-Sur-Yvette, 91190, France
[c] HNHP, UMR 7194, Muséum national d'Histoire naturelle, CNRS, MNHN, Paris, 75005, France
[d] Geo-Ocean, UMR 6538, Univ Bretagne Sud, Univ Brest, CNRS, Ifremer, Vannes, F-56000, France
[e] IMBE, UMR 7263, Aix Marseille Université, Avignon Université, CNRS, IRD, Aix-en-Provence, 13397, France
[f] AMAP, Univ Montpellier, CIRAD, CNRS, INRAE, Montpellier, 34398, France
[g] LGL-TPE, UMR 5276, Univ Lyon, ENS de Lyon, Université Lyon 1, CNRS, Lyon, 69364, France
[h] Sapienza University of Rome, Dipartimento di Scienze della Terra, Rome, 00185, Italy
[i] Instituto di Geologia Ambientale e Geoingeneria, CNR, Monterotondo, 00015, Italy
[j] Dipartimento di Scienze Fisiche, della Terra e dell'Ambiente, Università degli Studi di Siena, Siena, 53100, Italy
[k] GEOPS, UMR 8148, Université Paris-Saclay, CNRS, Orsay, 91405, France
[l] BioArch, UMR 7209, Muséum national d'Histoire naturelle, CNRS, MNHN, Paris, 75005, France

ARTICLE INFO

Handling Editor: Mira Matthews

Dataset link: https://doi.org/10.21233/KVNC-0856, http://www.neotomadb.org, https://doi.org/10.1594/PANGAEA.989985, https://doi.org/10.1594/PANGAEA.989981

Keywords:
Paleoclimatology
Southern italy
Holocene
Multi-proxy
Lipid-biomarkers (brGDGTs)
Pollen

ABSTRACT

Italy's Holocene climate can be characterised by a latitudinal division with a climatic contrast between the northern and southern regions, notably characterised by a stronger winter–summer precipitation seasonality in southern regions. The latitudinal boundary is located between latitudes 40° and 43°N, creating a climatic transition zone. However, the mechanisms underpinning this hydro-climatic partition remain poorly understood, due in part to a scarcity of precisely dated, high-resolution records at key latitudes. Lago Grande di Monticchio (~ 41°N) lies within this critical transitional band and presents a valuable opportunity to refine the latitudinal boundary location. Lago Grande di Monticchio is one of southern Italy's most comprehensively studied sediment archives, stretching back to the last interglacial. In this study, we employ a novel, high-resolution sediment core from Monticchio, applying a multi-proxy methodology that combines branched glycerol dialkyl glycerol tetraether (brGDGT) and pollen data to reconstruct seasonal temperature and precipitation changes during the Holocene. Results confirm that temperature reconstructions derived from brGDGT and pollen records are particularly consistent for most of the signal. Comparison with other palaeoclimate records and proxies in Italy allowed us to place Lago Grande di Monticchio's climate signal within southern climate regimes (i.e., summer cooling and aridity in contrast to wetter and warmer winters), corresponding to a stronger "Mediterraneanization" process throughout the Holocene. Multi-proxy comparison indicates that the most marked contrast during summer likely lies near the upper bound of 41°–43°N. Persistent inconsistencies in the transition zone suggest added climatic complexity around ~ 43°N, involving ocean-atmospheric teleconnections and local topography. We advocate further high-resolution, multi-proxy palaeoenvironmental studies in this transitional latitude band to refine understanding of the north–south hydro-climatic boundary across Italy in the Holocene.

* Corresponding author.
E-mail address: lea.d-oliveira@umontpellier.fr (L. d'Oliveira).

https://doi.org/10.1016/j.quascirev.2026.109873
Received 5 December 2025; Received in revised form 6 February 2026; Accepted 7 February 2026

1. Introduction

The geography of the Mediterranean Basin is unique and complex, characterised by sharp land-sea contrasts and enclosing mountain ranges. Its particular topography and location at the interface between tropical and north Atlantic atmospheric circulations subject the Mediterranean region to significant climatic gradients, associated with marked seasonality affecting temperatures and rainfall (Lionello et al., 2012). The climate of the Italian peninsula is primarily controlled by large-scale atmospheric circulation, particularly the mid-latitude westerlies and associated storm tracks, which govern most precipitation variability (Lionello et al., 2006). Winter rainfall dominates and is strongly modulated by storm-track position (Gaetani et al., 2011) and the North Atlantic Oscillation (NAO; Hurrell et al., 2003; Brandimarte et al., 2011): positive NAO phases shift westerlies poleward, reducing Mediterranean precipitation, while negative phases enhance cyclone activity over Italy. In summer, the westerlies weaken and migrate northward, allowing subtropical anticyclones and the descending branch of the Hadley cell to dominate, producing hot and dry conditions typical of Mediterranean climates (Lehmann and Coumou, 2015; Fratianni and Acquaotta, 2017). Recent studies showed a poleward expansion of the Hadley cell (Xian et al., 2021; Seo et al., 2023), resulting in the increased persistence of summer heat and drought in the Mediterranean. In addition, variability in the Atlantic Meridional Overturning Circulation (AMOC) indirectly affects Italian climate by modifying North Atlantic sea surface temperatures and atmospheric pressure gradients (Jacob et al., 2005; Bellomo et al., 2023), influencing storm tracks and subtropical circulation over southern Europe (Jackson et al., 2015; Li and Liu, 2025). According to Earth System Models simulations, the Mediterranean region is expected to experience a notable decrease in annual precipitation and localised flooding over the next few decades, accompanied by an increase in temperature (Giorgi and Lionello, 2008; Dubrovský et al., 2014; Guiot and Cramer, 2016; Tramblay et al., 2020; IPCC, 2023), significantly impacting human societies, biodiversity, land ecosystems, and water supplies. This underscores the need for a better understanding of the past, present and future climate dynamics and environmental responses in the Mediterranean region (e.g., Magny et al., 2013; Peyron et al., 2017; Di Rita et al., 2018b; Zielhofer et al., 2019).

Climate variability in the Mediterranean region during the Holocene (beginning 11,700 years ago) is documented through the use of various proxies, such as pollen data (e.g., Davis et al., 2003; Mauri et al., 2015; Peyron et al., 2017; Cruz-Silva et al., 2023; Liu et al., 2023), isotopic measurements from speleothems (e.g., Drysdale et al., 2006; Regattieri et al., 2014; Columbu et al., 2022), chironomids (Samartin et al., 2017), molecular biomarkers (Marriner et al., 2022; Rodrigo-Gámiz et al., 2022; Robles et al., 2023) or lake levels data (Magny et al., 2007, 2013). These studies revealed distinct spatio-temporal climate patterns across the central Mediterranean region, encompassing Southern France and Italy, marked by strong latitudinal contrasts. Particularly, a north–south climate division was recognised in Italy throughout the Holocene, with a latitudinal transition zone estimated between latitudes 40° and 43°N (Vannière et al., 2011; Peyron et al., 2011, 2013; Di Rita et al., 2018a; Robles et al., 2023; d'Oliveira et al., 2025). During the Early and Mid-Holocene, northern Italy experienced low summer precipitation, whereas southern regions exhibited an opposite pattern with higher moisture availability (d'Oliveira et al., 2025). This climatic gradient reversed during the mid-to-late Holocene, resulting in enhanced precipitation in the north and drier conditions in the south. The underlying mechanisms driving this north–south hydro-climatic pattern over the Italian Peninsula remain poorly understood (Magny et al., 2012, 2013; Peyron et al., 2013). Moreover, the scarcity of high-resolution and robustly dated palaeoclimatic records from sites located between 40° and 43°N makes it difficult to resolve these shifts at a finer spatial and temporal scale.

The Lago Grande di Monticchio (~ 41°N, 15°E, 650 m a.s.l.), a maar lake located at the top of the Mount Vulture volcanic complex at 656 m a.s.l., offers a valuable opportunity to investigate the north–south hydro-climate division, as it falls within the critical 40–43°N latitudinal band. The Lago Grande di Monticchio stands out as one of the most thoroughly studied sedimentary records in southern Europe, providing insight into the last climate cycle (Brauer et al., 2007; Wulf et al., 2008; Allen and Huntley, 2018). Its relative proximity to southern Italian Holocene active volcanoes led to the deposition of tephra layers in the record (e.g., Wulf et al., 2008), which constitutes a powerful tool to independently constrain the archive chronological framework using tephrochronology (major- and trace-element analyses of glass shards, direct/transferred radio-isotopic dating). Moreover, the lake is characterised by a rapid and continuous sedimentation rate, a clear stratigraphic layout and the possibility to transfer the dating results obtained for the same eruptive phase and establish a high-resolution age model based on the previously mentioned tephrochronological data combined with varve counting, guaranteeing a continuous fossil record dating back to the beginning of the last interglacial period (130,000 years ago). The earliest study, conducted by Watts (1985), focused on the lake palaeovegetation of the Last Glacial period, giving a preliminary understanding of the palaeoenvironmental history of Lago Grande di Monticchio. Subsequently, later studies developed the initial work of Watts (1985), focusing on geochemistry (Turton, 1993; Robinson, 1994; Narcisi, 1996), palaeomagnetism (Turton, 1993; Creer and Morris, 1996), sedimentology (Zolitschka and Negendank, 1993; Zolitschka, 1996; Narcisi, 1996; Brauer et al., 2000, 2007), tephrochronology and tephrostratigraphy (Newton and Dugmore, 1993; Wulf et al., 2004, 2006, 2008, 2012) and palynology (Huntley et al., 1996; Watts et al., 1996a,b; Allen et al., 1999; Huntley et al., 1999; Nimmergut et al., 1999; Watts et al., 2000; Allen et al., 2000, 2002; Brauer et al., 2007; Allen and Huntley, 2009, 2018). The palaeoclimatology of the region, mainly approached through palynology, has been the subject of several studies (Watts, 1985; Watts et al., 1996a,b; Zolitschka, 1996; Allen et al., 1999; Huntley et al., 1999; Allen et al., 2002), that underlay a complex relationship between southern Italian vegetation, North Atlantic atmospheric mechanisms and human exploitation throughout the Holocene. The relative importance of natural climate change and human activity as mechanisms driving vegetation change in Monticchio remains an open question (Allen et al., 2002), underlying the necessity of a multi-proxy palaeoclimate reconstruction approach.

Pollen is one of the most frequently used proxies to reconstruct past climate changes because, in addition to its excellent spatial coverage and preservation in sediments, the relationship between vegetation and regional climate is well known, making pollen-based palaeoclimate reconstructions robust (Chevalier et al., 2020). At Lago Grande di Monticchio, the first quantitative palaeoclimate reconstructions were obtained by Allen et al. (2002) and Allen and Huntley (2009); revealing abrupt environmental and climatic changes over the past 125,000 years. Other studies focused on key periods such as the Holocene (Allen et al., 2002; Allen and Huntley, 2009), the Eemian (Brewer et al., 2008) or the Late Glacial (Huntley et al., 1996) to investigate palaeoenvironment and palaeoclimate using pollen data. So far, pollen and diatoms have been the only proxies used to provide quantitative reconstructions of the Lago Grande di Monticchio palaeoclimate (Allen et al., 2002; Brewer et al., 2008; Allen and Huntley, 2009).

In addition to pollen data, the use of other proxies (e.g., isotopes, lake-levels and speleothems) has revealed the complex spatio-temporal patterns of Holocene climate change in this region (e.g., Peyron et al., 2011; Roberts et al., 2011; Bini et al., 2019). Combining independent proxies is essential for achieving more reliable climate reconstructions and understanding palaeoclimate changes (Camuera et al., 2023).

Lipid biomarkers such as branched glycerol dialkyl glycerol tetraether lipids (brGDGTs) are increasingly being used to reconstruct past temperature changes, in single-proxy studies (e.g., Ardenghi et al.,

2019; Rodrigo-Gámiz et al., 2022; Otiniano et al., 2024; Zander et al., 2024) but also in multi-proxy approaches, combined with pollen data (e.g., Martin et al., 2020; Dugerdil et al., 2021; Robles et al., 2022, 2023; d'Oliveira et al., 2023). These lipids, produced by bacteria, are found in both marine and terrestrial domains (e.g., Schouten et al., 2013; Zheng et al., 2015, 2018), and in a wide variety of terrestrial environments (e.g., lakes, soils and peats; Schouten et al., 2013). Over the last two decades, numerous studies demonstrated a relationship between environmental conditions (e.g., temperature and pH) and the structures of lipids synthesised by organisms (Weijers et al., 2004). Initially, Weijers et al. (2007) highlighted the relationships between temperature and Methylation of Branched Tetraethers (MBT) as well as between pH and Cyclisation of Branched Tetraethers (CBT). Later, after analytical improvements that made it possible to separate the co-eluting 5- and 6-methyl brGDGTs, De Jonge et al. (2014) updated the initial MBT and CBT to better temperature- and pH-correlated MBT'_{5Me} and CBT' index, respectively. As a result, several calibrations were proposed to quantify palaeotemperature from various sample types: soils (Peterse et al., 2012; De Jonge et al., 2014; Naafs et al., 2017a; Dearing Crampton-Flood et al., 2020), lake sediments (Russell et al., 2018; Martínez-Sosa et al., 2021; Raberg et al., 2021; Zhao et al., 2023), and peat (Naafs et al., 2017b). Following these analytical improvements, the presence of potential non-thermal influences on the distribution of 6-methyl brGDGTs in MBT'_{5Me}, associated with the salinity (e.g., Raberg et al., 2021; Wang et al., 2021) and pH of lakes (e.g., Tierney et al., 2010; Dang et al., 2016) was highlighted, suggesting the possibility of biased temperature reconstructions based on MBT'_{5Me}. The distribution of 6-methyl brGDGTs corresponds to the ratio of 5-methyl brGDGTs to 6-methyl brGDGTs (IR_{6Me}); the higher the ratio, the more abundant the 6-methyl isomers are compared to 5-methyl brGDGTs. Previous studies have shown that the reliability of temperature reconstructions based on MBT'_{5Me} decreases when the IR_{6Me} ratio is greater than 0.5 (Bauersachs et al., 2024) and that the correlation between MBT'_{5Me} and months above freezing air temperature increases when IR_{6Me} values are less than 0.4 (Novak et al., 2025). They highlighted the importance of the distribution of brGDGT compounds on MBT'_{5Me} and, therefore, the importance of taking brGDGT isomerisation into account when using them in palaeotemperature reconstructions. The isomerisation of brGDGTs IR_{6Me} was shown to be related to multiple environmental factors such as pH, salinity, O_2, sources and lake depth level (De Jonge et al., 2014; Ding et al., 2015; Yang et al., 2015; Naafs et al., 2017a; Dearing Crampton-Flood et al., 2020; Bauersachs et al., 2024; Baxter et al., 2024; Novak et al., 2025).

Other confounding factors, which could skew temperature reconstructions due to their impact on the compounds used to calculate the MBT'_{5Me}, have been identified. More specifically, in lacustrine environments, redox conditions (oxic vs. anoxic) at the surface and/or in the water column have an impact on the distribution and composition of bacterial communities, thereby affecting the MBT'_{5Me} index used in most calibrations (Raberg et al., 2025; Baxter et al., 2024; Harning et al., 2025). The isoGDGT-0 to Crenarchaeol ratio has been developed as a proxy for the presence of archaeal methanogens (Blaga et al., 2009), as crenarchaeol is biosynthesised by ammonia-oxidising archaea, while methanogenic archaea can biosynthesise isoGDGT-0. The higher the ratio, the more reducing (anoxic) the conditions. Overall, previous studies have demonstrated that brGDGT-based palaeotemperature reconstructions in lakes are more reliable when no reducing conditions are present (Weber et al., 2018; Baxter et al., 2024; Colcord et al., 2015; van Bree et al., 2020; Harning et al., 2025).

In addition, the establishment and development of Mediterranean vegetation has also been shaped by a long history of fires and land use under varying climatic conditions (Carcaillet et al., 2007; Leys et al., 2013; Lestienne et al., 2020). Several studies have shown that fire regimes do not have a linear relationship with climatic variations, and that an increase in human populations, along with changes in livestock and agricultural practices (Tinner et al., 2006; Vannière et al., 2008), can drastically increase the risk of fires (Carcaillet et al., 2002). Pollen data can therefore be combined with charcoal analysis to document the interactions between fire activity, human occupation and climate.

In this study, we aim to investigate the climate changes of the latitudinal band between 40–43°N at an intermediate elevation (~ 650 m a.s.l.) in Italy during the Holocene using a new sedimentary sequence taken from Lago Grande di Monticchio. We aim to provide robust estimates of the Late Glacial and Holocene temperature trends and patterns by a combination of two independent proxies: brGDGTs and pollen data. Several calibrations will be applied to the brGDGTs data, and several methods will be applied to the pollen data to improve the accuracy of our reconstructions. The signals from the different methods and calibrations will be combined to produce a single, robust climate signal for each parameter at Lago Grande di Monticchio. This multi-proxy and multi-method approach allowed us to assess the reliability of our temperature reconstruction. Pollen data will also be used to reconstruct the precipitation changes, particularly the summer precipitation, to better investigate the north–south pattern previously evidenced by lake levels and other proxies. Additionally, we compare our findings with charcoal analysed on the same core to document the Holocene fire activity. Our results will also be compared to other proxies like speleothems, chironomids, alkenones, and sedimentological markers to better understand seasonal dynamics across the Italian peninsula from the Early to the Late Holocene. Finally, we used our palaeoclimate reconstruction at Lago Grande di Monticchio and its comparison with other proxies and records to better understand the climate-forcing mechanisms (e.g., North Atlantic Oscillation, Intertropical Convergence Zone) involved in the latitudinal climate division in Italy during the Holocene.

2. Material and methods

2.1. Study area

Laghi di Monticchio are two maar lakes located west of Mount Vulture, near Melfi in the Basilicata region, southern Italy (Fig. 1a). Mount Vulture is a Quaternary volcano that last erupted approximately 130,000 years ago (Bonadonna et al., 1993; Villa and Buettner, 2009) and is the only volcano along the eastern margin of the Apennines mountain range. In comparison, about 100 km to the west, near Naples, there is a notable concentration of late Quaternary and contemporary volcanic activity (e.g., Somma-Vesuvius, Ischia, and Phlegraean Fields; Watts et al., 1996b; Di Vito et al., 1999; Cioni et al., 2008; Wulf et al., 2008; Sulpizio et al., 2010). The larger of the two lakes, Lago Grande di Monticchio, lies at an altitude of 656 m a.s.l., and has an average water depth of over 10 m (max ca. 39 m). Its surface area is ca. 40 ha, and its catchment is ca. 237 ha (Allen et al., 2002).

The site experiences a warm, temperate Mediterranean climate, with an average annual temperature and precipitation of 12.5 °C and 830 mm, respectively (Fick and Hijmans, 2017; ISPRA, 2023). The region is also characterised by a marked seasonality, with higher precipitation and lower temperatures in winter than in summer (winter: 5.9 °C and 160 mm; summer 19.9 °C and 80 mm; Fick and Hijmans, 2017).

Forests predominate on the inner slopes of the crater, the main tree species being *Fagus sylvatica*, occupying damper areas down to the lakes, and *Quercus cerris* (Allen et al., 2000). *Abies alba* are found at the top of Monte Vulture, while *Quercus pubescens* forests on the outer slope of the crater are a result, according to Watts et al. (1996b) and Allen et al. (2000), of early 20th-century plantings and are not naturally occurring. On the swampy shores of the lake, *Alnus glutinosa* accounts for a large part of the forest vegetation. Its presence results from human management, although it likely has natural origins as well (Watts et al., 1996b). There is little evidence of Mediterranean evergreen woodland at Lago Grande di Monticchio, with *Quercus ilex*

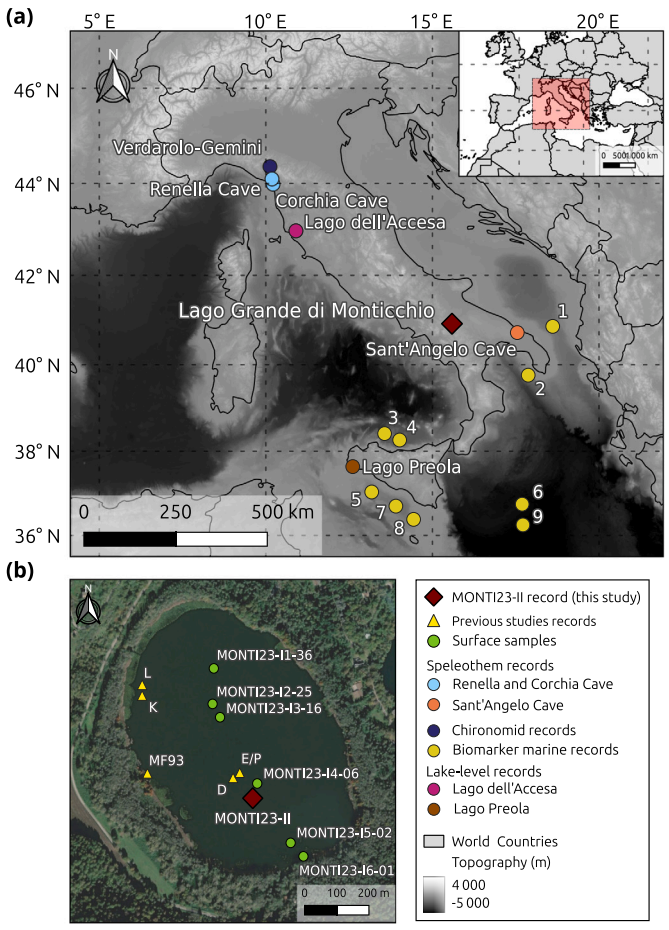

Fig. 1. (a) Location of the Lago Grande di Monticchio (red diamond); Holocene paleoclimate records inferred from various proxies are also plotted: speleothems (light blue and orange dots; Drysdale et al., 2006; Regattieri et al., 2014; Columbu et al., 2022), chironomids (dark blue dots; Samartin et al., 2017), lake-level (pink and brown dots; Magny et al., 2007, 2011), and marine biomarkers records (dark yellow dots, Table A.1; Emeis et al., 2000; Cacho et al., 2001; Doose, 2001; Emeis and Dawson, 2003; Giunta and Emeis, 2006; Versteegh et al., 2007; Incarbona et al., 2016). Topography basemap is from ETOPO Global Relief Model (NOAA National Centers for Environmental Information, 2022) (b) Aerial view of Lago Grande di Monticchio, including the location of the MONTI23-II core (red diamond), the six lacustrine surface samples named MONTI23-I1-36, MONTI23-I2-25, MONTI23-I3-16, MONTI23-I4-06, MONTI23-I5-02 and MONTI23-I6-01 (green dots), and the other cores previously investigated and used to create the composite pollen record (yellow triangles).

being the primary species identified. Genuine evergreen woodland and maquis only appear at lower elevations closer to the coast (Watts et al., 1996b; Allen et al., 2002).

Human presence near Monticchio is attested as early as the Middle Pleistocene in the Lower Palaeolithic sites of Notarchirico, Loreto (Venosa basin, ca. 18 km east of Monticchio; Lefèvre et al., 1994; Moncel et al., 2020; Pereira et al., 2024) and Cimitero di Atella (Atella basin, South of the Vulture; Rocca et al., 2023), and more closely in Rendina (Melfi, ca. 8 km north–east of Monticchio) 7000 years ago (6,200-5800 cal. BC; Cipolloni Sampo et al., 1977; Perrin and Binder, 2011) by agropastoral communities related to the Ceramica Impressa cultural sphere. In the caldera, human occupation is attested by the ruins of the 10th century abbey of Sant'Ippolito, which was succeeded in the 17th century by the abbey of San Michele (Allen et al., 2002).

2.2. Coring and surface sampling

The lipid biomarker analysis is carried out on the sedimentary sequence "MONTI23-II" (40°55′47" N; 15°36′21" E, red diamond on Fig. 1b), cored in May 2023 as a part of the ICARE and COMET projects (PI. A. Pereira and B. Giaccio). MONTI23-II is a 15 m sequence, cored 6 m below water level. The pollen-based climate reconstruction relies on the pollen samples obtained from the composite core "MONTICCHIO", encompassing sections LGM-D, -E/P, -K, -L and MF93 (yellow dots on Fig. 1b; Allen et al., 2002; Wulf et al., 2004), as no pollen analysis has yet been conducted on MONTI23-II.

Moreover, to have a better understanding of the modern pollen and brGDGT composition surrounding the lake, 12 surface samples were also collected: 6 from the lake interface (MONTI23-I) and 7 from the surrounding vegetation (MONTI23-PB). Lake interface surface samples were collected at different water depths of the lake, ranging from 36 to 1 m depth at 10 m intervals (grey dots on Fig. 1b). Surrounding vegetation surface samples (moss samples) were collected according to an altitudinal gradient, ranging from 1235 to 680 m, corresponding to different types of vegetation (e.g., beech forest, oak forest, hazel forest, etc.) close to Lago Grande di Monticchio.

2.3. Tephra sampling and glass analysis

The MONTI23-II core chronology is based on the geochemical analysis of ten tephra layers within the core. These tephra layers have been analysed in terms of major element composition, to provide geochemical correlations to specific volcanic sources and to individual events, and to use their related ages to establish a precise and robust age model (Table B.2, from Somma-Vesuvius and Phlegrean Fields).

Major element compositions of glass shards from selected tephra were determined at the joint Laboratory of Micro Analysis and Electron Microscopy (LAM2) of the CNR-IGAG and the Earth Sciences Department of "Sapienza" University of Rome using a JEOL JXA-iSP100 Super Probe equipped with five-WDS (Wavelength Dispersive Spectrometers). Operating conditions were set to 15 kV accelerating voltage, 10 nA beam current, and a defocused beam diameter of 10 μm. Element counting times were 20 s on the peak (half on the background) for all elements except for Na and Si (P:10 s; B:5 s), and F and S (P:30 s; B:15 s). Quartz (Si), ilmenite (Ti), anorthoclase (Al), chromite (Fe), olivine (Mg), diopside (Ca), albite (Na), orthoclase (K), apatite (P), fluorapatite (F), chlorite (Cl), baryte (S) and metals (Mn) were used as calibration standards. The accuracy of the measurements was assessed by measuring, before the analytical session, the Max Planck Institute artificial glass secondary standards GOR128-G, ATHO-G and StHs6/80-G (Jochum et al., 2006). All compositional data are shown as oxide weight percentages (wt%) in the Total Alkali vs Silica (TAS; Le Maitre et al., 2002) and bi-plots diagrams, with total iron measured as FeO and oxide data normalised to 100 % on a volatile-free basis (i.e., excluding F, Cl and S) for correlation purposes. Mean compositions for each tephra are reported with double the standard deviation (i.e., 2 sd, see Appendix section). The full glass composition and related discussion for each tephra are provided in the Appendix section and will not be discussed hereafter. Comparisons with available literature data are also provided, and the correlations of each tephra to the specific eruptions are summarised in Table 3.

2.4. brGDGT analysis and indexes

2.4.1. brGDGT analysis

BrGDGT analysis was conducted in the LGLTPE-ENS laboratory (Lyon, France) on fossil and modern samples: 107 samples from the MONTI23-II core (with a 5 to 10 cm sampling step) and 5 surface samples (lake interface MONTI23-I samples). Samples were freeze-dried for 24 to 72 h. After grinding and homogenisation, the total lipid fraction was extracted twice by microwave (MARS 6 CEM) at 70 °C

Table 1
Formulae used for computation of brGDGT indices, MAAT, MAF, and pH calibrations with their associated Root Mean Square Error criterion (RMSE, in degrees Celsius for MAAT and MAF).

Index	Formula	RMSE	Reference
MBT'_{5Me}	$\frac{(Ia+Ib+Ic)}{(Ia+Ib+Ic+IIa_{5Me}+IIb_{5Me}+IIc_{5Me}+IIIa_{5Me})}$	–	De Jonge et al. (2014)
CBT′	$log10\frac{(Ic+IIa_{6Me}+IIc_{6Me}+IIIa_{6Me}+IIIb_{6Me})}{(Ia+IIa+IIIa)}$	–	De Jonge et al. (2014)
IR_{6Me}	$\frac{IIabc_{6Me}+IIIab_{6Me}}{IIabc_{5Me}+IIIabc_{5Me}+IIabc_{6Me}+IIIab_{6Me}}$	–	De Jonge et al. (2014)
isoGDGT-0/Cren	$\frac{isoGDGT-0}{Crenarchaeol}$	–	Blaga et al. (2009)
$MAAT_{MBT'_{5Me}}$	$-1.21+32.42\times MBT'_{5Me}$	2.44	Russell et al. (2018)
$MAF_{MBT'_{5Me}}$	$4.81+15.64\times MBT'_{5Me}$	0.92	Bauersachs et al. (2024)
MAF_{mr}	$92+63.84^2-130.51\times(\frac{Ib_{5Me}}{Ib_{5Me}+IIb_{5Me}+IIIb_{5Me}})$ $-28.77\times(\frac{IIa_{5Me}}{Ia_{5Me}+IIa_{5Me}+IIIa_{5Me}})^2-72.28\times(\frac{IIb_{5Me}}{Ib_{5Me}+IIb_{5Me}+IIIb_{5Me}})^2$ $-5.88\times(\frac{IIc_{5Me}}{Ic_{5Me}+IIc_{5Me}+IIIc_{5Me}})^2+20.89\times(\frac{IIIa_{5Me}}{Ia_{5Me}+IIa_{5Me}+IIIa_{5Me}})^2$ $-40.54\times(\frac{IIIa_{5Me}}{Ia_{5Me}+IIa_{5Me}+IIIa_{5Me}})-80.47\times(\frac{IIIb_{5Me}}{Ib_{5Me}+IIb_{5Me}+IIIb_{5Me}})$	2.14	Raberg et al. (2021)
$pH_{CBT'}$	$8.95+2.65\times CBT'$	0.80	Russell et al. (2018)

with 10 ml of dichloromethane (DCM)/methanol (MeOH) mixture (3:1, v/v) and then filtered on SPE cartridge. 1000 ng of C_{46} GDGT (99 % n-hexane: 1 % isopropanol) was then added to the Total Liquid Extract (TLE) to serve as an internal standard (Hopmans et al., 2016). The TLE was then separated into polar and apolar fractions on a silica column with 5 ml of hexane/DCM (1:1) and 10 ml of DCM/MeOH (1:1), respectively. The samples were then analysed in hexane/isopropanol (99.8:0.2) by high-performance liquid chromatography with mass spectrometry (HPLC-MS, Agilent 1200). Ions in Selected Ion Monitoring (SIM) are detected for mass-to-charge ratios (m/z): 744 for the internal standard C_{46}, 1050, 1048, 1046, 1036, 1034, 1032, 1022, 1020, and 1018 for brGDGTs (Huguet et al., 2006). Concentrations are expressed in $\mu g\ g^{-1}_{[sed]}$. The relative abundances of each brGDGT are determined by the ratio of the proportion of the compound to the sum of all brGDGTs. Six samples with contrasting brGDGT compositions were measured and integrated six times to establish the reproducibility of the analytical setup.

2.4.2. Index calculation and temperature reconstruction

Different indices such as MBT'_{5Me}, CBT', IR_{6Me} and isoGDGT-0/Cren ratio were calculated for the MONTI23-II sequence and surface samples (Table 1). The Mean Annual Temperature (MAAT) and the mean temperature of Months Above Freezing (MAF) were reconstructed from three types of lacustrine calibrations: the linear relationship between MAAT/MAF and methylation indices (MBT'_{5Me}; Russell et al., 2018; Bauersachs et al., 2024), the multiple regression (mr) between MAF and fractional abundances of selected brGDGTs (Raberg et al., 2021), and the Bayesian calibration (Martínez-Sosa et al., 2021).

Changes in the water column and sediment pH can have a significant impact on bacterial communities and, as a result, affect brGDGT-based temperature reconstructions (De Jonge et al., 2014; Martínez-Sosa and Tierney, 2019). Hence, brGDGTs-based pH reconstruction, with a CBT'-based calibration (Table 1, De Jonge et al., 2014), of the MONTI23-II sequence has also been investigated.

2.5. Pollen samples

2.5.1. Fossil pollen samples

Extensive palaeoenvironmental research at Lago Grande di Monticchio has been conducted since the early 1980s, based on sedimentology, vegetation, and pollen data (Watts, 1985; Watts et al., 1996b; Zolitschka, 1996; Allen et al., 1999, 2000; Brauer et al., 2000; Allen et al., 2002; Brauer et al., 2007). Four subsequent coring campaigns (1990, 1994, and 2000) were conducted in the lake basin. They resulted in the recovery of nine overlapping sediment cores that form a continuous composite profile with a total length of 103.1 m covering the last climate cycle (Brauer et al., 2007).

In this study, we focus on the Younger Dryas and the Holocene periods. The composite fossil pollen sequence was extracted from the Neotoma international database (Allen et al., 2021, site name: Lago Grande di Monticchio, dataset ID: 47525, site ID: 3295); only the pollen samples corresponding to the last 13,000 years (approximately 8.17 m, encompassing the section LGM-D, -E/P, -K, -L and MF93, yellow dots on Fig. 1b) were kept for our study. The subsetted composite core was numerically resampled to limit the number of samples that were too close in time due to core overlap, potentially creating significant sample-to-sample variation. We resampled the composite core to reach at least 50 years between each pollen sample (Fig. C.1). The pollen taxa were homogenised, and the spores, aquatic and local hygro- to mesohygrophilous taxa, such as *Alnus, Salix, Populus* and Cyperaceae, were excluded for the palaeoclimate reconstruction.

2.5.2. Pollen surface samples analysis

Pollen surface samples from the lake interface and surrounding vegetation were chemically (HCl, KOH, HF and acetolysis) and physically (sieving between 200 and 10 μm) treated following the standard procedure (Moore et al., 1991). A total of 7 surface and 6 lake interface samples were analysed under a light microscope at a standard magnification of × 400. Pollen flora is identified using photo atlases (Reille, 1992; Beug, 2004). The pollen diversity is of 68 taxa.

An average of 316 terrestrial pollen grains was counted. Percentages were calculated on pollen sums excluding spores, *Alnus*, *Salix*, *Populus* and Cyperaceae.

Two pollen diagrams have been produced to represent the surrounding vegetation (Fig. 5a) and the lake interface (Fig. 5b) pollen rains. To conceptualise average pollen rain, an average pollen signal was estimated by averaging the different surface sample types depending on their environment types (surrounding vegetation or lake interface). MONTI23-PB mean corresponds to the average pollen signal of the vegetation surrounding the lake, and MONTI23-I mean corresponds to the average pollen signal of the sediment-water interface of the lake.

2.6. Pollen-based quantitative climate reconstruction: a multi-method approach

Various methods, based on different ecological and mathematical concepts, have been developed to reconstruct the climate from pollen data. These methods were initially designed to calibrate the relationship between modern pollen data (soils, mosses) and current climate parameters and to apply them to past pollen assemblages (transfer functions). Each method has its advantages and disadvantages, which can lead to different results depending on the techniques used (Chevalier et al., 2020). In this context, multi-method approaches can be applied to increase the reliability of palaeoclimatic reconstructions (Peyron et al., 2005; Brewer et al., 2008; Peyron et al., 2013, 2017; Salonen

et al., 2019; Dugerdil et al., 2021; Robles et al., 2022; d'Oliveira et al., 2023; Dugerdil et al., 2025). Our multi-method approaches include four different methods: two recent machine learning techniques based on regression trees (Random Forest and Boosted Regression Trees), a more classical "assemblages" approach, based on the principle of dissimilarity between fossil and modern assemblages (Modern Analogue Technique) to quantify climate parameters and a transfer function technique based on linear regressions (Weighted Averaging Partial Least Squares regression). These methods yield coherent results for the study of the last 13,000 years in the Mediterranean region (Robles et al., 2023; d'Oliveira et al., 2025; Sassoon et al., 2025).

The Boosted Regression Trees (BRT; Salonen et al., 2012, 2019) and Random Forest (RF; Breiman, 2001), methods based on machine learning principles, use regression trees to systematically partition pollen data through successive divisions based on the abundance observed in the pollen spectrum. This approach increases the probability of selecting under-represented samples in previous tree iterations (Chevalier et al., 2020). The boosting process of the BRT improves the model's predictive accuracy for elements that were previously less accurately forecasted (Salonen et al., 2019). For the BRT method, a minimum of 1000 trees was set to better optimise the parametrisation process (Elith et al., 2008).

The Modern Analogue Technique (MAT; Guiot, 1990) is a method often used for reconstructing past climates, recognised for its ease of use, efficiency, and sensitivity (e.g., for European large-scale studies; Davis et al., 2003; Mauri et al., 2015; Herzschuh et al., 2023; Geng et al., 2025). This approach measures the dissimilarity between fossil pollen assemblages and those of modern samples, selecting the closest modern counterparts as analogues.

The Weighted Averaging Partial Least Squares (WA-PLS) method, developed by ter Braak and Juggins (1993), serves as a transfer function and is frequently utilised in pollen-based palaeoclimate reconstructions. This method assumes that the relationship between the proportion of pollen and climate follows a unimodal pattern, suggesting that the abundance of a pollen type is closely linked to its environmental tolerance. WA-PLS determines the climatic optimum for a species using calibration data by calculating the average climatic conditions where the species is found, considering its abundance (Chevalier et al., 2020).

In this study, both annual and seasonal (winter and summer) temperatures (respectively, MAAT, Twin, and Tsum) and precipitation (respectively, MAP, Pwin, and Psum) will be reconstructed using the pollen data of Lago Grande di Monticchio. All these methods rely on a modern pollen dataset representing the full range of ecosystems that may have occurred in the past within the fossil record. The modern pollen dataset selected here is the "TEMPDB" dataset by d'Oliveira et al. (2025); it combines modern samples from Central and Western Europe and gathers temperate biomes (warm mixed forest, xerophytic wood/shrub, temperate deciduous forest, cool mixed forest, warm steppe, cold mixed forest, and cool steppe).

2.7. Charcoal extraction and quantification

A total of 1 cm^3 of sediment was subsampled every 10 cm along the sediment core using a manual punch to avoid contamination from the edges (Courtney Mustaphi et al., 2015). Each sample was treated in a solution containing 20 ml of sodium hypochlorite (NaClO), 3 g of sodium metaphosphate ($NaPO_3$), and 0.5 g of potassium hydroxide (KOH), and agitated for at least 24 h to activate the KOH and promote deflocculation (Carcaillet et al., 2001). This chemical treatment enables the separation of charcoal fragments from other organic matter. All samples were then sieved through a 160-µm mesh and rinsed with water (van Bellen et al., 2012; Adolf et al., 2018). This relatively fine mesh size was selected to allow the recovery of small charcoal particles typically produced by low-intensity grassland fires, in contrast to larger particles associated with forest fires (Higuera et al., 2009; Ali et al., 2009; Oris et al., 2014). Charcoal particles were hand-picked under a binocular microscope using a fine brush, then photographed and analysed using `ImageJ` software (Schneider et al., 2012).

The total number of particles and their morphometric characteristics (surface area, perimeter, length, and width) were automatically measured for each sample. The CHARnb (number of particles per cm^2 per year) values were calculated based on the sediment accumulation rates derived from the age–depth model. This metric provides information on charcoal input dynamics and can be used to infer both fire frequency and fire intensity (Ali et al., 2009; Lestienne et al., 2020).

2.8. Numerical analyses

To estimate the correlation between environmental (i.e., pH) and climatic (i.e., MAAT and MAF) variables inferred from brGDGTs in modern samples, a pair-wise correlation matrix was calculated using the `corrplot` package (version 0.95; Wei and Simko, 2024).

For pollen-based reconstruction methods (i.e., MAT, BRT, WA-PLS and RF), the reliability of the results was estimated by bootstrap cross-validation by calculating the values of the correlation coefficient between the variables (R^2) and those of the Root Mean Square Error criterion (RMSE) for the modern temperate climate dataset extracted from WorldClim 2.1 (Fick and Hijmans, 2017). The pollen-based reconstruction reliability results of each method used are summarised in Table 2. Pollen-based climate reconstructions and reliability tests (R^2 criterion and RMSE) were performed with the packages `rioja` (version 1.0.7; Juggins, 2024) and `dismo` (version 1.3.16; Hijmans et al., 2024).

The four applied methods (MAT, BRT, WA-PLS and RF) are combined to provide a unique and more robust climate signal for Lago Grande di Monticchio. This unique climate signal is based on a weighted-averaging approach. The weighted-averaged $\hat{x}$ prediction follows Eq. (1) for which n different methods are averaged together at each prediction time i using the inverse model performance criterion value (RMSE) of each method.

$$\hat{x}_i = \sum_{m=1}^{n} w_{i,m} \cdot x_{i,m} \tag{1}$$

Where $x_{i,m}$ is the prediction of model m at time i, and $w_{i,m}$ is its normalised weight. The weight of model m at time i is calculated following Eq. (2).

$$\tilde{w}_{i,m} = \frac{1}{\mathrm{RMSE}_m} \tag{2}$$

Where $\tilde{w}_{i,m}$ is the weight for model m at time i and RMSE_m the error of model m. The weights were then normalised to have their sum equal to 1 using Eq. (3).

$$w_{i,m} = \frac{\tilde{w}_{i,m}}{\sum_{m=1}^{n} \tilde{w}_{i,m}} \tag{3}$$

A correlation analysis was carried out between the reconstructions based on pollen and those based on brGDGTs, the latter being derived from two distinct sequences with different resolutions, to evaluate the robustness of our palaeoclimate reconstructions at Lago Grande di Monticchio. The higher the correlation between two independent proxies, the more robust the palaeoclimate reconstruction. Pollen- and brGDGTs-based climate signals were first transformed using the *zoo* function from the `zoo` package (version 1.8-13; Zeileis and Grothendieck, 2005), and an estimation of the Pearson's correlation coefficient (r) was calculated using the *CorIrregTimser* function from the `corit` package (version 0.0.0.9000; Reschke and Laepple, 2024). Following the approach of Reschke et al. (2019), since the correlation of time series is generally a function of time scale (i.e. the frequency range), a Gaussian filter is applied to the data in the time domain before estimating the correlation. As the time domain filters are applied at regular time positions, irregularly sampled time series were interpolated, using a linear interpolation method, to produce a regular time series before filtering. The time step of the interpolation was established as

Table 2
Performance results of the MAT, and BRT methods applied to the European temperate (TEMPDB) modern pollen dataset for mean annual (MAAT; °C), winter (Twin; °C) and summer (Tsum; °C) temperature and mean annual (MAP; mm), winter (Pwin; mm) and summer (Psum; mm) precipitation; *k* corresponds to the number of parameters for MAT and WA-PLS and tree complexity for BRT and RF that infer the best R^2 and calibration error (RMSE) values.

Parameter	Method	*k*	Nb tree	R^2	RMSE
MAAT	MAT	4	–	0.86	1.81
	BRT	10	2150	0.80	1.88
	WA-PLS	3	–	0.74	2.23
	RF	34	500	0.83	1.78
MAP	MAT	5	–	0.80	205.00
	BRT	10	3000	0.71	219.00
	WA-PLS	3	–	0.47	300.00
	RF	34	500	0.73	211.00
Twin	MAT	4	–	0.86	2.04
	BRT	10	2750	0.80	2.14
	WA-PLS	3	–	0.74	2.49
	RF	34	500	0.83	1.98
Pwin	MAT	4	–	0.77	75.00
	BRT	10	3000	0.66	80.40
	WA-PLS	3	–	0.36	112.00
	RF	34	500	0.67	79.00
Tsum	MAT	4	–	0.86	1.81
	BRT	10	2300	0.80	1.88
	WA-PLS	3	–	0.72	2.27
	RF	34	500	0.81	1.82
Psum	MAT	4	–	0.90	40.20
	BRT	10	3000	0.87	40.60
	WA-PLS	3	–	0.76	55.40
	RF	34	500	0.88	38.20

the mean temporal resolution of both time series (T_{res}), and the cut-off frequency of the applied filter was established to $0.5 \times T_{res}$ (Reschke et al., 2019). To assess the significance of the correlation between time series, we used an empirical permutation test adapted to temporal dependencies, which compares the observed correlation to a null distribution generated by permutations of the series, while preserving local dependency (block permutation test). Correlation coefficient between pollen- and brGDGTs-based climate signals was calculated for four time periods: Younger Dryas, Early Holocene, Middle Holocene and Late Holocene.

All numerical analyses and graphs were performed on R Studio (version 4.4.1; RStudio Team, 2020).

3. Results

3.1. Tephra sources

The major element compositions of the investigated tephras from Lago Grande di Monticchio are shown in Total Alkali vs Silica diagram (TAS; Le Maitre et al., 2002, Fig. 2a, 2b) and in the discrimination diagrams of 2c, 2d. All the investigated tephra samples fall into the high-K alkaline series and are classified as phonotephrites (TM23-3), tephri-phonolites (TM23-4b and TM23-19), phonolites (TM23-1, TM23-5, TM23-6, TM23-13 and TM23-17) and at the boundary between phonolites and trachytes (TM23-7, TM23-9, TM23-19, 2a, b). The alkali contents and ratios (i.e., K_2O/Na_2O) are variable. It is > 1 for TM23-3, TM23-4b, TM23-9, TM23-17, TM23-19, while it is> 1 for samples TM23-1 and TM23-13, and is approximately ±1 for tephras TM23-5 and TM23-6. The CaO/FeO is > 0.6 for all the samples, and it is ±1 for samples TM23-1, TM23-3, TM23-4b, TM23-5, TM23-6 (Fig. 2c). A detailed discussion of the geochemical features of each tephra layer, in addition to the associated figures, can be found in the Appendix section (Figs. D.2–D.4). Features such as the Cl content > 0.3 wt% are distinctive of Somma-Vesuvius, Phlegraean Fields and Ischia (e.g., Tomlinson et al., 2015). The distinct CaO/FeO ratios and the relationship between CaO/FeO and Cl (Giaccio et al., 2017a) were a useful tool to distinguish the sources. In addition, the alkali ratio (i.e., K_2O/Na_2O) further helps discriminate eruptions sourced at Somma-Vesuvius (generally characterised by Low Alkali Ratio, LAR) from those sourced at Phlegraean Fields (High Alkali Ratio, HAR). Tephra layers were correlated to 10 previously characterised and sometimes dated eruptions (Figs. 2a, 2b, 2c, 2d, Table 3, Figs. D.2, D.3, D.4). On this basis, six tephra layers are attributed to the Somma-Vesuvius, and correlated to the 1631 CE and 512 CE historical eruptions, the inter Avellino-Pompeii (AP) −3 and −2 eruptions, and finally the Pomici di Avellino and Mercato eruptions (Table 3, Figs. D.2, D.3, D.4). The remaining four tephra layers were attributed to the Phlegraean Fields volcanic complex and correlated to Astroni 1, Agnano Monte Spina (AMS), Pomici Principali (PP) and the Neapolitan Yellow Tuff (NYT) eruptions (Figs. D.2, D.3, D.4). A detailed description of tephra correlations and figures is provided in the Appendix section.

3.2. Bayesian age model

The age model relies on ten published radiocarbon ages (Table 3) and covers the last 13,000 years. These ages were recalculated here according to the IntCal20 (Reimer et al., 2020) calibration. To facilitate comparisons with previous cores already studied in Lago Grande di Monticchio, correlations with tephras presented by Wulf et al. (2008) are reported in Table 3. The age–depth model was produced with *Chronomodel 3.2.9* software (Lanos and Dufresne, 2019). Historical ages are defined as events in the model. The resulting age model of the first 10 m of the MONTI23-II core is shown in Fig. 2e, with an error envelope expressed at 2σ. It results in a mean sedimentary rate of 73 $cm.ka^{-1}$, with a drop to 30.9 $cm.ka^{-1}$ between AP3 and AMS tephra layer.

3.3. BrGDGT analysis and climate reconstruction

3.3.1. Compound concentrations

For MONTI23 lacustrine surface samples, the average concentration of brGDGTs is 5.8 ± 3.9 μg $g^{-1}_{[sed]}$ (0.7–17.4 μg $g^{-1}_{[sed]}$). The MONTI23-II core samples have a higher average concentration of brGDGTs than the surface samples: 6.5 ± 2.8 μg $g^{-1}_{[sed]}$ (2.8–11.2 μg $g^{-1}_{[sed]}$).

3.3.2. Relative abundances

Average analytical errors are calculated from the averaged standard deviations (sd) of replicate measurements for brGDGTs (sd = 7.5 %, *n* = 107).

BrGDGT relative abundances in MONTI23 lacustrine surface samples show the dominance of tetramethylated (Ia) and pentamethylated (IIa) (18.9 % and 19.8 % respectively; Figs. 3a, E.5b. Hexamethylated (IIIa) brGDGTs have a lesser relative abundance in the core (8.7 %, Figs. 3a, E.5b). In surface samples, brGDGTs are dominated by pentamethylated (IIa) compounds with an average relative abundance of 53.0 % (Figs. 3a, E.5b). Tetra- and hexamethylated brGDGTs have a comparable relative abundance in the core (respectively 23.5 % and 23.6 %, Figs. 3a, E.5b).

MBT'_{5Me} index ranges between 0.30 and 0.55 (sd = 0.02, *n* = 107; Fig. 4a). Minimal values were observed during the Younger Dryas event, between 12,900 and 11,400 cal. BP (average value of 0.34), before an abrupt increase at the onset of the Holocene. From 11,400 cal. BP to approximately 870 cal. BP, MBT'_{5Me} values are relatively stable and range between 0.38 and 0.55 (average value of 0.44). A decrease of MBT'_{5Me} values follows this stable period from 870 cal. BP onward, with values ranging from 0.36 to 0.47 (average value of 0.39). The CBT' index does not show the same trends as the MBT'_{5Me} and ranges from −0.6 to −0.2 (sd = 0.03, *n* = 107; Fig. 4b). A slight continuous increase over time is observed, although punctuated by falls in CBT' values between 7800 and 7100 cal. BP, and several successive ones between 6300 and 2800 cal. BP. The pH, inferred from the CBT'-based calibration of Russell et al. (2018), varies from 7.20 to 8.36

Table 3
MONTI23-II tephras included in the age model correlated with the respective tephra layers from Wulf et al. (2004). The volcanic sources identified and the related radiocarbon dates used to build the age model are also presented. All ages are calibrated with Intcal20[a] (Reimer et al., 2020) or Marine20[b] (Heaton et al., 2020).

TM23	TM (Wulf et al., 2008)	Eruption	^{14}C age	CalBP	Reference
TM23-1	TM-1	1631	–	319	Wulf et al. (2008)
TM23-2	TM-2a	PM1	–	1438	Rolandi et al. (1998)
TM23-4b	TM-3b	AP3	2710 ± 60	2849 ± 62[a]	Rolandi et al. (1998)
TM23-5	TM-3c	AP2	3227 ± 80	3227 ± 80[a]	Rolandi et al. (1998)
TM23-6	TM-4	Avellino	3550 ± 20	3837 ± 48[a]	Passariello et al. (2010)
TM23-7	TM-5a	Astroni 1, 3	3820 ± 50	4177 ± 83[a]	Di Vito et al. (1999)
					Isaia et al. (2009)
TM23-9	TM-5c	Agnano Monte Spina	4130 ± 50	4640 ± 87[a]	Andronico et al. (1995)
			4000 ± 50	4580 ± 90[a]	de Vita et al. (1999)
				4610 ± 104	Chronomodel age
TM23-13	TM-6b	Mercato	8098 ± 71	9024 ± 140[a]	Wulf et al. (2004)
TM23-17	TM-7a	Pomici Principali	10320 ± 50	12169 ± 166[a]	Di Vito et al. (1999)
TM23-19	TM-8	Neapolitan Yellow Tuff	12260 ± 110	14157 ± 198[a]	Siani et al. (2004)[a]
			12260 ± 110	13886 ± 287[b]	Mean Bronk Ramsey et al. (2015)

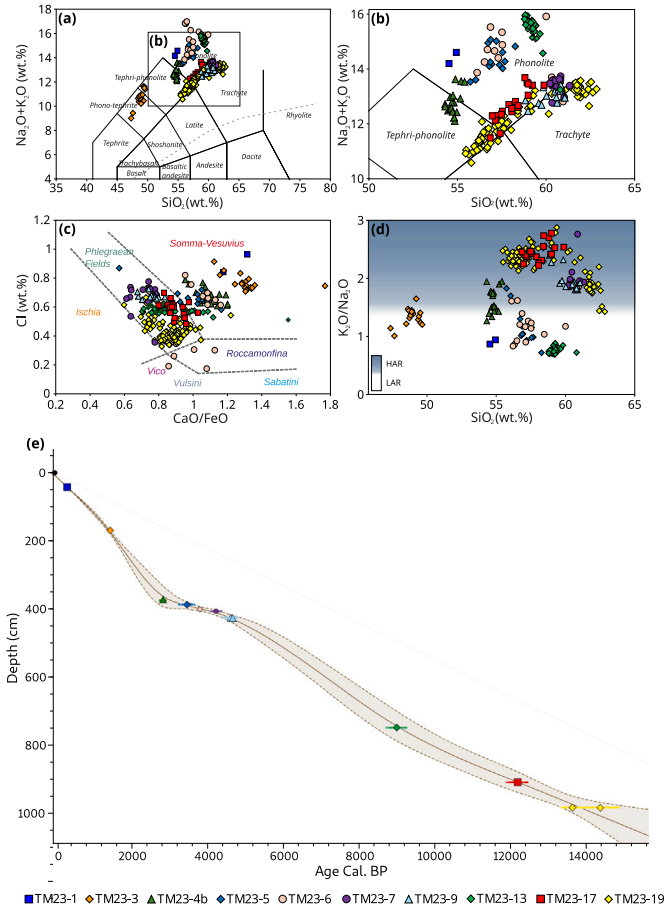

Fig. 2. Major element composition of the samples used in the age model. (a) and (b) Total alkali (K_2O/Na_2O, wt%) vs silica (SiO_2, wt%) diagrams (TAS, Le Maitre et al., 2002); (c) CaO/FeO ratio vs chlorine (Cl, wt%) diagram (modified after Giaccio et al., 2017a); (d) Silica (SiO_2, wt%) vs total alkali (K_2O/Na_2O, wt%). (e) Age-depth model of the MONTI23-II sequence, based on tephrochronologically correlated radiocarbon ages found in Table 3 and built with the *Chronomodel 3.2.9* software (Lanos and Dufresne, 2019), using 3 chains for the MCMC settings, a burn-in iteration of 1000, baths of 100 iterations, an acquisition of 100,000 iterations and a thinning of 10.

and reflects the CBT' trends (Fig. 4d). The IR_{6Me} ratio ranges between 0.28 and 0.67 (sd = 0.02, n = 107; Fig. F.6c). Trends similar to those observed for CBT' are observed, with a slight continuous increase over time, punctuated by decreases in IR_{6Me} values between 7800 and 7100 cal. BP, and several successive decreases between 6300 and 2800 cal. BP. The isoGDGT-0/Cren ratio ranges between 62.67 and 1288.60 (sd = 73.11, n = 107; Fig. F.6d). Relatively high values (> 200) are observed throughout the Holocene, punctuated by phases of even higher values (> 500) between 10,800–9100 cal. BP, 8000–7000 cal. BP, 6900–6300 cal. BP, 3800–2000 cal. BP and 1400–1200 cal. BP.

The correlation matrix between CBT'-based pH and MBT'$_{5Me}$-based MAAT and MAF reconstructions (Fig. G.7) suggests a strongly significant positive correlation between reconstructed temperature (i.e., MAAT and MAF) with r-values ranging from 0.90 to 1.00. Between $pH_{CBT'}$ and MAAT/MAF (MAF_mr, MAF_Bayeasian, MAAT_MBT'$_{5Me}$, MAF_MBT'$_{5Me}$), lower r-values (< 0.20) are present, suggesting no significant correlation between the environmental and climatic variable inferred from brGDGTs.

3.3.3. BrGDGT-based temperature reconstructions

The four calibrations used to estimate the annual temperature from the MONTI23-II record show similar trends (red curve on Fig. 4d). (1) The Younger Dryas period (12,900–11,700 cal. BP) is characterised by very low temperature values, corresponding to temperature anomalies of −3.1 °C (method-averaged values around 9.3 °C) compared to modern-day conditions. Cold conditions are followed by (2) stable warmer conditions between 11,700 and 3200 cal. BP, oscillating around present-day values (method averaged value of 12.5 °C). During this stable period, maximum temperatures are recorded from 7100 to 6100 cal. BP. The last 3000 cal. BP are then characterised by (3) a progressive temperature decrease, accentuated during the previous 870 cal. BP (Fig. 4d), during which temperature anomalies of −1.2 °C are present. Among the calibrations, the MAF_MBT'$_{5Me}$ calibration shows lower variation amplitudes than the others, even though it is based on the same index.

3.4. Pollen analysis and climate reconstruction

3.4.1. Pollen surface samples

Surface samples from the surrounding vegetation (Fig. 5a) have been sampled according to an altitudinal gradient, ranging from 680 (close to the lake elevation) to 1235 m a.s.l. An elevation-dependent variability for various taxa is evidenced, such as *Fagus* (from 10 to 70 %), *Quercus* (from 10 to 45 %), *Corylus* (from 2 to 20 %) and *Pinus* (from 2 to 15 %), while the AP proportion is similar from one sample to another (between 80 and 90 %).

Surface samples from the lake interface (Fig. 5b) have been sampled according to a water depth gradient, ranging from 2 to 36 m. Contrary to surface samples from the surrounding vegetation, the lake interface samples show a homogeneous pollen rain signal from one depth to another. High percentages of *Alnus* (≥ 40 %) and *Salix* (~ 10 %) are found in lake interface samples; much less are present in MONTI23-PB samples corresponding to the surrounding vegetation (< 10 %). The high percentage of *Alnus* and *Salix* in lake surface samples support

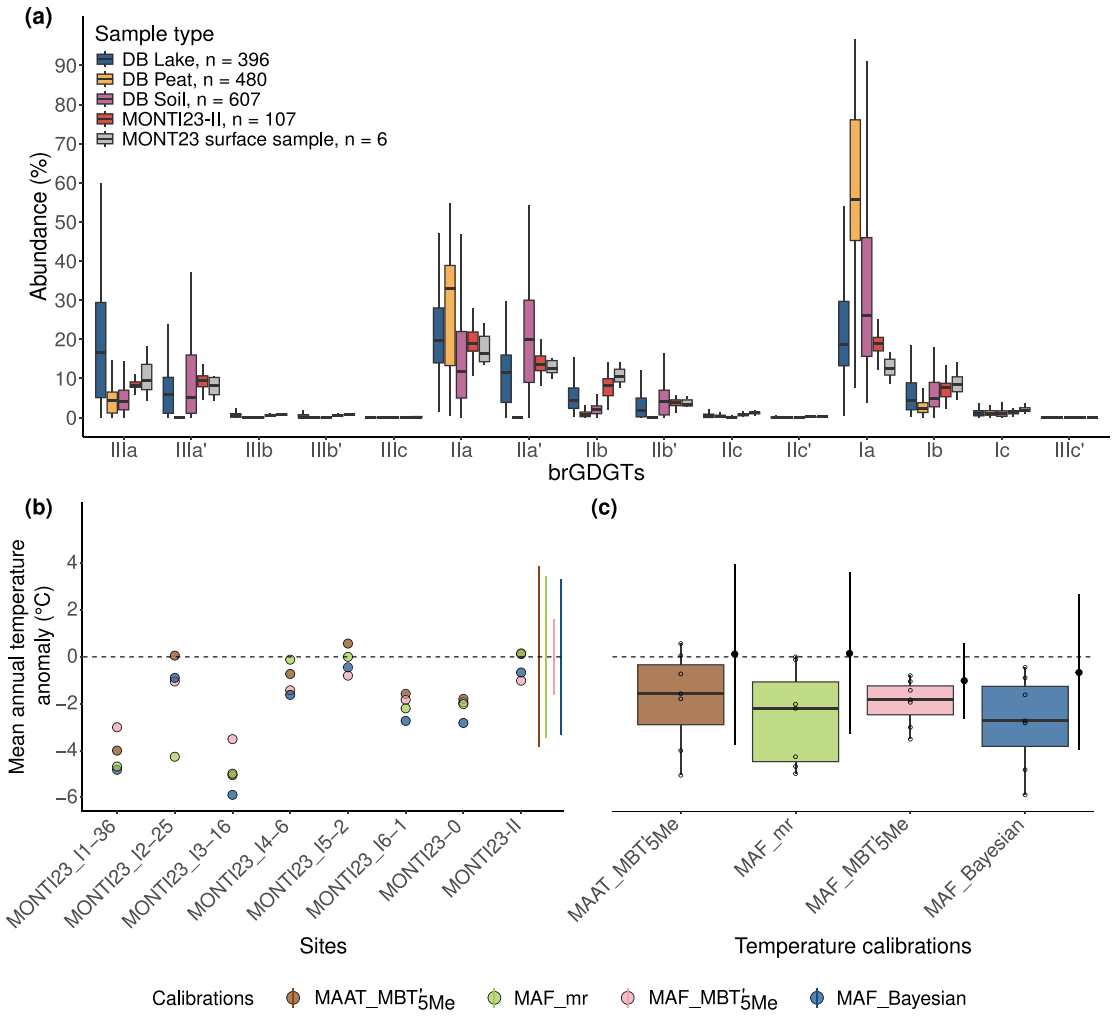

Fig. 3. (a) GDGT compounds relative abundance (%) of brGDGTs for MONTI23-II core samples (in red) and averaged MONTI23 lacustrine surface samples (in grey) and for global lake (Martínez-Sosa and Tierney, 2019, in blue), peat (Naafs et al., 2017b, in yellow) and soil databases (Yang et al., 2014; Naafs et al., 2017a; Dearing Crampton-Flood et al., 2020, in pink). (b) Reconstructed MAAT and MAF from each calibration expressed as anomalies with respect to the mean annual temperatures measured at Monticchio (~ 12.3 °C). The errors (RMSE) of each calibration applied to the MONTI23-II core, found in Table 1, are represented by the lateral lines on the right side. (c) Boxplot representing the results of the calibrations applied to the MONTI23 lacustrine surface samples (n = 6). Black points with error bars next to each calibration correspond to temperature anomalies of MONTI23-II core samples.

its qualification as a local mesohygrophilous taxon and therefore their removal from the fossil pollen dataset used for the palaeoclimatic reconstruction.

Surface samples from the surrounding vegetation (Fig. 5a) and the lake interface (Fig. 5b) have each been averaged to represent the average pollen rain of each environment. Both MONTI23-PB and MONTI23-I mean are dominated by arboreal taxa (AP ≥ 80 %), mostly by *Quercus*, *Fagus* and *Corylus*. Mediterranean taxa are also represented in lake interface samples with *Quercus ilex*-type and *Olea*.

The tree pollen diversity of these surface samples is similar to that observed in the vegetation (Watts et al., 1996b; Allen et al., 2000, 2002) and the percentages are close to those of the youngest sample in the Monticchio fossil sequence.

3.4.2. Pollen-inferred climate reconstructions

There is a relatively good consistency between the four methods used to quantitatively reconstruct temperatures and precipitation (Fig. 6). For temperatures (Figs. 6a–c), WA-PLS and MAT methods show the highest variability, while the BRT method shows the lowest. Precipitation reconstructions are associated with stronger model-to-model variability and performance differences (Table 2), in particular for annual (MAP) and winter (Pwin) precipitation (Figs. 6d–f); WA-PLS and MAT are also the methods that show the highest variability.

Annual conditions. The weight-averaged annual temperature (red curves on Fig. 6a) obtained from the four methods shows (1) cold conditions from 12,800 to 7300 cal. BP (ranging on average between 8.5–11.9 °C), followed by (2) warmer conditions between 7300 and 3100 cal. BP, with temperatures close to modern day (ranging on average between 10.2–13.1 °C) and a slight thermal maximum around 3400 cal. BP (average temperature maximum of 13.1 °C). This warm period is followed by (3) slightly cooler, stable temperatures, close to modern-day values (averaging 9.8–13.0 °C).

The weight-averaged annual precipitation (red curves on Fig. 6d) shows (1) dry conditions from 12,800 to 10,800 cal. BP (averaging between 525–699 mm), followed by (2) wetter conditions from 10,800 to 3000 cal. BP (ranging on average between 562–836 mm). This maximum precipitation is followed by (3) a gradual aridification trend until around 1800 years (averaging 596–798 mm), before wetter conditions, closer to modern-day values, take place.

Seasonal conditions. Weight-averaged winter and summer temperatures show the same trends as the weight-averaged annual temperature (red curves on Figs. 6a, 6b, 6c), with (1) cold conditions from 12,800

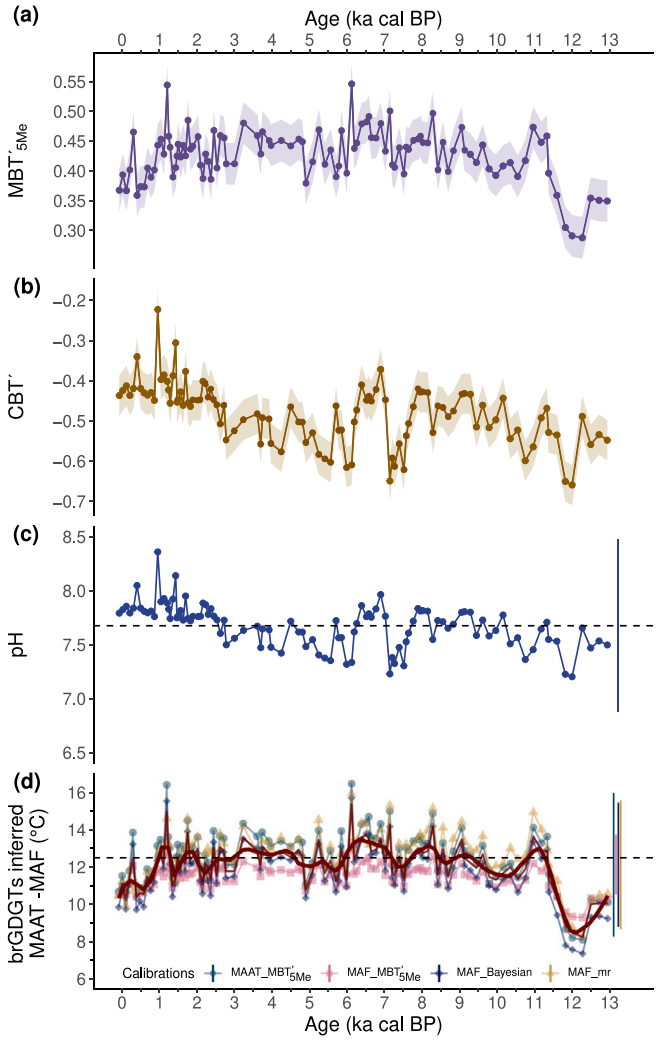

Fig. 4. (a) Index of the degree of methylation (MBT'$_{5Me}$). (b) Index of the degree of cyclisation (CBT'). (c) pH reconstruction based on lacustrine calibration of Russell et al. (2018, CBT'). (d) Mean Annual Temperature (MAAT) and mean temperature of Months Above Freezing (MAF) reconstructions based on lacustrine calibrations of Russell et al. (2018, MAAT_MBT'$_{5Me}$), Bauersachs et al. (2024, MAF_MBT'$_{5Me}$), Martínez-Sosa et al. (2021, MAF_Bayesian) and Raberg et al. (2021, MAF_mr). The red and the bold red curves correspond respectively to the calibration-averaged and the smoothed calibration-averaged temperature signal. The standard deviation of each calibration applied to the MONTI23-II core is represented by the lateral lines on the right side and centred on the average values. Dashed black line: modern estimated mean annual temperature at Lago Grande di Monticchio (data from WorldClim 2.1, Fick and Hijmans, 2017).

to 7800 cal. BP, followed by (2) warmer conditions from 7800 to 2500 cal. BP, before (3) relatively stable conditions from 2500 cal. BP onward.

Similarly to temperatures, weight-averaged winter precipitation (Pwin) exhibits a similar trend to annual precipitation (red curves on Fig. 6d). Winter precipitation shows (1) relatively dry conditions from 12,800 to 10,800 cal. BP, followed by (2) wetter conditions from 10,800 cal. BP onward. The late Holocene gradual aridification trend observed for annual precipitation is less pronounced for winter precipitation. In contrast to annual and winter conditions, summer precipitation (Psum) shows a different trend, i.e., a progressive aridification throughout the Holocene, with a more pronounced aridification during the last 2500 cal. BP (Fig. 6f).

Overall, weight-averaged temperature seasonality is relatively constant throughout time (i.e., summer and winter gradual warming), while seasonality of rainfall is becoming more pronounced, with increasingly wet winters and increasingly dry summers (Fig. 7c).

3.5. Pollen- and brGDGT-based temperature correlation

The correlation analysis aimed to determine the relationships between pollen- and brGDGT-based temperature reconstructions using an estimation of Pearson's correlation coefficient *r*-value. Correlation coefficients of the smoothed averaged pollen and brGDGT-based signals (bold red curves on Figs. 7a, 7b) were calculated for key periods as the Younger Dryas (12,900–11,700 cal. BP), the Early Holocene (11,700–8200 cal. BP), the Mid-Holocene (8200–4200 cal. BP) and the Late Holocene (4200 cal. BP–modern times) periods (Fig. 7). For all four periods, the correlation analysis between pollen- and brGDGT-based reconstructions shows correlations with *r*-values ranging from −0.01 to 1.00. The Younger Dryas and Early Holocene periods have the highest positive correlation values (respective *r*-values of 1.00 and 0.92, *p*-value < 0.001). The Middle Holocene period is characterised by a negative near null *r*-value of −0.01 (*p*-value > 0.05), highlighting the non-correlation between the two proxies.

3.6. Fire activity inferred from charcoal analysis

The CHARnb values range between 0 and 12.90 #.cm^{-2}.year^{-1}. Based on the analysis of the CHARnb signal (Fig. 7d), three main phases were identified, reflecting contrasting dynamics in charcoal influx: (1) between 9000 and 7500 cal. BP, characterised by high charcoal influx values, mostly above 5 #.cm^{-2}.year^{-1}, indicating a high frequency of fire events and/or a high availability of combustible biomass. (2) between 7500 and 800 cal. BP, marked by a decrease in charcoal flux, with values approximately three times lower than those of the first phase. However, a notable peak is observed between 2780 and 2000 cal. BP, indicating a temporary resurgence of fire activity during this interval. (3) from 800 cal. BP onwards, characterised by a significant increase in charcoal influx values, again exceeding the 5 #.cm^{-2}.year^{-1} threshold, with values about five times higher than those in the previous period. Regarding variations in fuel types over time, the W/L ratio indicates a dominance of herbaceous fires during the Holocene. However, some peaks corresponding to burned tree occurs during several periods: 7000–6200, 2200–1200 and 600 cal. BP up to the present condition.

4. Discussion

4.1. BrGDGTs inferred mean annual temperature

4.1.1. Relevance of the selected brGDGTs calibrations

The brGDGTs compounds repartition obtained from the Monticchio sequence and lacustrine surface samples are consistent with both global soil and lake databases, with a dominance of pentamethylated brGDGTs and similar abundances of tetra- and hexamethylated brGDGTs (Fig. H.8). Previous studies have shown that brGDGT compounds behave differently in those two environments (i.e., lake and soil, Tierney and Russell, 2009; Dearing Crampton-Flood et al., 2020; Martínez-Sosa et al., 2021). This difference leads to a "cold bias" when reconstructing mean annual air temperature (MAAT) using a soil-based calibration on lake sediment (Tierney and Russell, 2009; Tyler et al., 2010; Russell et al., 2018). In addition, the MONTI23-II compounds brGDGT-IIIa and -IIa, involved in the calculation of the MBT'$_{5Me}$ index used for the MAAT reconstruction, have higher abundances than those found in the soil databases and correspond more closely to the lacustrine databases (Figs. 3a, H.8). Moreover, the application of the BIGMaC algorithm, developed by Martínez-Sosa et al. (2023), classified all MONTI23-II samples as *Lake-type*. The brGDGT compounds repartition and BIGMaC

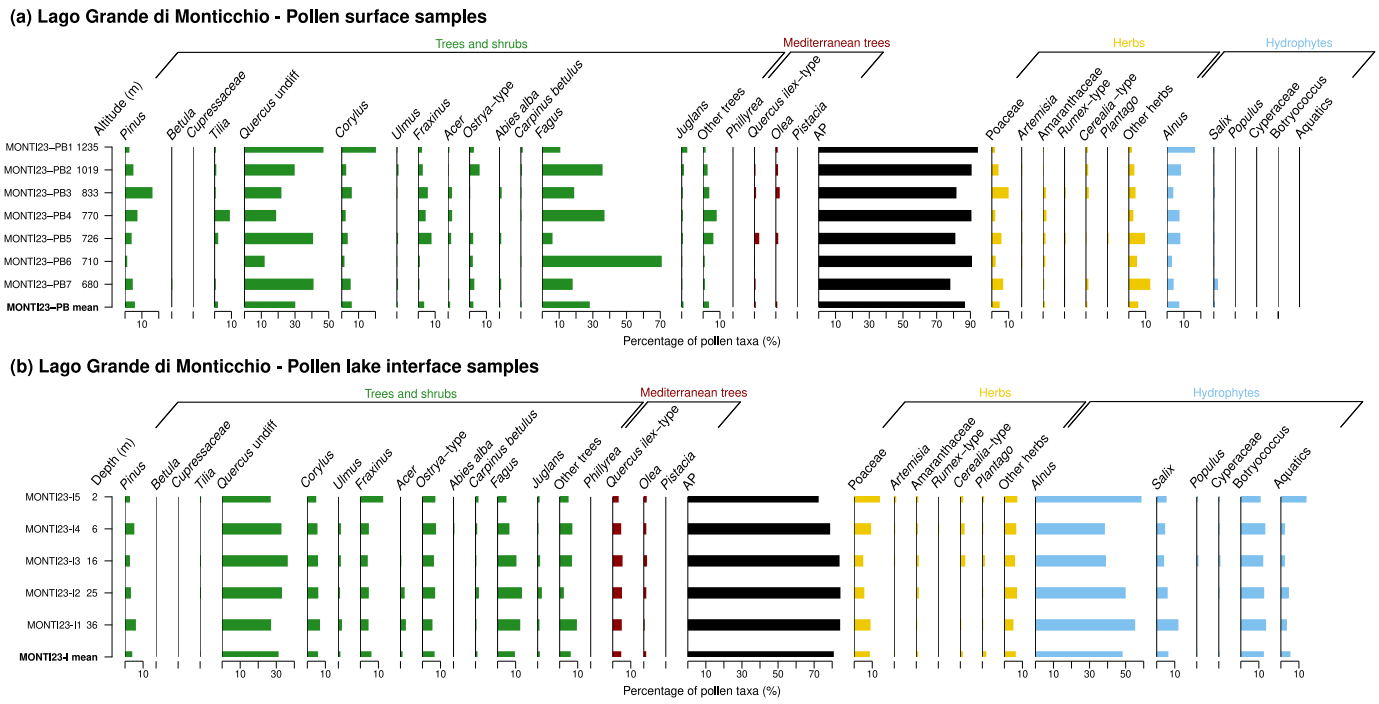

Fig. 5. Simplified pollen diagram of (a) the 7 surface samples (MONTI23-PB) and (c) 5 lake interface samples (MONTI23-I). Grouping selected tree and shrub taxa (green), Mediterranean tree taxa (red), herbaceous taxa (yellow), arboreal pollen (AP, black) and hydrophytes (blue). Percentages were calculated on pollen sums excluding spores, *Alnus*, *Salix*, *Populus* and Cyperaceae.

classification support the application of strictly lacustrine calibrations, as the brGDGT assemblage observed in the MONTI23-II sequence is consistent with the global lacustrine brGDGT assemblage and samples classified as *Lake-type* only.

Surface samples were collected from sediments at various depths (i.e., 36, 35, 16, 6, 2, and 1 m). Surface temperature reconstructions using different calibrations on samples MONTI23_I1-36, MONTI23_I2-25 and MONTI23_I3-16, taken from sediments at depths of 36, 25 and 16 m, respectively, show high variability from one sample and calibration to another, with temperature anomalies ranging from 0 to −6 °C (Fig. 3b). Conversely, samples MONTI23_I4-6, MONTI23_I5-2 and MONTI23_I6-1, taken at depths of 16, 2 and 1 m respectively, show more reliable variability with temperature anomalies ranging from 0.6 to −3 °C (Fig. 3b). There appears to be a difference in behaviour between the 'deep' samples (> 10 m) and the 'shallow' samples, with the former showing a colder bias. The different temperature reconstructions of the MONTI23-0 top core indicate temperature anomalies of −2 to −3 °C, which are closer to those observed for the 'shallow' samples, particularly MONTI23_I6-1, than to those of the 'deep' samples. MONTI23-II was sampled at a depth of 6 m. The good consistency between the different reconstructions of the 'shallow' surface samples and that of the MONTI23-0 top core, combined with the low anomaly values, highlights the reliability of the calibrations applied to MONTI23-II.

Now considering the calibrations individually, the MAAT_MBT'$_{5Me}$ and MAF_mr calibrations (brown and green dots and boxes respectively in Figs. 3b, 3c) have the greatest dispersion, particularly accentuated by the 'deep' samples. However, these two calibrations, based on MBT'$_{5Me}$ and multiregression, generally provide the best current reconstructions for the 'shallow' samples (average anomaly of −1 and −2 °C, respectively) and for MONTI23-0 (average anomaly around −2 °C). The MAF_Bayesian calibration (blue dots and boxes in Figs. 3b, 3c), has a slightly lower dispersion, but is associated with larger anomalies on 'shallow' samples (average anomaly of −3 °C) and on MONTI23-0 (−3 °C), making it generally less reliable than the MAAT_MBT'$_{5Me}$ and MAF_mr calibrations. Finally, the MAF_MBT'$_{5Me}$ calibration has the lowest dispersion of all calibrations (pink dots and box in Figs. 3b, 3c), across all surface samples. However, it is associated with larger anomalies than the MAAT_MBT'$_{5Me}$ and MAF_mr calibrations on 'shallow' samples (average anomaly of approximately −3 °C) and on MONTI23-0 (−2 °C). This allows us to conclude that the MAAT_MBT'$_{5Me}$ and MAF_mr calibrations are the most reliable of the four calibrations applied to MONTI23-II and that the Bayesian MAF calibration appears to be the least reliable.

4.1.2. Palaeoclimate interpretation

Several studies have highlighted the relationship linking environmental conditions (i.e., temperature and pH) and the structure of biomolecules synthesised by brGDGT producers (Weijers et al., 2007), resulting in the definition of the 5-methyl isomer-based methylation index (MBT'$_{5Me}$) and the 6-methyl isomer-based cyclisation index (CBT', De Jonge et al., 2014). In lacustrine environments, the MBT'$_{5Me}$ has been used to define calibrations to estimate the mean annual temperature (MAAT, Russell et al., 2018) and the month above freezing temperature (MAF, Martínez-Sosa et al., 2021; Raberg et al., 2021; Bauersachs et al., 2024), while the CBT' index has been used to reconstruct pH changes (Sanchi et al., 2015; Russell et al., 2018). Previous studies highlighted the effect of pH variation on brGDGT compounds involved in the MBT'$_{5Me}$ index, and therefore its impact on the reconstructed temperature derived from it (De Jonge et al., 2014; Martínez-Sosa and Tierney, 2019).

Here, the correlation matrix indicates no significant correlation between brGDGT-inferred pH and temperature reconstructions at Monticchio (Pearson r values < 0.2 in Fig. G.7). This suggests that for the Monticchio core, the pH variations throughout the Holocene were not linked to climatic changes and/or that the reconstructed temperatures were not impacted by changes in pH, supporting the reliability of our temperature reconstruction for the Holocene.

Moreover, studies demonstrated that the isomerisation of brGDGTs (IR_{6Me}; De Jonge et al., 2014), which can be related to multiple environmental factors such as pH, salinity, O_2 and sources, is related to

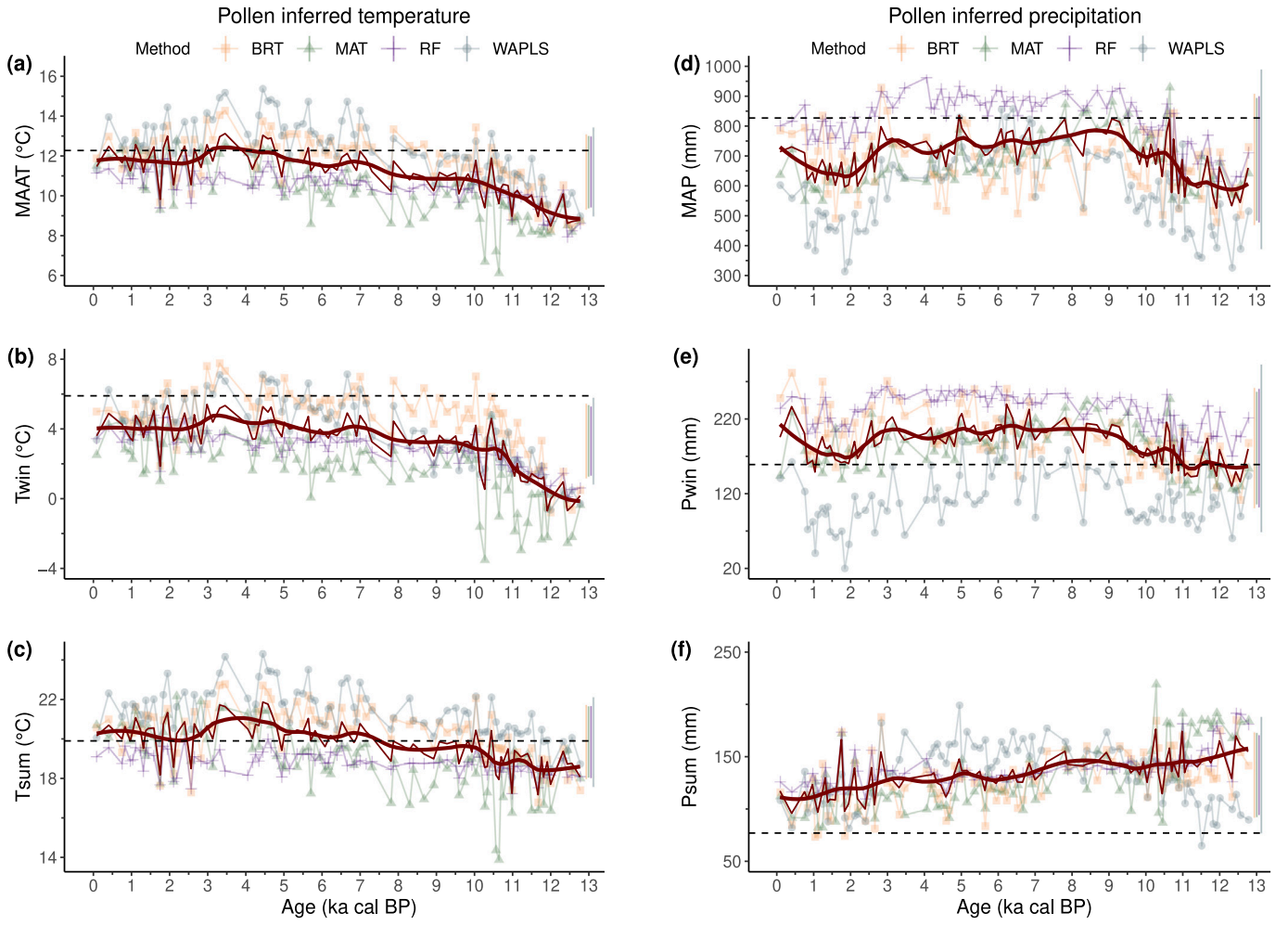

Fig. 6. Pollen inferred reconstruction of the mean (a) annual (MAAT, °C), (b) winter (Twin, °C), (c) summer (Tsum, °C) temperature and mean (d) annual (MAP, mm), (e) winter (Pwin, mm), (f) summer (Psum, mm) precipitation for the MAT (green lines and triangles), BRT (orange lines and triangles), WA-PLS (grey lines and circles) and RF (violet lines and crosses) methods. The red and the bold red curves correspond to the averaged and the smoothed averaged palaeoclimate signal for all climate parameters. Lateral lines on the right represent the method errors (RMSE), centred on the average climate values, found in Table 2. Dashed black lines: modern estimated climate values for MAAT, Tsum, Twin, MAP, Pwin and Psum at Lago Grande di Monticchio (data from WorldClim 2.1, Fick and Hijmans, 2017).

shifts in temperature (Weber et al., 2018; Wu et al., 2021; Bauersachs et al., 2024; Novak et al., 2025). Bauersachs et al. (2024) showed that for Central European lakes with IR_{6Me} values > 0.5, the MBT'_{5Me} frequently shows values too low compared to measured MAATs, and MBT'_{5Me}-reconstructed temperatures in these lakes deviate from measured MAATs by several degrees. They therefore proposed a cut-off value of 0.50 for the IR_{6Me}, after which MBT'_{5Me}-reconstructed MAATs from lacustrine archives should be regarded as unreliable. In their study, Novak et al. (2025) demonstrated that, for middle and high latitude lakes, restricting the data to samples with an IR_{6Me} value < 0.4 eliminates the non-thermal overprint on the fossil record. Previous studies showed that higher dissolved O_2 in lakes can lead to a lower isomerisation (Weber et al., 2018; Wu et al., 2021) and an increase in brGDGT concentrations (Martínez-Sosa and Tierney, 2019), highlighting possible non-thermal effects on brGDGTs composition.

At Monticchio, IR_{6Me} values are mostly under this cut-off value of 0.5; very few samples present IR_{6Me} values higher than that (Fig. F.6c). Overall, no high variations of MBT'_{5Me} values are associated with high IR_{6Me} values (> 0.5, Figs. F.6a, F.6c). Some of them (e.g., at 400, 1200 and 6400 cal. BP) correspond to abnormally high outlier values of CBT' values, but this is not the case for all of them (e.g., at 6900, 9100–9300 cal. BP), and it does not impact MBT'_{5Me} values (Figs. F.6a–F.6c). This suggest that, in accordance to Bauersachs et al. (2024), close to cut-off value of 0.5 can still yield reliable palaeotemperature reconstructions, but their interpretation must be made with caution. Similarly, while most of the IR_{6Me} values are higher than 0.4 at Monticchio, no significant variation in MBT'_{5Me} values is linked to exceeding the threshold value of 0.4 for IR_{6Me}. This supports the precedent observations and the overall reliability of MBT'_{5Me}-based palaeotemperature reconstructions at Monticchio, although caution is required when interpreting samples with high IR_{6Me} values (Bauersachs et al., 2024; Novak et al., 2025). In addition, IR_{6Me} and brGDGTs concentration ($\sum$[brGDGTs]) are not correlated (Fig. I.9), supporting the general absence of a non-thermal effect of isomerisation on brGDGT concentrations and abundances.

Oxic vs. anoxic conditions were suggested to bias brGDGT-inferred palaeotemperature reconstructions, notably by altering not only the MBT'_{5Me} temperature index, but also the fractional abundance of high-abundance compounds such as Ia, IIIa, and IIIa', indispensable to nearly all brGDGT temperature calibrations (Raberg et al., 2025). The isoGDGT-0 to crenarchaeol ratio serves as an indicator for the presence of archaeal methanogens (Blaga et al., 2009). Higher values of the isoGDGT-0/Cren ratio are likely associated with periods of reduced conditions characterised by low oxygen levels, which in turn favour the growth of archaeal methanogens.

Monticchio's high iso-GDGT0/Cren ratio points to mostly anoxic/reducing conditions. Variation of the iso-GDGT0/Cren ratio, however,

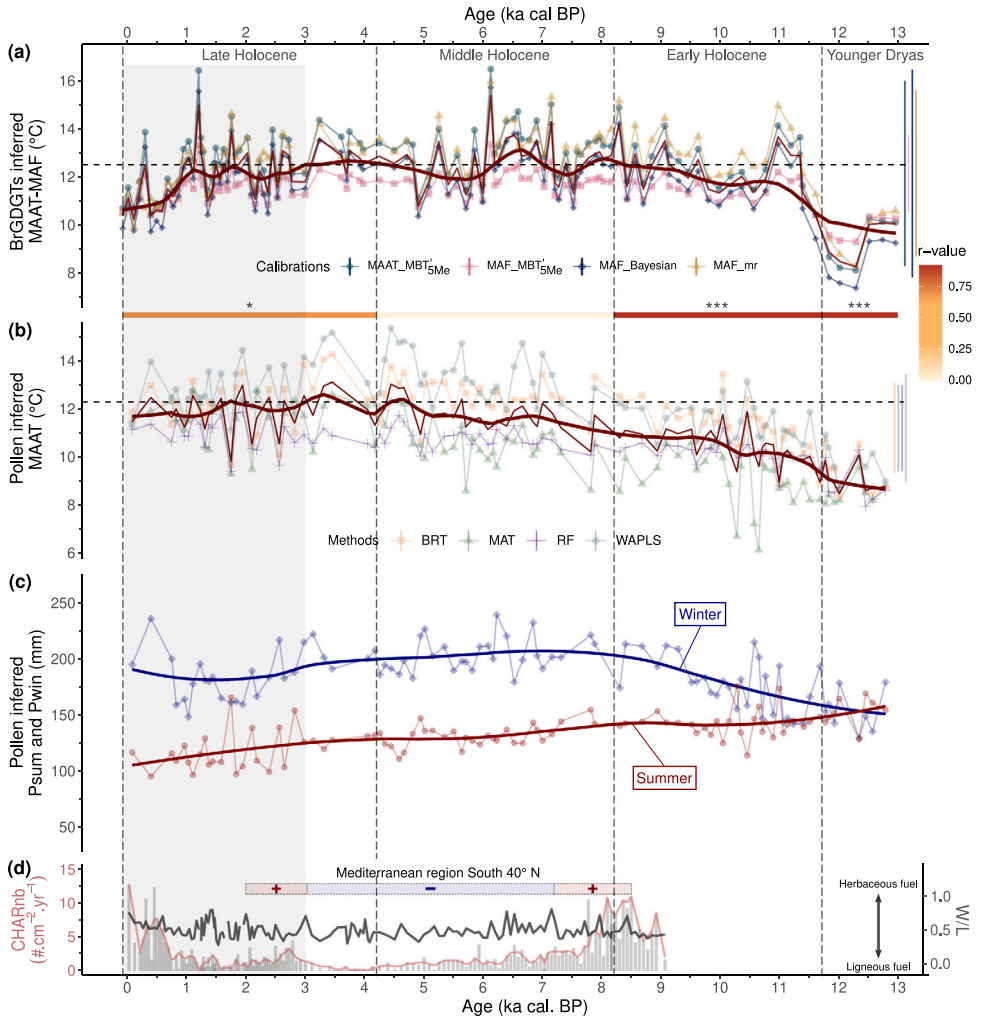

Fig. 7. (a) brGDGT-inferred Mean Annual Air Temperature (MAAT) and mean temperature of Months Above Freezing (MAF) reconstructions based on lacustrine calibrations of Russell et al. (2018, MAAT_MBT'$_{5Me}$), Bauersachs et al. (2024, MAF_MBT'$_{5Me}$), Martínez-Sosa et al. (2021, MAF_Bayesian) and Raberg et al. (2021, MAF_mr). (b) Pollen inferred mean annual temperature (MAAT) for the MAT (green lines and triangles), BRT (orange lines and triangles), WA-PLS (grey lines and circles) and RF (violet lines and crosses) methods. The red and the bold red curves correspond respectively to the calibrations-averaged and the smoothed calibrations-averaged palaeoclimate signal. Lateral lines on the right represent the calibration and method errors (RMSE) found in the Tables 1, 2. Estimation of Pearson's correlation coefficient (r) values for each time period, highlighted by the vertical dashed lines, is represented between panels (a) and (b). * block permutation p-value ≤ 0.05, ** block permutation p-value < 0.01, *** block permutation p-value < 0.001. (c) Pollen-inferred summer (Psum, red curve) and winter (Pwin, blue curve) precipitation (mm) at Lago Grande di Monticchio. (d) Charcoal-inferred CHARnb (#.cm^{-2}.yr^{-1}, number) and width/length ratio (W/L) for MONTI23-II. Fire activity of the Mediterranean region south of latitude 40°N, inferred from z-scores of transformed charcoal influx by Vannière et al. (2011), is represented by red (more activity) and blue (less activity) rectangles. Dashed horizontal black line: modern estimated mean annual temperature and seasonal (summer and winter) precipitation at Lago Grande di Monticchio (data from WorldClim 2.1, Fick and Hijmans, 2017).

does not coincide with high variation of MBT'$_{5Me}$ values (Figs. F.6a, F.6d). This suggest that, while anoxic/reducing conditions may impact the overall reliability of brGDGT-base palaeotemperature reconstruction (Harning et al., 2025; Raberg et al., 2025), in Lago Grande di Monticchio, the MBT'$_{5Me}$-based calibration can still be applied to quantitatively reconstruct palaeotemperatures.

4.2. Pollen-inferred annual and seasonal palaeoclimate

First studies focusing on palaeovegetation and palaeoclimate (Allen et al., 1999, 2002) aimed to reconstruct three bioclimate parameters (e.g., temperature of the coldest month, growing degree days over 5 °C and the ratio of potential evapotranspiration). In their study (pink curve in Fig. 8c), cold winter conditions are evidenced during the Younger Dryas (YD), followed by a warming trend during the early Holocene (EH), which culminates in close to modern winter temperatures during the Mid-Holocene (MH).

In our study, the winter temperature trend reconstructed from a multi-method approach (red curve in Fig. 8c) is consistent with those climate trends, depicting a winter warming throughout the Holocene. Overall, between our study and that of Allen et al. (2002), the winter temperature reconstructions are consistent and follow the increasing trend of winter insolation at those latitudes (black curves in Fig. 8a; Cruz-Silva et al., 2023; Liu et al., 2023; d'Oliveira et al., 2025). The pollen-based summer precipitation curve (red curve in Figs. 7c, 8h) indicates wetter conditions from the Younger Dryas onward, suggesting a shift towards drier summer conditions throughout the Holocene. In Mediterranean regions, summer rainfall can be related to fluctuating lake levels, as it reflects regional summer hydrological changes (Magny et al., 2007). The summer precipitation pattern at Monticchio would have caused lake levels to remain high from the Early to Mid-Holocene, followed by a decline after 6000 cal. BP, similar to the observations at Lago Preola in southern Italy (Fig. 8h; Magny et al., 2011). The

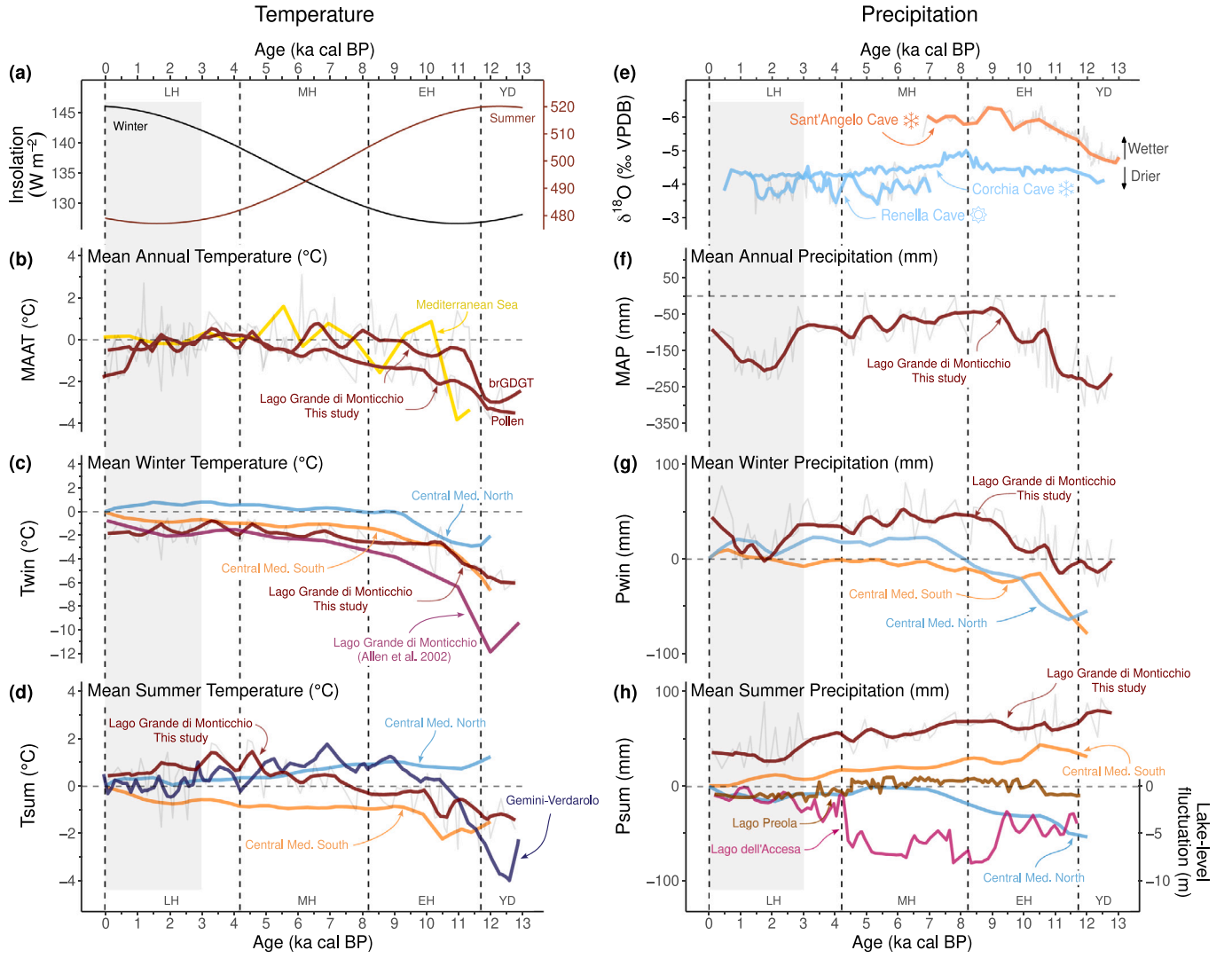

Fig. 8. Selected palaeoclimate records over the Holocene for Italy. (a) Summer (June, red curve) and winter (December, black curve) insolation for latitude 43°N (W m^{-2}, Laskar et al., 2004). (b) Mean annual temperature anomaly (MAAT, °C) at Lago Grande di Monticchio reconstructed from pollen and brGDGTs data (red curves, this study) and Southern Italian Sea surface temperature anomaly (SST) reconstructed from biomarker records (detailed in Table A.1). (c) Mean winter temperature anomaly (Twin, °C) reconstructed from pollen data for Northern and Southern Central Mediterranean (respectively light blue and orange curves, d'Oliveira et al., 2025) and for Lago Grande di Monticchio (red and pink curves for respectively this study and Allen et al., 2002). (d) Mean summer temperature anomaly (Tsum, °C) reconstructed from pollen data for Northern and Southern Central Mediterranean (respectively light blue and orange curves, d'Oliveira et al., 2025) and for Lago Grande di Monticchio (red curve, this study) and from chironomid data for Gemini-Verdarolo sites (northern Italy) (dark blue curve Samartin et al., 2017). (e) $\delta^{18}O$ (‰VPDB) measurement from speleothems data for Corchia Cave (Regattieri et al., 2014), Renella Cave (Drysdale et al., 2006) and Sant'Angelo cave (Columbu et al., 2022). (f) Mean annual precipitation anomaly (MAP, mm) at Lago Grande di Monticchio reconstructed from pollen data (red curve, this study). (g) Mean winter precipitation anomaly (Pwin, mm) reconstructed from pollen data for Northern and Southern Central Mediterranean (respectively light blue and orange curves, d'Oliveira et al., 2025) and for Lago Grande di Monticchio (red curve, this study). (h) Left: Mean summer precipitation anomaly (Psum, mm) reconstructed from pollen data for Northern and Southern Central Mediterranean (respectively light blue and orange curves, d'Oliveira et al., 2025) and for Lago Grande di Monticchio (red curve, this study). Right: Lake-level fluctuations at Lago dell'Accesa (expressed in absolute elevation in m a.s.l.) and at Lago Preola (interpreted from correspondence analysis scores; CA) from sedimentology analysis (respectively pink and brown curves, Magny et al., 2007, 2011). The period highlighted in grey corresponds to the period when the human impact was identified in the sedimentary record of Lago Grande di Monticchio.

fluctuations in summer precipitation and lake levels are further evidenced by the presence of *Alnus* (alder) around the lake. At Monticchio, *Alnus*, which is confined to the wetlands at the edge of the lake, appear as early as 10,000 cal. BP but was not present continuously or in high proportions (< 20 %) and disappears around 8000 cal. BP before reappearing in high proportions (> 60 %) around 7000 cal. BP (Fig. 5a). In their early study, Allen et al. (2002) proposed several reasons for the sudden disappearance of alder around 8000 cal. BP and its subsequent return around 7000 cal. BP. One explanation was that increased precipitation could submerge the *Alnus* fringe, drowning the trees. Conversely, prolonged drought could lower the lake level to a point where the trees could no longer survive due to drought. Contrary to what is proposed by Allen et al. (2002) to explain *Alnus* presence evolution around the lake edges, our findings reveal that the sudden re-emergence of *Alnus* around 7000 cal. BP followed a period of gradual summer aridification that resulted in lower summer precipitation levels. These low summer rainfalls likely led to declines in lake levels (Magny et al., 2011, 2012), thus enabling the growth of *Alnus* in the humid areas near the lake due to an expansion of the potential zone for *Alnus* occupation.

Overall, the temperature and precipitation signals of Lago Grande di Monticchio (red curves in Fig. 8) can be linked to the palaeoclimatic signals from the southern Italian regions, i.e., progressive warming and aridification of summer conditions, and warming and humidification of winter conditions. This pattern translates to an enhanced precipitation seasonality during the Holocene (Figs. 7c, 8g, 8h). This well-known "Mediterraneanization" process surrounding the Mediterranean Sea has been highlighted by previous studies (Roberts et al., 2011; Sadori et al., 2011; Joannin et al., 2014; Finné et al., 2019; d'Oliveira et al., 2025) during the Mid- and Late Holocene.

4.3. A multi-proxy temperature reconstruction from the Lago Grande di Monticchio record

One of the aims of our multi-proxy study is to reconstruct and better understand the climatic variability in the zone between 40–43°N in Italy. The location of the Lago Grande di Monticchio, in this transitional region, makes the study of its sedimentary record particularly important. The comparison of two independent climate proxies, namely pollen and brGDGTs, enabled us to verify the robustness of the temperature reconstructions for the Holocene and the end of the Lateglacial. The temperature trends reconstructed from both proxies show similar trends, highlighted by relatively good positive correlation coefficient values (Pearson r-value ≥ 0.60) between 13,000 and 8200 cal. BP (Figs. 7a, 7b).

During the Younger Dryas period (12,900–11,700 cal. BP), cold conditions are evidenced, followed by a warming during the Early Holocene (11,700–8200 cal. BP). The Mid-Holocene (8200–4200 cal. BP) corresponds to the period with the least correlation (Pearson r-value close to zero). During this period, a mid-Holocene thermal maximum (HTM) is recorded by brGDGTs data (Fig. 7a), similar to what is observed in the sea surface temperature of the southern Italian Mediterranean Sea (yellow curve in Fig. 8b, extracted from the study of Marriner et al., 2022), while no HTM is present in pollen data during this period; temperatures are characterised by continuous warming (Fig. 7b). Finally, the Late Holocene period (4200 cal. BP to modern times) is characterised by a thermal maximum around 3500 cal. BP with pollen data, followed by similar cooling trends between the two proxies. The positive correlation (Pearson r-value of 0.7) during the Late Holocene supports a reliable temperature reconstruction during this period.

4.4. Anthropogenic activity and fire history at Lago Grande di Monticchio

Addressing the influence of human impact on vegetation is crucial when using pollen data to reconstruct past climates of recent periods, such as the Late Holocene. Numerous studies have indicated that human activities, such as land clearing for agriculture, can result in an inflated representation of non-arboreal pollen and fire activity (Vannière et al., 2008, 2011). Pastoralism activities and, more generally, an increase in herbivory pressure (including wild herbivory impact) have an impact on the vegetation structure, favouring herbaceous and shrubby vegetation community (Biancari et al., 2024). Inflated representation of non-arboreal pollen can lead to skewed palaeoclimate reconstructions, where shifts in vegetation do not accurately reflect climatic changes (Birks et al., 2010; Mauri et al., 2015). In the central Mediterranean region and in Italy, studies revealed that before 4000 cal. BP, climatic variations were the primary drivers of vegetation changes (Sadori et al., 2011) and fire activity (Vannière et al., 2008, 2011). However, after this period, it appeared that both human activities and climatic changes contributed to the observed changes in vegetation and the increase in fire activity (Sadori et al., 2011; Vannière et al., 2011).

At Lago Grande di Monticchio, charcoal analysis indicates a phase of intense fire activity between 9000 and 7500 cal. BP (Fig. 7d). This phase is associated with increasing forested fuel (Fig. 7d). This trend is also evident in other records from the Central Mediterranean regions located south of 40°N (blue and red rectangle in Fig. 7d; Vannière et al., 2011) and in Sardinia (Beffa et al., 2016; Pedrotta et al., 2021). According to Vannière et al. (2011), who investigated the fire regime in this area, the charcoal records from the central Mediterranean (between 40–45°N) indicate an increase in fire occurrences between 8000 and 4000 cal. BP, much later than observed in Monticchio. In contrast, sites in the southern regions (south 40°N), such as Gorgo Basso, Lago di Pergusa, and Biviere di Gela, show a decrease in fire activity from 7000 to around 4000 cal. BP, often linked to wetter than present summer conditions. These distinctive patterns may be influenced by the interactions between the Central Mediterranean, North Atlantic atmospheric and oceanic cells, and low-latitude monsoon areas (Broccoli et al., 2006; Roberts et al., 2011; Vannière et al., 2011; Brogli et al., 2019). Additionally, shifts in orbital parameters, including summer insolation, might have indirectly caused abrupt changes in fire activity by affecting rainfall distribution and intensity, temperature, and seasonal variations. A clear seasonal pattern, characterised by dry summers and wet winters, would likely promote fire activity (Vannière et al., 2008; Beffa et al., 2016; Pedrotta et al., 2021). Looking at fuel type, the fires recorded at Lago Grande di Monticchio appear to involve a mixture of herbaceous and woody biomass, as suggested by relatively high W/L values (W/L ratio < 0.5, Fig. 7d). Pollen data, however, indicate high proportions of tree pollen throughout the Holocene (> 80 %, Fig. C.1). Such discrepancies could be explained if fires mainly affected the herbaceous layer rather than the surrounding forested areas close to the lake. In this case, elongated charcoal particles would primarily reflect the burning of herbaceous fuels, whereas more compact particles would be related to woody biomass (Umbanhowar and Mcgrath, 1998; Enache and Cumming, 2007; Mustaphi and Pisaric, 2014). Consequently, the charcoal record would mainly reflect local fire activity, while the pollen record would integrate a broader, regional signal of vegetation composition, as commonly observed in palaeoecological studies (Vannière et al., 2003; Leys et al., 2014; Lestienne et al., 2020). In addition, the interpretation of the W/L ratio may be limited during periods of low charcoal abundance, reducing its reliability between ca. 7500 and 1500 cal. BP (Aleman et al., 2013).

During the Late Holocene, the human impact increased. In south–eastern Italy, human settlements are recorded as early as 8000 cal. BP (Guilaine et al., 2019; Manen et al., 2019). At Lago Grande di Monticchio, *Cerealia*-type and *Plantago lanceolata*-type are recorded around this period (Fig. 5). The presence of these taxa is consistent with human presence in the region during the Middle Holocene, but their impact on the vegetation is not evidenced in the pollen assemblages. However, the effect of human activity increases, from 3000 cal. BP onwards, with the appearance of more regular percentages of *Cerealia*-type and higher percentages of *Olea* and *Juglans*, suggesting that cultivation was becoming more common. Human impact is also recorded by a strong increase in fire activity from 3000 cal. BP onward. From other Italian charcoal records, Vannière et al. (2008) evidenced that a combination of drier climate conditions and human actions contributed to increased fires from 4000 cal. BP onward. They suggested that the increase in human population during the Bronze Age (4300–3000 cal. BP) and the more intensive land-use affected fire activity. At Lago Grande di Monticchio, significant human settlement began in the 10th century BC (about 1000 years ago) with the construction of the Benedictine abbey of San'Ippolito (Allen et al., 2002). This is reflected in our results by a clear rise in fire activity at that time (Fig. 7d).

Those observations suggest that, while climate must have been a driver of vegetation dynamics from 3000 cal. BP onward, human influence must also be considered. The absence of a clear relationship between fire and vegetation until 3000 cal. BP supports the reliability of our palaeoclimatic reconstructions based on pollen data, as the vegetation recorded at Lago Grande di Monticchio appears to be independent of fire activity from the Younger Dryas to the Late Holocene. Therefore, it is important to be cautious when interpreting the results of the pollen-based climate reconstructions from 3000 cal. BP to the modern period (grey period on Figs. 7 and 8).

4.5. The north–south pattern of seasonal temperature and precipitation in the Italian peninsula

Over the past decade, several studies have highlighted a north-south climate divide in the central Mediterranean throughout the Holocene, separating the northern and southern climate regions. The latitudinal boundary remains uncertain and is thought to lie between latitudes 40 and 43°N, creating a climate transition zone (Magny et al., 2012; Peyron et al., 2011; Magny et al., 2013; Peyron et al., 2013; Di Rita et al., 2018a; Robles et al., 2023; d'Oliveira et al., 2025). Within this framework, the location of Lago Grande di Monticchio (~ 41°N) presents a valuable opportunity to refine the latitudinal boundary location (Fig. 9). Our quantitative palaeoclimate reconstructions highlighted the absence of an HTM and the presence of a "Mediterraneanization" process taking place during the mid-Holocene, i.e., wet (dry) summer (winter) conditions during the Younger Dryas and Early Holocene, followed by drier (wetter) summer (winter) conditions during the Middle and Late Holocene.

Previous studies showed that southern regions (below 40°N) are characterised by a marked "Mediterraneanization" process during the Holocene (Roberts et al., 2011; Di Rita et al., 2018a; d'Oliveira et al., 2025) and the absence of a summer and/or annual HTM (d'Oliveira et al., 2025). Our quantitative palaeoclimate reconstructions of Lago Grande di Monticchio (red curves on Fig. 8) show good consistency with the climate of southern regions. Summer aridification is also reflected by the lake-level fluctuations of the Sicilian site Lago Preola (Magny et al., 2007, 2011, brown curve Fig. 8h), with the presence of high lake-level between 11,500–4500 cal. BP, followed by a marked decrease between 4500 and 3400 cal. BP. A similar pattern is illustrated by the decreasing water depth level of Lago Trifoglietti between 9000–4000 cal. BP (Joannin et al., 2012). Wet winter conditions at the onset of the Holocene (11,700 cal. BP) are also observed in the winter precipitation signal at Sant'Angelo cave (Figs. 8e, 9b), inferred by oxygen stable isotope ($\delta^{18}O$; Columbu et al., 2022). In addition, Mediterranean vegetation at Monticchio, with the presence of *Quercus ilex*-type, *Phillyrea* around 7000 cal. BP and later of *Olea* and *Pistacia* (Fig. C.1), is also consistent with the records of Lago Alimini Piccolo (~ 40°N, Di Rita and Magri, 2009) and Lago di Battaglia (~ 41°N, Caroli and Caldara, 2007). Those two records present the establishment of a similar vegetation around 6000 cal. BP and an increasing aridification trend from 4200 cal. BP onwards. This suggests that the lower latitudinal limit of the transition zone should be located above not only 40°N but also 41°N (Fig. 9). Lago Grande di Monticchio record allows us to propose a new lower latitudinal boundary, above 41°N, that restricts the climatic transition zone between 41 and 43°N rather than between 40 and 43°N.

While Lago Grande di Monticchio has allowed us to specify the lower latitudinal limit of the climatic transition zone (now above 41°N, Fig. 9), uncertainties remain regarding the upper latitudinal boundary, currently proposed to be around 43°N. Northern regions (above 43°N) are climatically defined by wetter summer and winter conditions throughout the Holocene and the presence of a summer and/or annual HTM (Roberts et al., 2011; Di Rita et al., 2018a; d'Oliveira et al., 2025, Fig. 9). In the Alps and northern Apennines, pollen, chironomid, lake-level and speleothem records illustrate this pattern (Figs. 8, 9). Pollen data highlighted wetter summer and winter conditions during the early-to-mid Holocene (Figs. 9c, 9d) as well as the presence of a summer HTM, also present with chironomid data at Gemini-Verdarolo lakes (Fig. 8d; Samartin et al., 2017). Further south, close to the upper boundary of the latitudinal boundary (~ 43°N), lake-level data at Lago dell'Accesa indicate dry conditions from 12,000 to 4200 cal. BP with low lake-level values, while pollen data from d'Oliveira et al. (2025) suggest rather humid conditions during this period (Fig. 8h). In addition, d'Oliveira et al. (2025) highlighted that the most significant climatic contrast arises for the summer season between Lago dell'Accesa (~ 42°N) and Lago del Greppo (~ 44°N). These inconsistencies point to underlying complexities and factors affecting the climatic dynamics at the higher latitudes of the transition zone (~ 43°N).

Among those factors, the type of proxy used to reconstruct the palaeoclimate is of great importance. Indeed, the multi-proxy approach permits overcoming the biases inherent in proxies, but certain characteristics specific to proxies must be taken into account. One of them concerns the consistency of comparisons of reconstructed climate parameters, meaning that from one proxy to another, the reconstructed parameter may not always be the same. This is the case for the changes in $\delta^{18}O$ isotopic values from speleothems. In the studies of Drysdale et al. (2006), Regattieri et al. (2014), and Columbu et al. (2022), those variations are interpreted as an indirect measure of winter (i.e., Corchia Cave and Sant'Angelo Cave) or summer precipitation (i.e., Renella Cave). Those indirect measurements of seasonal precipitation may not fully align with winter and summer pollen-based precipitation parameters, which can result in climatic contrasts related to the type of proxy rather than to different atmospheric dynamics. Moreover, studies suggest that the latitudinal boundary varied through time and space in the Mediterranean region (Vannière et al., 2011; Magny et al., 2013; Robles et al., 2023; d'Oliveira et al., 2025). As such, it may also be possible that the transition zone between northern and southern climate regions was a diffuse rather than a clear and distinct boundary, resulting in a latitudinal climate gradient that may have slightly moved through time and space. Further multi-proxy investigations in northern latitudes, closer to the upper latitudinal boundary (~ 43°N), are needed to obtain a more complete picture of Holocene climate variability in the Italian Peninsula.

Finally, the reconstructed palaeoclimate dynamics may be impacted by the combination of records at different elevations. The intricate topography of Italy and its central location within the Mediterranean region result in diverse precipitation patterns influenced by various meteorological processes (Silvestri et al., 2022). Indeed, the climate of the Mediterranean basin is strongly influenced by its orography and land-sea distribution, since these factors partly shape the expression of the regional climate and its teleconnections with global mechanisms (Lionello et al., 2006). It therefore seems necessary to gain a better understanding of the climatic mechanisms affecting the Mediterranean Basin and their evolution and connections during the Holocene. The final part of the discussion attempts to provide a framework for these mechanisms, their functioning, their interactions and their evolution during the Holocene.

4.6. Mediterranean climate forcing mechanisms

Studies proposed that the Holocene climate of the Mediterranean region was shaped by the complex interplay of several global forcing mechanisms, resulting in distinct temporal variability and pronounced spatial heterogeneity (Roberts et al., 2011; Fletcher et al., 2013; Magny et al., 2013; Zanchetta et al., 2016; Ayache et al., 2018; Di Rita et al., 2018a; Columbu et al., 2022; Lionello et al., 2024). These mechanisms included (1) changes in tropical system dynamics, often modulated by orbital and solar forcing, (2) oceanic circulation, and (3) atmospheric oscillations in the high northern latitudes (Roberts et al., 2011; Magny et al., 2013; Zanchetta et al., 2016; Di Rita et al., 2018a; Columbu et al., 2022).

Millennial climate variability during the Holocene is mainly influenced by orbital forcing (i.e., obliquity, precession and eccentricity), whose variations cause significant redistributions of energy, both seasonally and latitudinally (Bradley, 2003). On a large-scale, shifts in Hadley Cell circulation can be directed by changes in the temperature gradient between polar and equatorial regions, themselves resulting from differential radiation anomalies (Bradley, 2003). The Hadley circulation (HC) is a vital global atmospheric system that moves moisture from the tropics to the subtropics, impacting the regional hydrological cycle. It consists of two cells in each hemisphere, with an ascending

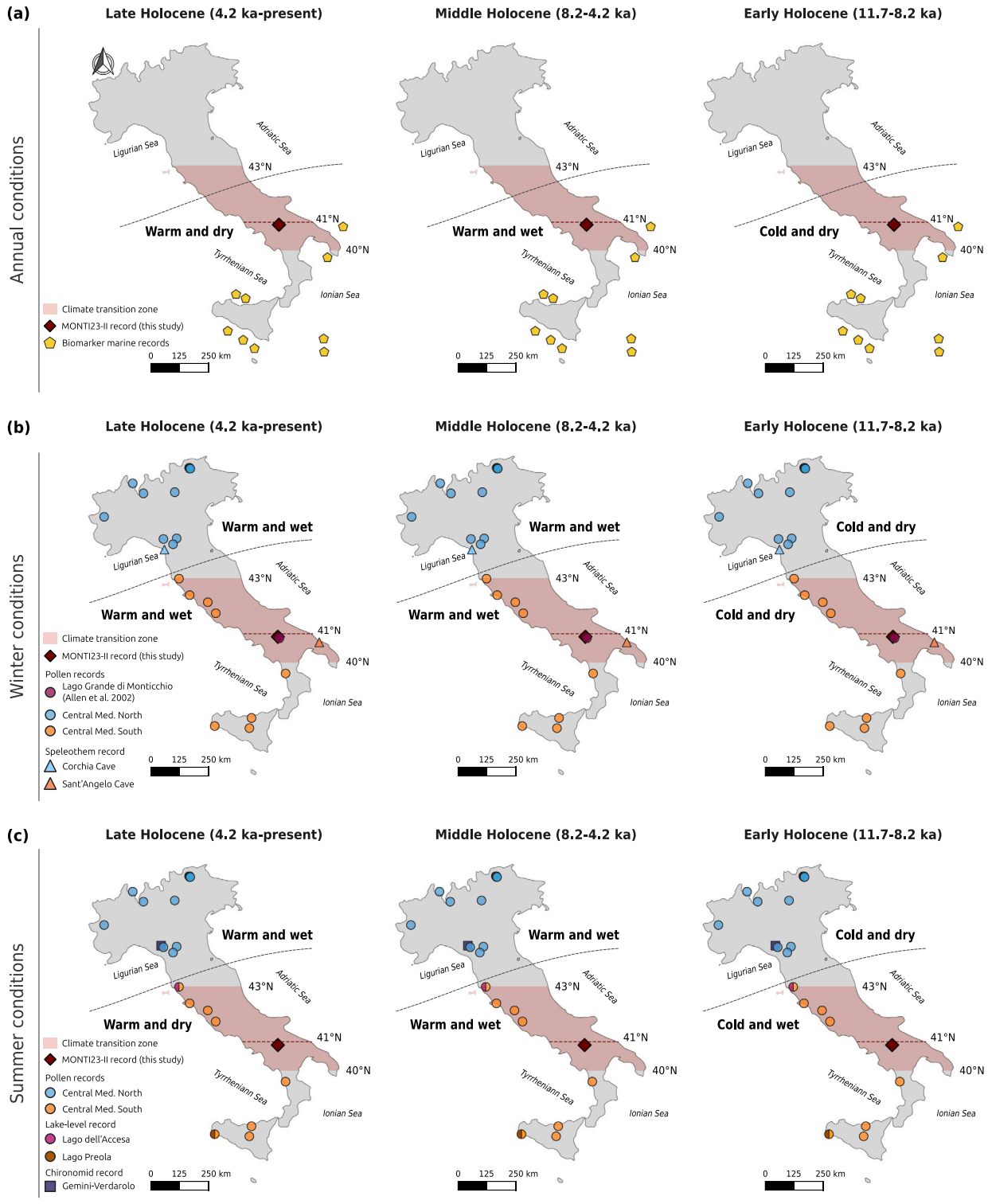

Fig. 9. Selected palaeoclimate records over the Holocene for Italy. (a) Annual, (b) winter and (c) summer conditions, with the location of Lago Grande di Monticchio (MONTI23-II, red diamond and study of Allen et al., 2002, pink dot), pollen records of southern (orange dots) and northern (blue dots) Central Mediterranean regions (d'Oliveira et al., 2025), speleothems (light blue and orange triangle; Drysdale et al., 2006; Regattieri et al., 2014; Columbu et al., 2022), chironomids (dark blue rectangle; Samartin et al., 2017), lake-level (pink and brown dots; Magny et al., 2007, 2011), and marine biomarkers records (dark yellow pentagons, Table A.1; Emeis et al., 2000; Cacho et al., 2001; Doose, 2001; Emeis and Dawson, 2003; Giunta and Emeis, 2006; Versteegh et al., 2007; Incarbona et al., 2016). The red band correspond to the hypothesised location of the climate transitional zone.

branch at the Intertropical Convergence Zone (ITCZ) and descending branches in the subtropics (Lionello et al., 2024). The HC determines summer dryness in the Mediterranean, as its descending limb moves northward from the Sahara to encompass the southern Mediterranean region (Egypt and southern Levant; Roberts et al., 2011). Summer aridity is tightly linked to the HC's summer extension and strength in the southern limits of the Mediterranean basin (Lionello et al., 2006; Desprat et al., 2013). The ITCZ is a narrow equatorial band of intense convective activity whose position and strength regulate the global water cycle and are intrinsically connected to the HC (Yuan et al., 2023; Bian et al., 2025). The decrease of the Northern Hemisphere solar insolation throughout the Holocene lead to a general cooling, a southern shift of the ITCZ and a weakened summer monsoon system (Wanner et al., 2011). During the early-to-mid Holocene period, a strong insolation seasonality favoured a northward shift of the boreal summer ITCZ (Menviel et al., 2021; Bian et al., 2025), which brought enhanced summer rainfall to tropical north Africa, corresponding to the African Humid Period (AHP). During the mid-Holocene (~ 6000 cal. BP), the Northern Hemisphere insolation seasonality progressively decreased, reducing the cross-equatorial circulations. This led to a gradual but continuous southward shift of the ITCZ (Haug et al., 2001; Braconnot et al., 2007), a summer cooling trend and a weakening summer monsoon system (Wanner et al., 2008, 2011). The weakening of the summer monsoon system has gradually increased aridity in subtropical Africa and Asia (Roberts et al., 2011), leading to a time-transgressive termination of the AHP, as early as 5500 cal. BP in the north-eastern regions of the African continent, and later (~ 2500 cal. BP) at lower latitudes (Shanahan et al., 2015; Lézine et al., 2017; Dallmeyer et al., 2020).

Although it is unlikely that the summer monsoon had a direct influence on the northern Mediterranean coast during the Holocene, links between the position of the ITCZ and the Mediterranean summer anticyclonic system have already been proposed to explain the hydrological variability of central Italy at the beginning of the last glacial period (115.0–92.3 ka; Regattieri et al., 2015). Regattieri et al. (2015) suggested that the northward shift of the ITCZ during this period may have strengthened and displaced the summer high-pressure system northward, amplifying summer aridity and winter wetness due to the persistence of high Mediterranean Sea temperatures along the Apennines ridge. This hypothesis, linking the position of the ITCZ and seasonal precipitation (i.e., northward shift of the ITCZ amplifying summer aridification and winter wetness) in the Central Mediterranean during the Holocene, remains to be verified. At Lago Grande di Monticchio, during the early and middle Holocene, as the ITCZ shifted northward, our reconstructions suggest relatively wet but drying summer conditions. At the same time, winter precipitation reached its maximum (Figs. 8g, 8h), supporting the hypothesis stated above. In this sense, the southward shift of the ITCZ around 5500 cal. BP should lead to wetter summers and drier winters. At Monticchio, from 5500 cal. BP onwards, summer aridification is still present but slowed down, and winter conditions are less wet (Figs. 8g, 8h). This pattern is observed until 3000 cal. BP, when summer aridification resumes and appears to impact winter conditions. 3000 cal. BP marks the appearance of anthropogenic pollen markers at Monticchio (*Ceralia*-type, *Plantago lanceolata*-type, *Olea*, and *Juglans*), highlighting human influence on the vegetation (Fig. C.1). The latest climate patterns derived from pollen data from Monticchio from 3000 cal. BP onwards should therefore be interpreted with caution. Considering this, the link between the position of the ITCZ and the evolution of seasonal precipitation patterns in Monticchio during the Holocene seems to be coherent with our palaeoclimatic reconstructions, at least up to 3000 cal. BP. This suggests that the position of the ITCZ and the strength of the HC may have had an impact on the climate of southern Italy, but other mechanisms may also have been at work. A better understanding of the influence of these overlaps and their spatial extent could shed light on the possible mechanisms.

The Atlantic Meridional Overturning Circulation (AMOC) serves as a critical oceanic forcing mechanism, playing a key role in the global climate system through its heat and freshwater transports, which help maintain a relatively warm north-western European climate (Ayache et al., 2018). The AMOC's surface limb moves warm, salty waters towards the high latitudes of the North Atlantic, where they cool and sink. Studies have evidenced centennial- to millennial-scale variations in the AMOC during the Holocene, switching between strong and weak states (Thornalley et al., 2011), directly impacting western European climate. Changes in AMOC intensity are partly caused by atmospheric factors, in particular the North Atlantic Oscillation (NAO) (Li et al., 2013; Sun et al., 2015; Wang et al., 2017; Xu et al., 2019). NAO variations are hypothesised to influence the AMOC by modifying air–sea fluxes. The NAO operates via a spatial dipole with pressure centres near the Azores and Iceland, and modulates the strength and direction of the westerly winds belt (Hurrell, 1995; López-Moreno et al., 2011; Ait Brahim et al., 2019). Positive (negative) phase results in the reinforcement (weakening) and displacement to the north (south) of the pressure centres, directly affecting precipitation patterns across the Mediterranean region by creating dry (wet) conditions in northern and central Mediterranean borderlands (Southern France, Iberian Peninsula, North Africa) and wet (dry) conditions in southern ones (Middle East) (Wanner et al., 2008). While the NAO is often noted for its short-term variability, observations indicate that it also displays annual and longer-term variations in addition to its sub-seasonal fluctuations (Olsen et al., 2012; Wang et al., 2017). A positive NAO (NAO+) strengthens the AMOC by extracting heat from the subpolar gyre and increasing deep-water formation (Delworth and Zeng, 2016). In contrast, a negative NAO (NAO-) will lead to reduced westerly winds over the North Atlantic, less heat extraction, reduced deep-water formation, and a subsequent weakening of the AMOC. A weakened AMOC reduces the northward transport of warm water, contributing to regional cooling and decreased (increased) summer precipitation in northern (southern) Europe, often associated with a summer NAO-signal (Jackson et al., 2015; Li and Liu, 2025). Holocene AMOC fluctuations have been suggested to control the presence of a North Atlantic dipole similar to the NAO (Schulz et al., 2007; Fletcher et al., 2013; Smith et al., 2016).

During the Holocene, the NAO was suggested as the dominant atmospheric driver of the hydro-climate variability over the Mediterranean Basin (Magny et al., 2013; Delworth and Zeng, 2016; Zanchetta et al., 2016; Di Rita et al., 2018a; Columbu et al., 2022). Predominantly negative NAO conditions (NAO-) during the Early and Late Holocene were associated with a southern shift of the westerly wind belt, increasing winter precipitation in northern Morocco (Ait Brahim et al., 2019) and northern Italy (Corchia Cave, Fig. 8e; Regattieri et al., 2014), high lake-level in central-northern Italy (summer precipitation; Magny et al., 2007) and glacier advancements in the Apennines (winter precipitation; Giraudi et al., 2011). Conversely, more positive NAO conditions (NAO+) dominated during the Mid-Holocene, which initiated a lake-level minimum in central-northern Italy (Lago dell'Accesa, Fig. 8h; Magny et al., 2013) and a maximum in southern Italy (Lago Preola, Fig. 8h). At Monticchio, winter precipitation also seems to be influenced by the NAO, as similar trends are present throughout the Holocene (i.e., relatively dry winter conditions during the Early and Late Holocene and wetter ones during the Mid-Holocene). Throughout the Holocene, the AMOC likely underwent an initial enhancement, followed by a general weakening trend from approximately 6000–7000 cal. BP to 2000 cal. BP (Ayache et al., 2018). A progressive weakening of the AMOC during the mid-Holocene is not in accordance with our summer precipitation reconstruction at Lago Grande di Monticchio (Fig. 8h), which shows a gradual summer aridification throughout time instead of a dry early-to-mid Holocene followed by wetter summer conditions. However, this pattern is present at higher latitudes, at north 43°N central Mediterranean (orange curve in Fig. 8h). This may suggest that the influence of the AMOC intensity on southern Europe stops or

decreases significantly at the climate transition zone around 40–43°N and that other climate forcing takes over for regions further south.

The Mediterranean region exhibits distinct temporal periodicities and is a major climate transition, with palaeohydrological changes occurring in response to a combination of orbital, ice-sheet, and solar forcing factors (Magny et al., 2013; Di Rita et al., 2018a; Columbu et al., 2022) and an intricate, spatially reorganised ocean-atmospheric teleconnection between monsoon systems and summer weather conditions (Regattieri et al., 2015; Finné et al., 2019). Speleothems (Drysdale et al., 2006; Regattieri et al., 2015; Zanchetta et al., 2016; Columbu et al., 2022) and lake-level fluctuations (Magny et al., 2007, 2011, 2013) in Italy reveal contrasting hydrological responses across the region, influenced by complex interactions among these climate systems and atmospheric circulation. In an earlier study, Roberts et al. (2011) proposed that the rainfall changes were often patchy in their distribution across the Mediterranean basin, especially in the western Mediterranean region. The existence of clearly opposing hydrological trends between the south-western Mediterranean (wet periods) and the central-southern Mediterranean (dry periods, e.g., the Gaeta archives; Di Rita et al., 2018b) suggests that complex atmospheric circulation patterns were at work. These potentially involved the NAO and the dynamics of the North African anticyclone (Di Rita et al., 2018a), the latter being partly influenced by large-scale circulations (position of the ITCZ and the descending branch of HC; Chen, 2005; Djebbar et al., 2020). This complexity aligns with the "Mediterraneanization" process after 8000 cal. BP, where the region evolved towards characteristically wet winters and dry summers (Sadori et al., 2011; Vannière et al., 2011; d'Oliveira et al., 2025), which is also observed at Lago Grande di Monticchio (Fig. 8h).

The complex interaction between several global forcing mechanisms highlights the sensitivity of the Mediterranean climate to changes at different geographical and temporal scales. Beyond the complex ocean-atmospheric teleconnection, the contrasted north-south climate pattern is likely to be also related to the intricate land-sea geography, local topography of the Mediterranean basin (Roberts et al., 2011; Finné et al., 2019). The actual cause of this north-south climate contrast on the Italian peninsula remains unclear, although several hypotheses have been put forward. A better understanding of global forcing mechanisms on a regional scale, particularly in a region with complex topography and surrounded by sea (the Italian peninsula), could help to refine the climate mechanisms involved in this north-south division during the Holocene.

5. Conclusion

In this study, we aimed to quantitatively reconstruct the climate evolution of the latitudinal band between 40° and 43°N in Italy during the Holocene using a new sedimentary record from Lago Grande di Monticchio. The reliability of our palaeoclimate reconstruction was assessed using two independent proxies, i.e., pollen and brGDGTs, on which a multi-method and multi-calibration approach was applied to reconstruct mean annual temperature. Pollen data were also used to reconstruct seasonal (summer, winter) temperatures and precipitation to better investigate the north–south pattern previously evidenced by lake levels and other proxies.

Our results enabled us to verify the robustness of the temperature reconstructions for the Holocene and the end of the Late Glacial, with similar annual temperature patterns between pollen- and brGDGT-based signals. First, cold conditions were present during the Younger Dryas, followed by a warming during the Early Holocene. The Mid-Holocene period showed less coherence, with an early mid-Holocene thermal maximum (HTM) with brGDGTs data and a later one, during the mid-to-late Holocene transition, with pollen data. A similar cooling trend is present during the Late Holocene. The charcoal analysis, as well as pollen data, highlighted the period from 3000 cal. BP to modern day, during which the human and climate impact became indistinguishable. During this period, fire activity intensified, anthropogenic taxa increased, and other human indicators (i.e., archaeological artefacts) were attested.

The second objective of this study was to explore the regional climate variability of the Italian peninsula using other proxies and locations, and to precisely locate the north–south latitudinal limitation boundaries located between 40–43°N. Compared to other studies based on various proxies (i.e., pollen, chironomids, speleothems, alkenones and lake-level fluctuations), the Lago Grande di Monticchio climate signal can be linked to southern (south of 43°N), rather than northern (north of 43°N) climate regions. Southern regions are characterised by summer cooling and aridification trends alongside winter warming and humidification trends during the Holocene. The location of Lago Grande di Monticchio in the transitional zone that climatically divides the northern from the southern regions is supported by the pronounced "Mediterraneanization" process and the absence of a marked mid-Holocene summer thermal maximum.

Comparative analysis with records located within this transitional zone supports the southern climate attribute of Lago Grande di Monticchio, but the precise latitudinal boundary of the transition remains unclear. From previous studies, the most significant climatic contrast arises during summer between Lago dell'Accesa (~ 42°N) and Lago del Greppo (~ 44°N), where opposing climatic trends are evident around the 43°N mark. This suggests that the latitudinal divide influencing the climate of the Italian peninsula during the Holocene is likely situated at the higher end of the 41–43°N range.

The Holocene climate of the Mediterranean region was shaped by the complex interplay of global forcing mechanisms, primarily including the dominant atmospheric North Atlantic Oscillation (NAO), the oceanic Atlantic Meridional Overturning Circulation (AMOC), and tropical system dynamics (ITCZ/Hadley Cells). Changes in Earth's orbital parameters influenced the position of the ITCZ, which governed summer aridity and resulted in a widespread climate shift around 5000 cal. BP, linked to its southward migration. Throughout the Holocene, the region experienced dry episodes with distinct temporal periodicities, reflecting oscillations in the North Atlantic westerlies. After 8000 cal. BP, the region generally evolved towards a "Mediterraneanization", characterised by wet winters and dry summers, but rainfall changes were spatially patchy. This resulted in significant spatial heterogeneity, including opposed hydrological trends between the south-western and south-central Mediterranean areas, underscoring the role of complex ocean-atmospheric teleconnections and local topography.

Although limitations affect the multi-proxy approach used to reconstruct the palaeoclimate, whether applied to a single record (e.g., proxy bias) or encompassing multiple records (e.g., site-related effects, altitude, proxy bias, temporal resolution), it remains a powerful tool for better understanding the spatial and temporal variability of climate. Our palaeoclimate reconstruction at Lago Grande di Monticchio has provided a more accurate understanding of the climate transition zone for intermediate elevations. Further multi-proxy investigations are needed at higher latitudes, at similar and/or lower and higher elevations, to obtain a more complete picture of Holocene climate variability in the central Mediterranean. The climatic mechanisms responsible for the particular climate pattern of the Mediterranean during the Holocene remain uncertain. It would be interesting to investigate the forcings of global mechanisms on a regional scale to help refine our understanding of the factors involved in this north-south climate contrast during the Holocene.

CRediT authorship contribution statement

Léa d'Oliveira: Conceptualisation, Software, Formal analysis, Investigation, Writing – original draft, Review & editing, Visualisation. **Adrien Maignan:** Formal analysis, Writing – original draft, Review & editing. **Odile Peyron:** Conceptualisation, Writing – review & editing,

Supervision. **Sébastien Joannin:** Conceptualisation, Writing – review & editing, Supervision. **Nathalie Combourieu-Nebout:** Conceptualisation, Writing – review & editing, Supervision. **Marion Genet:** Formal analysis, Writing – original draft, Review & editing. **Marion Lestienne:** Formal analysis, Writing – original draft, Review & editing. **Lucas Dugerdil:** Software, Formal analysis, Writing – review & editing. **Giada Fernandez:** Formal analysis, Writing – review & editing. **Biagio Giaccio:** Formal analysis, Writing – review & editing. **Lorenzo Monaco:** Formal analysis, Writing – review & editing. **Sébastien Nomade:** Resources, Writing – review & editing. **Alison Pereira:** Resources, Writing – review & editing. **Vincent Scao:** Resources. **Edouard Regnier:** Resources. **Marie Balasse:** Writing – review & editing, Funding acquisition. **Guillemette Ménot:** Conceptualisation, Resources, Writing – review & editing, Supervision.

Declaration of competing interest

The authors declare the following financial interests/personal relationships which may be considered as potential competing interests: Given his role as an editor of Quaternary Science Reviews, B. Giaccio had no involvement in the peer review of this article and had no access to information regarding its peer review. Full responsibility for the editorial process for this article was delegated to another journal editor. If there are other authors, they declare that they have no known competing financial interests or personal relationships that could have appeared to influence the work reported in this paper.

Acknowledgements

This research was funded, in whole or in part, by ANR AUTUMN-LAMBS, Grant ANR-22-CE27-0011. The Monticchio coring as well as the establishment of the tephra-based age model of the record were funded by the French and Italian projects ICARE ("Inter-Calibration 40Ar/39Ar et Radiocarbone en Europe entre 10 000 et 40 000 ans BP", LEFE-INSU,2022–2024, A. Pereira coordinator) and COMET ("Consolidating the radiocarbon calibration over the 12–55 ka interval using paired 14C and 40Ar/39Ar dating of Mediterranean tephra", MUR, PRIN 2022; grant 2022MS9KWR, B. Giaccio coordinator). This project was also supported by the DT-INSU (CNRS). We would like to thank L. Augustin, T. Popp, A. De Moya, and F. Arnaud for their contributions in this context. Conference funding was provided by the Association des Palynologues de Langue Française (APLF). The work of data contributors, data stewards, and the Neotoma community is gratefully acknowledged. This is ISEM contribution ISEM 2026-047.

Appendix A. Central mediterranean sea surface temperature

Table A.1
Fossil marine biomarker records used for the Central Mediterranean Sea Surface Temperature (SST) reconstruction represented in Fig. 1a. Each record's climate parameters were averaged in a 100-year bin increment. The binned values of each record were averaged to produce a regional SST signal for the southern Italian region. The average signal was then transformed into anomalies with respect to the reconstructed modern average value.

ID	Sitename	Latitude (°N)	Longitude (° E)	Reference
1	AD91-17	40.87	18.64	Giunta and Emeis (2006)
2	GT89-3	39.76	17.90	Versteegh et al. (2007)
3	BS79-38	38.41	13.56	Cacho et al. (2001)
4	BS79-33	38.26	14.03	Cacho et al. (2001)
5	M40-4-SL78	37.04	13.19	Emeis and Dawson (2003)
6	M25_4-KL11	36.76	17.72	Emeis et al. (2000)
7	ANSIC-03_342	36.70	13.92	Incarbona et al. (2016)
8	ANSIC-03_407	36.38	14.45	Incarbona et al. (2016)
9	KC01	36.25	17.74	Doose (2001)

Appendix B. Tephra sampling for age-depth model

Table B.2
Tephra from MONTI23-II used for the age model.

Tephra	Sample label	Borehole and section depth (cm)	Composite depth (cm)		Tephra thickness (cm)
			Top	Base	
TM23-1	MON23-1	A01_40-41	40	41	1
TM23-2	MON23-3/4	B01_130-131	169.8	171.8	2
TM23-4b	MON23-7	A02_180-181	353	354	1
TM23-5	MON23-8	B02_127-129	383.3	385.3	2
TM23-6	MON23-9	B02_147.5	403.5	403.8	0.3
TM23-7	MON23-12	B02_172	428.1	428.3	0.2
TM23-9	MON23-13	A03_157-159	548.5	549	0.5
TM23-13	MON23-17/18	B04_65-67	738	744	6
TM23-17	MON23-22	A05_98-101	901.1	904.6	3.5
TM23-19	MON23-24	B05_105-108	977.3	981.3	4

Appendix C. Pollen diagram

The last 13,000 cal. BP vegetation has already been described in detail in the previous studies of Huntley et al. (1996, 1999) and Allen et al. (2002). The first period of the pollen diagram (M-1), corresponding to the Younger Dryas period (12,900–11,700 cal. BP), is marked by the lowest percentages of trees (60–80 %). *Quercus* (deciduous) represent the major proportion of arboreal pollen (50–60 %). Smaller proportion of other trees taxa such as *Betula*, *Pinus*, *Ulmus*, *Fraxinus*, *Tilia* and *Fagus*. Poaceae and *Artemisia* represent the highest proportion of the herbaceous taxa. The second period (M-2), expanding from 11,500 to around 9900 cal. BP, correspond to a higher proportion of arboreal pollen taxa (~ 90 %). The drop in *Artemisia*, *Quercus*, *Betula* and Poaceae coincide with the apparition of *Corylus* and *Ostrya*-type, and the increase of *Ulmus* and *Fraxinus*. This period also corresponds to the appearance of the Mediterranean taxon *Phillyrea* in small proportions (< 5 %). During the third period (M-3, 9900–7100 cal. BP), *Quercus* and *Corylus* proportions drop, while *Ostrya*-type, *Fagus* and *Phillyrea* percentages increase. *Abies*, *Caprinus betulus* and Mediterranean *Quercus ilex*-type taxa appears during this period. The presence of the hygrophilous taxon of *Alnus* is found around the lake. The fourth period (M-4) extends from 7100–3000 cal. BP, and corresponds to the highest tree diversity of the sequence with the presence of *Quercus* (deciduous), *Ostrya*-type, *Abies alba*, *Carpinus betulus*, *Corylus* and higher percentages of *Quercus ilex*-type (~ 20 %). *Plantago* appears in small proportions while hydrophytes (*Alnus* and aquatics) increases. The fifth short period (M-5, 3000–2300 cal. BP) corresponds to a peak in *Corylus* and *Carpinus betulus* while *Quercus* deciduous significantly drops. Finally, the sixth period (M-6), extending from 2300 cal. BP to modern-day corresponds to higher Mediterranean taxa with the appearance of *Olea* and *Pistacia* and the presence of *Quercus ilex*-type and *Phillyrea*. *Corylus*, *Carpinus betulus*, *Abies* and *Ulmus* percentages drops while *Quercus* deciduous and *Fagus* increases. Anthropogenic taxa appear during this last period, with the apparition of *Juglans* and *Cerealia*-type, and the increase of Poaceae.

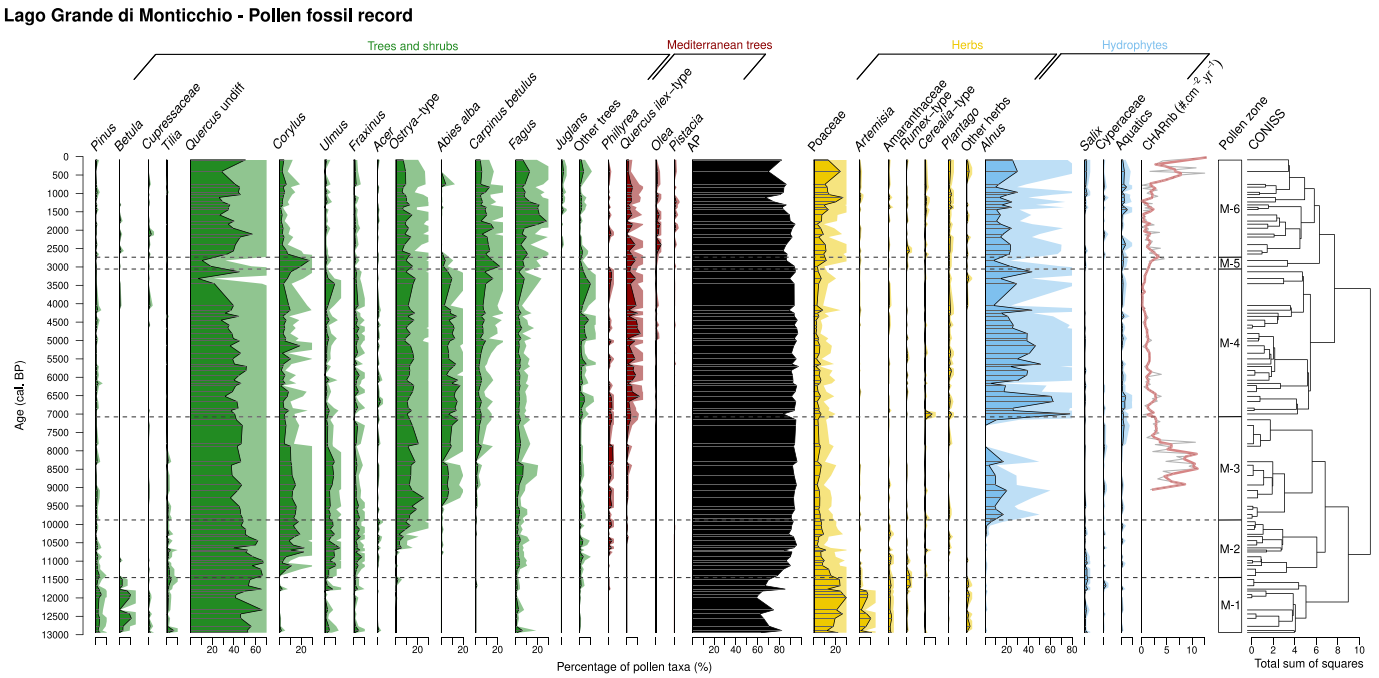

Fig. C.1. Simplified pollen diagram of the re-sampled composite core of Lago Grande di Monticchio and charcoal-inferred CHARnb (#.cm^{-2}.yr^{-1}, number). Grouping selected tree and shrub taxa (green), Mediterranean tree taxa (red), herbaceous taxa (yellow), arboreal pollen (AP, black) and hydrophytes (blue). Percentages were calculated on pollen sums excluding spores, *Alnus*, *Salix*, *Populus* and Cyperaceae. Dashed black lines delineate six zones based on CONISS (constrained incremental sum-of-squares agglomerative clustering) hierarchy classification method described by Grimm (1987).

Appendix D. Tephra compositions and correlations

D.1. Somma-vesuvius tephra

D.1.1. TM23-1 vs 1631 CE

Only two analytical data points were acquired for the first tephra layer, TM23-1. The composition of the glass is phonolitic (Fig. 2b), with a SiO_2 content of 54.7 ± 0.2 wt% and an alkali sum (Na_2O+K_2O) of 12.4 ± 0.2 wt% (Fig. D.2a). The alkali ratio (K_2O/Na_2O) is low (between 0.9 and 0.95), the CaO/FeO ratio is 1.25 ± 0.05, and the Cl content is between 0.9 ± 0.1 wt%. The stratigraphic position in the core and the major element content suggest the 1631 CE eruption as a potential correlative (Santacroce et al., 2008). The 1631 CE has been identified with a composition corresponding to that of ND14Q_SW/15 and ND14Q-33/34 samples (Fig. D.2a) from the southern Adriatic Sea (Totaro et al., 2022). Further occurrences have been found in southern Italy, at the San Vito (SV 9.50, Russo Ermolli et al., 2024) and Lago Grande di Monticchio (TM-1, Wulf et al., 2004) sequences.

D.1.2. TM23-3 vs 512 CE

TM23-3 is fairly homogeneous in composition, with a silica content of 48.9 ± 1.2 wt% and an alkali sum of 10.7 ± 1.4 wt% (Fig. D.2b). The alkali ratio is 1.4 ± 0.3, the CaO/FeO is 1.3 ± 0.3, and the Cl content is 0.8 ± 0.1 wt%. This tephra can be classified as a tephri-phonolite to phono-tephrite (Fig. 2b), similar to the 512 AD eruption of the Somma-Vesuvius (Cioni et al., 2008). The alkali ratio is medium-low (i.e., K_2O/Na_2O between 1.01 and 1.86); it can thus be classified as a Low Alkali Ratio (LAR) eruption (Fig. 2d). The 512 CE has a peculiar CaO composition that ranges between 7 and 12 wt% (Fig. D.2b, Santacroce et al., 2008), in agreement with our data. TM23-3 composition perfectly matches the composition of three samples from the Adriatic Sea (i.e., ND14Q_67b, ND14Q_AR2/48b and ND14Q_AR2/49b, Totaro et al., 2022), which can also be correlated to a tephra from Lago Grande di Monticchio (TM-2a, Wulf et al., 2004) and tentatively to one from Lake Prespa (PT0915-1, Damaschke et al., 2013).

D.1.3. TM23-4b and TMM23-5 vs AP3-AP2

TM23-4b has a slightly heterogeneous composition, and can be classified as a tephri-phonolite/phonolite (Fig. 2b), with a SiO_2 content of 55.0 ± 3.2 wt% and an alkali sum of 12.6 ± 2.0 wt% (Figs. D.2c, D.2d. The alkali ratio (K_2O/Na_2O) is 1.2 ± 0.6, the CaO/FeO is 1.0 ± 0.5, and the Cl content is 0.7 ± 0.4 wt%.

TM23-5 has instead a homogeneous composition and can be classified as a phonolite (Fig. 2b), with a SiO_2 content of 57.0 ± 1.3 wt% and an alkali sum of 14.3 ± 1.0 wt% (Fig. D.2c). The alkali ratio (K_2O/Na_2O) is 1.2 ± 0.6, the CaO/FeO is 1.0 ± 0.3, and the Cl content is 0.7 ± 0.1 wt%.

The composition of the glass shards allowed the identification of two eruptions that occurred between the Avellino and Pompeii eruptions from Somma-Vesuvius (Andronico and Cioni, 2002), the inter Avellino-Pompeii (AP) eruptions AP-3, correlated to the TM23-4b sample, and AP-2, correlated to the TM23-5 samples, respectively. An increase in SiO_2 and Na_2O+K_2O from a tephri-phonolitic AP-3 composition to a phonolitic AP-2 composition (Santacroce et al., 2008) is recorded in the Adriatic Sea (ND14Q/121a, ND14Q_AR2/104, ND14Q_AR2/106, Totaro et al., 2022), in the San Vito (SV 33.50) sequence and the Lago Grande di Monticchio (TM-3b and TM-3c, Wulf et al., 2004). AP-3 and AP-2 eruptions are the only well-dated of the AP series, with ages of 2849 ± 62 cal. BP (1σ) and 3425 ± 93 cal. BP (1σ) respectively (recalculated from Rolandi et al., 1998).

D.1.4. TM23-6 vs Pomici di Avellino eruption

TM23-6 falls in the phonolitic field in the TAS diagram (Fig. 2b), with a SiO_2 between 56.1 and 60.9 wt% and an alkali sum between 12.9 and 17.0 wt% (Fig. D.3a). The alkali ratio spans from 0.8 to 1.9,

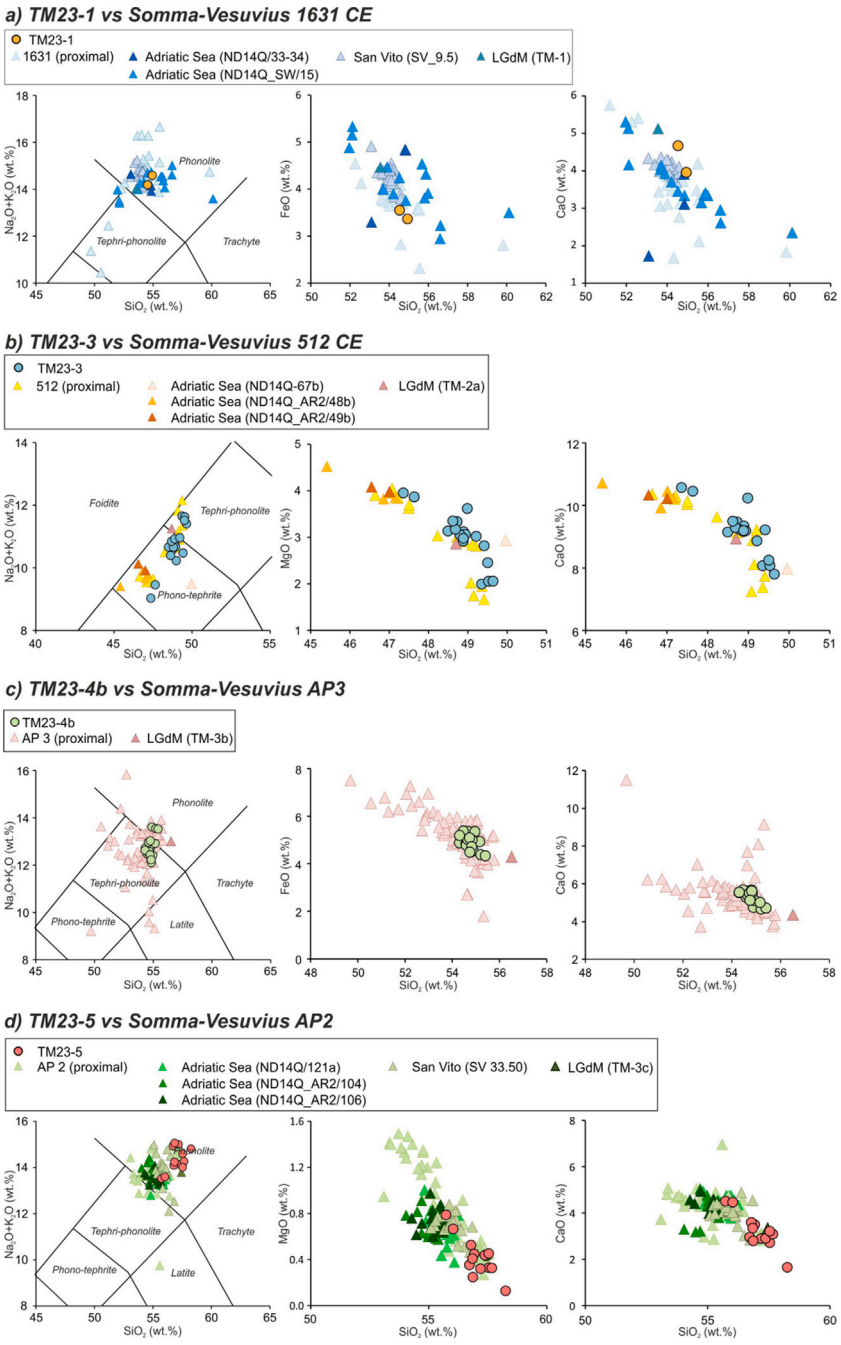

Fig. D.2. Total Alkali Silica (TAS; Le Maitre et al., 2002) diagram, SiO_2 vs FeO, SiO_2 vs CaO and SiO_2 vs FeO diagrams of (a) TM23-1, (b) TM23-3, (c) TM23-4b and (d) TM23-5 tephras.

the CaO/FeO between 0.8 and 1.2, and the Cl content between 0.2 and 0.8 wt%. The major element composition suggests the Somma-Vesuvius as the source of this tephra deposit. The phonolitic composition of the sample and the low alkali ratio (K_2O/Na_2O = 1.35 ± 0.77) point towards the Avellino eruption, with several occurrences that have been found in proximal (e.g., Sulpizio et al., 2008) and distal (Fernandez et al., 2023, and references therein) settings, e.g., in Lago Grande di Monticchio (TM-4, Wulf et al., 2004), Vico (Fernandez et al., 2023), Mezzano (e.g., Ramrath et al., 1999; Sulpizio et al., 2008), Accesa (Magny et al., 2007), Albano, Nemi (Calanchi and Dinelli, 2008), and Shkodra (Sulpizio et al., 2010) lakes. Further occurrences of this tephra have been found in the San Vito sequence (SV 25.50, SV 26.10 and SV 35.40, Fig. D.3, Russo Ermolli et al., 2024) and in the Adriatic Sea (ND14Q/127a, Totaro et al., 2022). This well-known Bronze Age eruption is an important marker horizon layer (e.g., Sevink et al., 2021). Although multiple ^{14}C ages are available in the literature (Delibrias et al., 1979; Marzocchella et al., 1994; Andronico et al., 1995; Watts et al., 1996b; Rolandi et al., 1998), we choose to retain the latest and most accurate age of 3837 ± 48 cal. BP (1σ, recalculated from Passariello et al. (2010), obtained on a goat bone buried by the Avellino eruption.

D.1.5. TM23-13 vs Mercato

TM23-13 shows a phonolitic composition (Fig. 2b), with a SiO_2 content of 59.2 ± 0.7 wt% and an alkali sum of 15.5 ± 1.0 wt% (Fig. D.3). The alkali ratio is 0.8 ± 0.1, the CaO/FeO varies from 0.7 to 1.1, and the Cl content is 0.6 ± 0.1 wt%. The TM23-13 tephra shows a composition

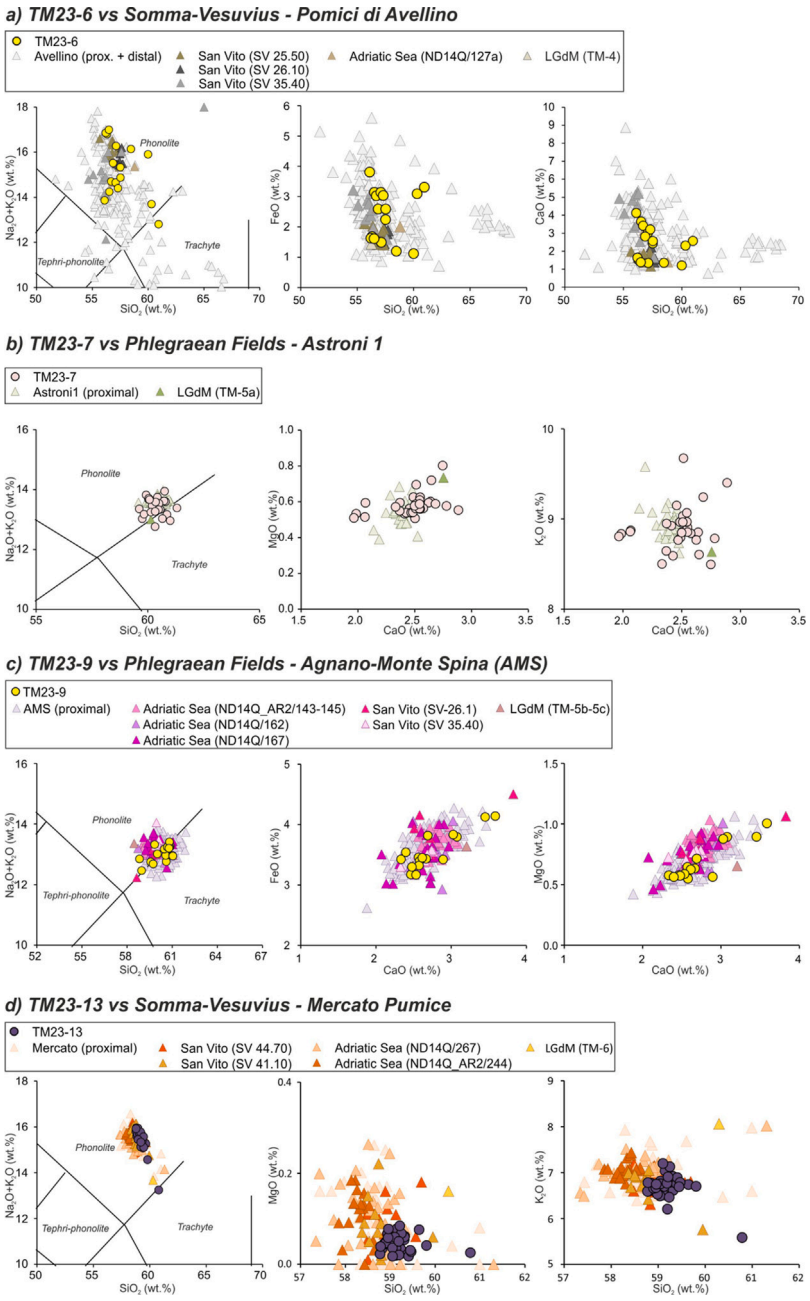

Fig. D.3. Total Alkali Silica (TAS; Le Maitre et al., 2002) diagram, SiO_2 vs FeO, SiO_2 vs CaO, CaO vs MgO, CaO vs K_2O, CaO vs FeO, SiO_2 vs MgO and SiO_2 vs K_2O diagrams of (a) TM23-6, (b) TM23-7, (c) TM23-9, and (d) TM23-13 tephras.

that partially overlaps with the Pomici di Avellino eruption (Santacroce et al., 2008). However, its homogeneous composition shows lower CaO (> 2 wt%), FeO (> 2.5 wt%) and TiO_2 (< 0.4 wt%) contents, suggesting a correlation with the Mercato Pumice eruption (Fig. D.3d, Santacroce et al., 2008), which has also been found in the Adriatic sea (Totaro et al., 2022) in the San Vito sequence (Russo Ermolli et al., 2024) in Lago Grande di Monticchio (TM-6b, Wulf et al., 2004) and lake Prespa (Damaschke et al., 2013). This eruption has been dated at 9024 ± 140 cal. BP (1σ, Wulf et al., 2004).

D.2. Phlegraean fields tephra

D.2.1. TM23-7 vs Astroni 1

TM23-7 is fairly homogeneous and spans the range between the phonolite and trachyte fields (Fig. 2b), with a SiO_2 content of 60.2 ± 1 wt% and an alkali sum (Na_2O+K_2O) of 13.6 ± 0.6 wt% (Fig. D.3). The alkali ratio (K_2O/Na_2O) is 1.9 ± 0.3, the CaO/FeO ratio is 0.8 ± 0.1, and the Cl content is 0.7 ± 0.1 wt%. The CaO/FeO vs Cl diagram confirms that this tephra layer originated from the Campi Flegrei (Fig. 2a–d). The glass is characterised by a High Alkali Ratio (1.9 ± 0.3, Isaia et al., 2009). The results allowed us to correlate the TM23-7 tephra with the proximal (Smith et al., 2011) and distal (TM-5a, Wulf et al., 2004) Astroni 1 eruptions, dated to 4177 ± 83 cal. BP (1σ, recalculated from Di Vito et al., 1999; Isaia et al., 2009).

D.2.2. TM23-9 vs Agnano Monte Spina (AMS)

TM23-9 has a heterogeneous composition and spans the range between the phonolite and trachyte fields (Fig. 2b), with a SiO_2 content of 60.3 ± 1.4 wt% and an alkali sum of 13.0 ± 0.5 wt% (Fig. D.3c). The alkali ratio is 2.0 ± 0.4, the CaO/FeO ratio is 0.8 ± 0.1, and the

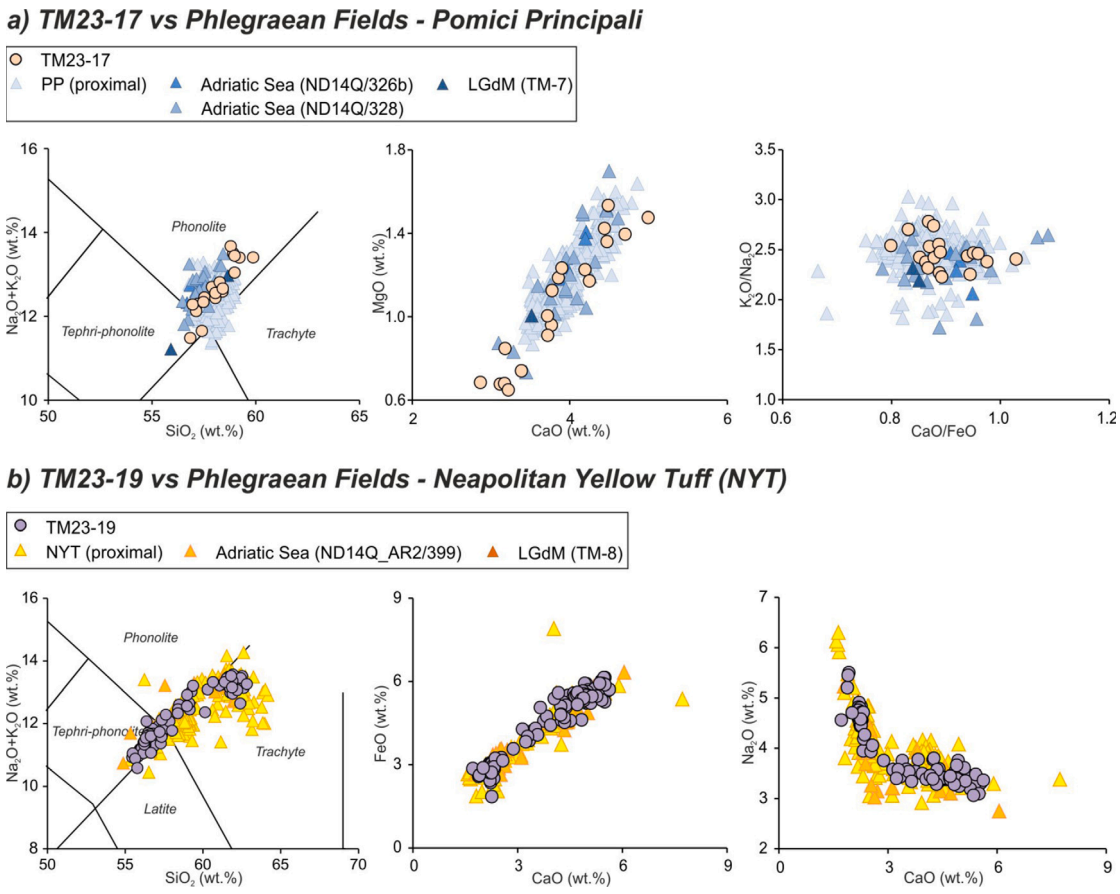

Fig. D.4. Total Alkali Silica (TAS; Le Maitre et al., 2002) diagram, CaO vs MgO, CaO/FeO vs. K_2/Na_2, CaO vsFeO and CaO vs Na_2O diagrams of (a) TM23-17 and (b) TM23-19 tephras.

Cl content is 0.7 ± 0.1 wt%. The CaO/FeO vs Cl diagram allowed the attribution of this tephra layer to the Campi Flegrei complex (CaO/FeO = 0.8 ± 0.1, Cl content = 0.7 ± 0.1 wt%). The alkali ratio is high (K_2O/Na_2O = 2.0 ± 0.4). The tephra can be correlated to the Agnano-Monte Spina eruption (Smith et al., 2011) and is also recorded in the San Vito sequence (Fig. D.3, Russo Ermolli et al., 2024), in the Adriatic Sea (Totaro et al., 2022) and in Lago Grande di Monticchio (TM-5c, Wulf et al., 2004). Two ages are available for these eruptions, one at 4640 ± 87 cal. BP (1σ, Andronico et al., 1995) and the other at 4580 ± 90 cal. BP (1σ, de Vita et al., 1999). For more accuracy, and since these two ages were obtained on different direct materials, their average age is used, resulting in a Chronomodel calculated age of 4610 ± 104 cal. BP.

D.2.3. TM23-17 vs Pomici Principali (PP)

TM23-17 composition is mostly phonolitic (Fig. 2b), with a SiO_2 content of 58.1 ± 1.7 wt% and an alkali sum of 12.7 ± 1.2 wt% (Fig. D.4a). The alkali ratio is 2.5 ± 0.3, the CaO/FeO is 0.9 ± 0.1, and the Cl content 0.6 ± 0.1 wt%. The Cl content and the CaO/FeO ratio suggest Campi Flegrei as the source of this tephra. The glass composition on the TM23-17 is coherent with the Pomici Principali tephri-phonolite to phonolite composition D.4a, found in proximal (Smith et al., 2011) and distal (TM-7a, Wulf et al., 2004) settings. The Pomici Principali eruption was previously dated at 12,169 ± 166 cal. BP (recalculated from Di Vito et al., 1999).

D.2.4. TM23-19 vs Neapolitan Yellow Tuff (NYT)

The chemistry of TM23-19 is based on 95 individual data points. It spans the tephri-phonolite/phonolite fields in the TAS diagram (Fig. 2b), with an average SiO_2 content of 58.5 ± 4.8 wt% and an average alkali sum of 12.2 ± 1.7 wt% (Fig. D.4b). The alkali average ratio is 2.3 ± 0.6, the average CaO/FeO ratio is 0.9 ± 0.2, and the Cl content varies between 0.3 and 0.7 wt%. This composition points to Campi Flegrei as a source and is consistent with the composition of the Neapolitan Yellow Tuff eruption (Deino et al., 2004, e.g.,). The distal correlatives of this eruption were found in several settings, e.g., in the Tyrrhenian (Paterne et al., 1988) and Adriatic (e.g., Siani et al., 2004; Totaro et al., 2022) seas, in Lago Grande di Monticchio (TM-8, Wulf et al., 2004), in San Gregorio Magno (Petrosino et al., 2019) in Croatia (Radić, 2007), in Fucino (Giaccio et al., 2017b), and in northern and eastern Europe (Schmidt et al., 2002; Lane et al., 2011). This eruption was dated on a tephra layer recovered in a marine core by Siani et al. (2004). The radiocarbon date obtained using the IntCal20 calibration curves is 14,157 ± 198 cal. BP (1σ), while the radiocarbon age obtained using the Marine20 calibration curves is 13,686 ± 155 cal. BP (1σ). Due to the uncertainty of the Marine20 calibration accuracy, the approach suggested by Bronk Ramsey et al. (2015) is applied, i.e., average age between the two radiocarbon calibrations, resulting in an age of 13,886 ± 287 cal. BP (1σ).

Appendix E. BrGDGT compounds relative abundances

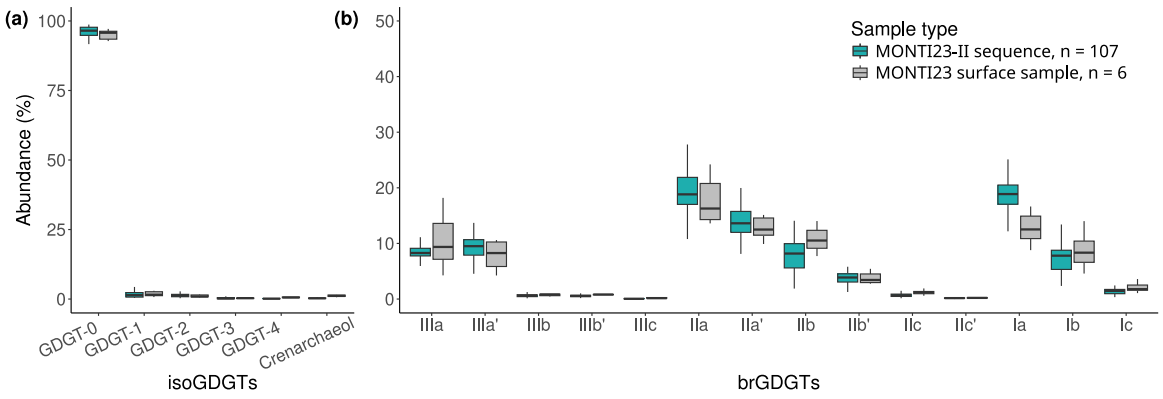

Fig. E.5. GDGT compounds relative abundance (%) of (a) isoGDGTs and (b) brGDGTs for the MONTI23-II core (n = 107, blue) and MONTI23 lacustrine surface samples (n = 6, grey).

Appendix F. GDGT indices

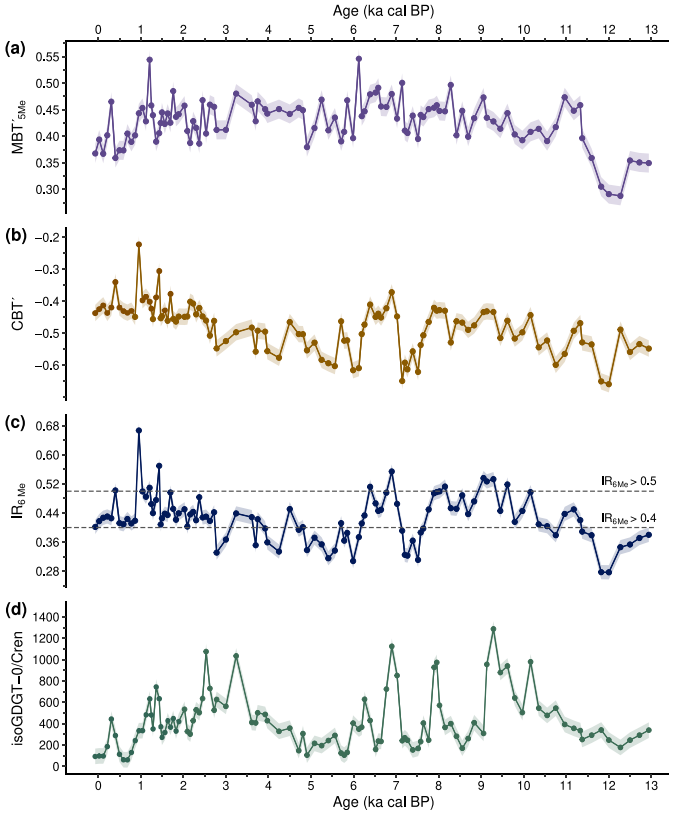

Fig. F.6. (a) Index of the degree of methylation (MBT'$_{5Me}$; De Jonge et al., 2014). (b) Index of the degree of cyclisation (CBT'; De Jonge et al., 2014). (c) Isomer ratio of 6-methyl brGDGTs vs. 5-methyl penta and hexamethylated brGDGTs (IR$_{6Me}$; De Jonge et al., 2014). (d) IsoGDGT-0 over Crenarchaeol ratio (isoGDGT-0/Cren; Blaga et al., 2009).

Appendix G. Correlation matrix

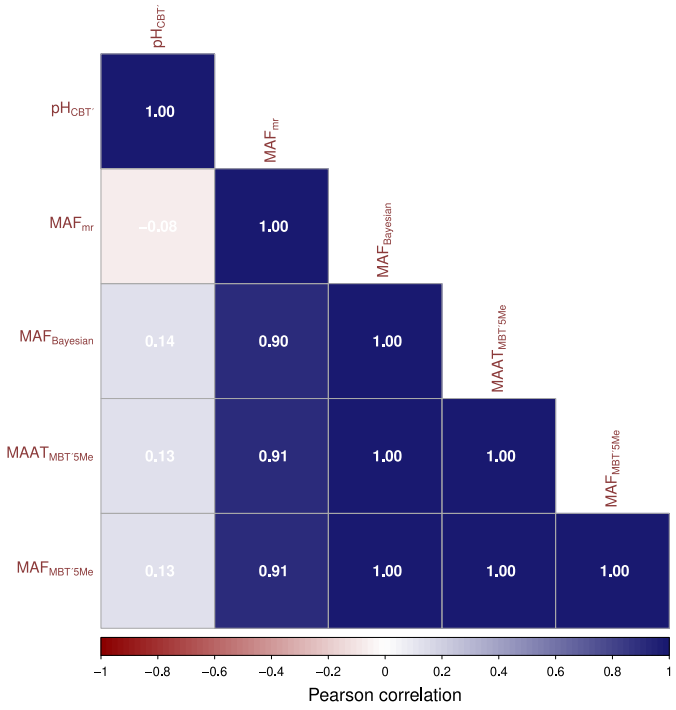

Fig. G.7. Heatmap of pair-wise correlations between pH and temperature (MAAT and MAF) inferred from brGDGTs.

Appendix H. brGDGT analysis: fractional abundances of tetra-, penta-, and hexamethylated brGDGTs

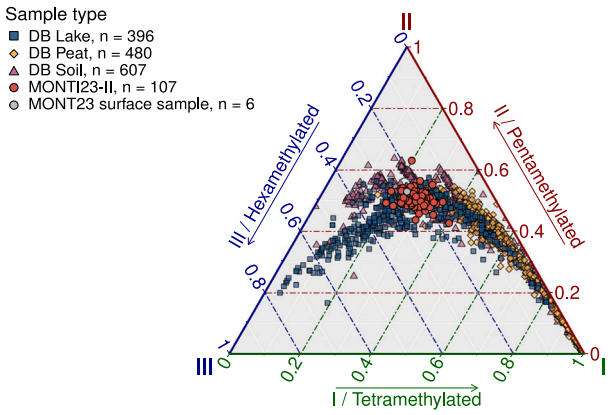

Fig. H.8. Ternary plot of fractional abundances of tetra-, penta-, and hexamethylated brGDGTs for MONTI23-II core samples (red dots) and averaged MONTI23 lacustrine surface samples (grey dots) and for global lake (Martínez-Sosa et al., 2021, blue squares), peat (Naafs et al., 2017b, yellow lozenges) and soil databases (Yang et al., 2014; Naafs et al., 2017a; Dearing Crampton-Flood et al., 2020, pink triangles).

Appendix I. BrGDGT isomerisation vs. brGDGTs concentration

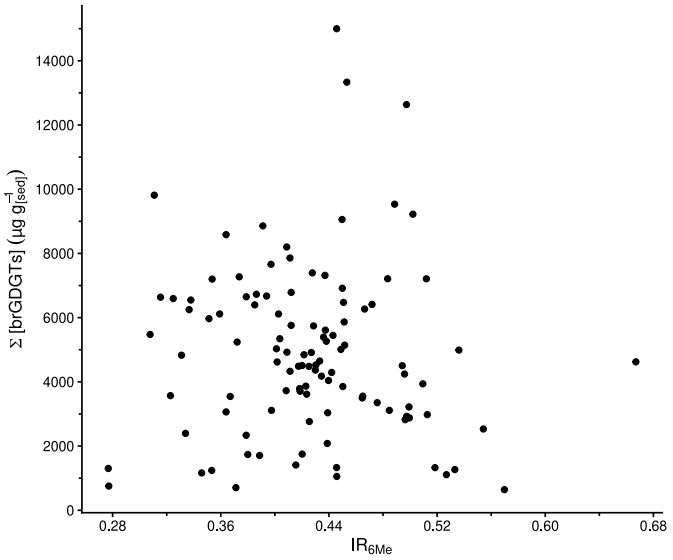

Fig. I.9. BrGDGT isomerisation (IR_{6Me}; De Jonge et al., 2014) vs. sum of all brGDGTs concentrations ($\sum$[brGDGTs]). The concentration of the sum of all brGDGTs encompasses 5- and 6-methyl brGDGTs (Ia, Ib, Ic, IIa, IIb, IIc, IIIa, IIIb and IIIc) and is expressed in µg $g^{-1}_{[sed]}$.

Data availability

Lago Grande di Monticchio pollen dataset (https://doi.org/10.21233/KVNC-0856) were obtained from the Neotoma Paleoecology Database (http://www.neotomadb.org). Lago Grande di Monticchio pollen-based palaeoclimate reconstructions are available at https://doi.org/10.1594/PANGAEA.989985. Lago Grande di Monticchio GDGT data and brGDGT-based palaeoclimate reconstructions are available at https://doi.org/10.1594/PANGAEA.989981.

References

Adolf, C., Wunderle, S., Colombaroli, D., Weber, H., Gobet, E., Heiri, O., van Leeuwen, J.F.N., Bigler, C., Connor, S.E., Gał ka, M., La Mantia, T., Makhortykh, S., Svitavská-Svobodová, H., Vannière, B., Tinner, W., 2018. The sedimentary and remote-sensing reflection of biomass burning in Europe. Glob. Ecol. Biogeogr. 27 (2), 199–212. http://dx.doi.org/10.1111/geb.12682, _eprint: https://onlinelibrary.wiley.com/doi/pdf/10.1111/geb.12682.

Ait Brahim, Y., Wassenburg, J.A., Sha, L., Cruz, F.W., Deininger, M., Sifeddine, A., Bouchaou, L., Spötl, C., Edwards, R.L., Cheng, H., 2019. North atlantic ice-rafting, ocean and atmospheric circulation during the holocene: Insights from western mediterranean speleothems. Geophys. Res. Lett. 46 (13), 7614–7623. http://dx.doi.org/10.1029/2019GL082405, URL: https://agupubs.onlinelibrary.wiley.com/doi/10.1029/2019GL082405.

Aleman, J.C., Blarquez, O., Bentaleb, I., Bonté, P., Brossier, B., Carcaillet, C., Gond, V., Gourlet-Fleury, S., Kpolita, A., Lefèvre, I., Oslisly, R., Power, M.J., Yongo, O., Bremond, L., Favier, C., 2013. Tracking land-cover changes with sedimentary charcoal in the Afrotropics. Holocene 23 (12), 1853–1862. http://dx.doi.org/10.1177/0959683613508159.

Ali, A.A., Higuera, P.E., Bergeron, Y., Carcaillet, C., 2009. Comparing fire-history interpretations based on area, number and estimated volume of macroscopic charcoal in lake sediments. Quat. Res. 72 (3), 462–468. http://dx.doi.org/10.1016/j.yqres.2009.07.002.

Allen, J.R.M., Brandt, U., Brauer, A., Hubberten, H.-W., Huntley, B., Keller, J., Kraml, M., Mackensen, A., Mingram, J., Negendank, J.F.W., Nowaczyk, N.R., Oberhänsli, H., Watts, W.A., Wulf, S., Zolitschka, B., 1999. Rapid environmental changes in southern Europe during the last glacial period. Nature 400 (6746), 740–743. http://dx.doi.org/10.1038/23432.

Allen, J.R., Huntley, B., 2009. Last interglacial palaeovegetation, palaeoenvironments and chronology: a new record from lago grande di monticchio, southern Italy. Quat. Sci. Rev. 28 (15–16), 1521–1538. http://dx.doi.org/10.1016/j.quascirev.2009.02.013, URL: https://linkinghub.elsevier.com/retrieve/pii/S0277379109000729.

Allen, J.R.M., Huntley, B., 2018. Effects of tephra falls on vegetation: A late-quaternary record from southern Italy. J. Ecol. 106 (6), 2456–2472. http://dx.doi.org/10.1111/1365-2745.12998.

Allen, J.R.M., Huntley, B., Watts, W.A., 2021. Lago Grande di Monticchio pollen dataset. http://dx.doi.org/10.21233/KVNC-0856, URL: https://data.neotomadb.org/47525.

Allen, J.R., Watts, W.A., Huntley, B., 2000. Weichselian palynostratigraphy, palaeovegetation and palaeoenvironment; the record from lago grande di monticchio, southern Italy. Quat. Int. 73–74, 91–110. http://dx.doi.org/10.1016/S1040-6182(00)00067-7, URL: https://linkinghub.elsevier.com/retrieve/pii/S1040618200000677.

Allen, J.R.M., Watts, W.A., McGee, E., Huntley, B., 2002. Holocene environmental variability-the record from Lago Grande di Monticchio, Italy. Quat. Int. 88, 69–80. http://dx.doi.org/10.1016/S1040-6182(01)00074-X.

Andronico, D., Calderoni, G., Cioni, R., Sbrana, A., Sulpizio, R., Santacroce, R., 1995. Geological map of Somma-Vesuvius volcano. Period. Miner. 64 (1–2), 77–78.

Andronico, D., Cioni, R., 2002. Contrasting styles of mount vesuvius activity in the period between the avellino and pompeii plinian eruptions, and some implications for assessment of future hazards. Bull. Volcanol. 64 (6), 372–391. http://dx.doi.org/10.1007/s00445-002-0215-4.

Ardenghi, N., Mulch, A., Koutsodendris, A., Pross, J., Kahmen, A., Niedermeyer, E.M., 2019. Temperature and moisture variability in the eastern mediterranean region during marine isotope stages 11–10 based on biomarker analysis of the tenaghi philippon peat deposit. Quat. Sci. Rev. 225, 105977. http://dx.doi.org/10.1016/j.quascirev.2019.105977.

Ayache, M., Swingedouw, D., Mary, Y., Eynaud, F., Colin, C., 2018. Multi-centennial variability of the AMOC over the holocene: A new reconstruction based on multiple proxy-derived SST records. Glob. Planet. Change 170, 172–189. http://dx.doi.org/10.1016/j.gloplacha.2018.08.016, URL: https://linkinghub.elsevier.com/retrieve/pii/S0921818118301231.

Bauersachs, T., Schubert, C.J., Mayr, C., Gilli, A., Schwark, L., 2024. Branched GDGT-based temperature calibrations from central European lakes. Sci. Total Environ. 906, 167724. http://dx.doi.org/10.1016/j.scitotenv.2023.167724.

Baxter, A.J., Peterse, F., Verschuren, D., Maitituerdi, A., Waldmann, N., Sinninghe Damsté, J.S., 2024. Disentangling influences of climate variability and lake-system evolution on climate proxies derived from isoprenoid and branched glycerol dialkyl glycerol tetraethers (GDGTs): the 250 kyr lake Chala record. Biogeosciences 21 (11), 2877–2908. http://dx.doi.org/10.5194/bg-21-2877-2024, URL: https://bg.copernicus.org/articles/21/2877/2024/.

Beffa, G., Pedrotta, T., Colombaroli, D., Henne, P.D., Van Leeuwen, J.F.N., Süsstrunk, P., Kaltenrieder, P., Adolf, C., Vogel, H., Pasta, S., Anselmetti, F.S., Gobet, E., Tinner, W., 2016. Vegetation and fire history of coastal north-eastern sardinia (Italy) under changing Holocene climates and land use. Veg. Hist. Archaeobotany 25 (3), 271–289. http://dx.doi.org/10.1007/s00334-015-0548-5, URL: http://link.springer.com/10.1007/s00334-015-0548-5.

van Bellen, S., Garneau, M., Ali, A.A., Bergeron, Y., 2012. Did fires drive Holocene carbon sequestration in boreal ombrotrophic peatlands of eastern Canada? Quat. Res. 78 (1), 50–59. http://dx.doi.org/10.1016/j.yqres.2012.03.009.

Bellomo, K., Meccia, V.L., D'Agostino, R., Fabiano, F., Larson, S.M., von Hardenberg, J., Corti, S., 2023. Impacts of a weakened AMOC on precipitation over the euro-atlantic region in the EC-Earth3 climate model. Clim. Dyn. 61 (7), 3397–3416. http://dx.doi.org/10.1007/s00382-023-06754-2.

Beug, H.J., 2004. Leitfaden der Pollenbestimmung für Mitteleuropa und angrenzende Gebiete. Dr. Friedrich Pfeil München, München, p. 542.

Bian, J., Räisänen, J., Seppä, H., 2025. Mid-holocene intertropical convergence zone migration: connection with hadley cell dynamics and impacts on terrestrial hydroclimate. Clim. Past 21 (7), 1209–1233. http://dx.doi.org/10.5194/cp-21-1209-2025, URL: https://cp.copernicus.org/articles/21/1209/2025/.

Biancari, L., Aguiar, M.R., Eldridge, D.J., Oñatibia, G.R., Le Bagousse-Pinguet, Y., Saiz, H., Gross, N., Austin, A.T., Ochoa, V., Gozalo, B., Asensio, S., Guirado, E., Valencia, E., Berdugo, M., Plaza, C., Martínez-Valderrama, J., Mendoza, B.J., García-Gómez, M., Abedi, M., Ahumada, R.J., Alcántara, J.M., Amghar, F., Anadón, J.D., Aramayo, V., Arredondo, T., Bader, M.Y., Bahalkeh, K., Salem, F.B., Blaum, N., Boldgiv, B., Bowker, M., Branquinho, C., Bu, C., Byambatsogt, B., Calvo, D.A., Castillo Monroy, A.P., Castro, H., Castro-Quezada, P., Chibani, R., Conceição, A.A., Currier, C.M., Donoso, D.A., Dougill, A., Ejtehadi, H., Espinosa, C.I., Fajardo, A., Farzam, M., Ferrante, D., Fraser, L.H., Gaitán, J.J., Gherardi, L.A., Gusmán-Montalván, E., Hernández-Hernández, R.M., Hölzel, N., Huber-Sannwald, E., Hughes, F.M., Jadán, O., Jeltsch, F., Jentsch, A., Ju, M., Kaseke, K.F., Kindermann, L., Köbel, M., Le Roux, P.C., Liancourt, P., Linstädter, A., Liu, J., Louw, M.A., Maggs-Kölling, G., Issa, O.M., Marais, E., Margerie, P., Messeder, J.V.S., Mora, J.P., Moreno, G., Munson, S.M., Oliva, G., Pueyo, Y., Quiroga, R.E., Reed, S.C., Rey, P.J., Rodríguez, A., Rodríguez, L.B., Rolo, V., Ruppert, J.C., Sala, O., Salah, A., Stavi, I., Stephens, C.R.A., Swemmer, A.M., Teixido, A.L., Thomas, A.D., Throop, H.L., Tielbörger, K., Travers, S.K., Van Den Brink, L., Wagner, V., Wamiti, W., Wang, D., Wang, L., Wolff, P., Yahdjian, L., Zaady, E., Maestre, F.T., 2024. Drivers of woody dominance across global drylands. Sci. Adv. 10 (41), eadn6007. http://dx.doi.org/10.1126/sciadv.adn6007.

Bini, M., Zanchetta, G., Perşoiu, A., Cartier, R., Català, A., Cacho, I., Dean, J.R., Di Rita, F., Drysdale, R.N., Finnè, M., Isola, I., Jalali, B., Lirer, F., Magri, D., Masi, A., Marks, L., Mercuri, A.M., Peyron, O., Sadori, L., Sicre, M.A., Welc, F., Zielhofer, C., Brisset, E., 2019. The 4.2 ka BP event in the mediterranean region: an overview. Clim. Past 15 (2), 555–577. http://dx.doi.org/10.5194/cp-15-555-2019.

Birks, H.J.B., Heiri, O., Seppä, H., Bjune, A.E., 2010. Strengths and weaknesses of quantitative climate reconstructions based on late-quaternary biological proxies. Open Ecol. J. 3, 68–110.

Blaga, C.I., Reichart, G.J., Heiri, O., Sinninghe Damsté, J.S., 2009. Tetraether membrane lipid distributions in water-column particulate matter and sediments: a study of 47 European lakes along a north–south transect. J. Paleolimnol. 41 (3), 523–540. http://dx.doi.org/10.1007/s10933-008-9242-2, URL: http://link.springer.com/10.1007/s10933-008-9242-2.

Bonadonna, F., Brocchini, D., Laurenzi, M., Principe, C., Ferrara, G., Follieri, M., Girotti, O., Kotasakis, T., Taddeucci, A., Turner, C., 1993. Mt. Vulture volcano. Chronostratigraphy and paleogeographic implications. In: Symposium: Quaternary Stratigraphy in Volcanic Areas. INQUA subcommission on European Quaternary stratigraphy, p. 13.

ter Braak, C.J.F., Juggins, S., 1993. Weighted averaging partial least squares regression (WA-PLS): an improved method for reconstructing environmental variables from species assemblages | SpringerLink. Hydrobiologia 269/270, 485–502. http://dx.doi.org/10.1007/BF00028046, URL: https://link.springer.com/article/10.1007/BF00028046.

Braconnot, P., Otto-Bliesner, B., Harrison, S., Joussaume, S., Peterchmitt, J.Y., Abe-Ouchi, A., Crucifix, M., Driesschaert, E., Fichefet, T., Hewitt, C.D., Kageyama, M., Kitoh, A., Loutre, M.-F., Marti, O., Merkel, U., Ramstein, G., Valdes, P., Weber, L., Yu, Y., Zhao, Y., 2007. Results of PMIP2 coupled simulations of the mid-holocene and last glacial maximum - part 2: feedbacks with emphasis on the location of the ITCZ and mid- and high latitudes heat budget. Clim. Past 3 (2), 279–296. http://dx.doi.org/10.5194/cp-3-279-2007, Publisher: Copernicus GmbH, URL: https://cp.copernicus.org/articles/3/279/2007/.

Bradley, R., 2003. Chapter 2 climate forcing during the holocene. PAGES News 11, http://dx.doi.org/10.22498/pages.11.2-3.18.

Brandimarte, L., Di Baldassarre, G., Bruni, G., D'Odorico, P., Montanari, A., 2011. Relation between the north-atlantic oscillation and hydroclimatic conditions in mediterranean areas. Water Resour. Manag. 25 (5), 1269–1279. http://dx.doi.org/10.1007/s11269-010-9742-5, URL: http://link.springer.com/10.1007/s11269-010-9742-5.

Brauer, A., Allen, J.R.M., Mingram, J., Dulski, P., Wulf, S., Huntley, B., 2007. Evidence for last interglacial chronology and environmental change from Southern Europe. Proc. Natl. Acad. Sci. 104 (2), 450–455. http://dx.doi.org/10.1073/pnas.0603321104.

Brauer, A., Mingram, J., Frank, U., Günter, C., Georg Schettler, Wulf, S., Zolitschka, B., Negendank, J.F., 2000. Abrupt environmental oscillations during the early weichselian recorded at Lago Grande di monticchio, southern Italy. Quat. Int. 73–74, 79–90. http://dx.doi.org/10.1016/S1040-6182(00)00066-5.

van Bree, L.G.J., Peterse, F., Baxter, A.J., De Crop, W., van Grinsven, S., Villanueva, L., Verschuren, D., Sinninghe Damsté, J.S., 2020. Seasonal variability and sources of in situ brgdgt production in a permanently stratified African crater lake. Biogeosciences 17 (21), 5443–5463. http://dx.doi.org/10.5194/bg-17-5443-2020, Publisher: Copernicus GmbH, URL: https://bg.copernicus.org/articles/17/5443/2020/.

Breiman, L., 2001. Random forests. Mach. Learn. 45 (1), 5–32. http://dx.doi.org/10.1023/A:1010933404324.

Brewer, S., Guiot, J., Sánchez-Goñi, M., Klotz, S., 2008. The climate in Europe during the Eemian: a multi-method approach using pollen data. Quat. Sci. Rev. 27 (25–26), 2303–2315. http://dx.doi.org/10.1016/j.quascirev.2008.08.029.

Broccoli, A.J., Dahl, K.A., Stouffer, R.J., 2006. Response of the ITCZ to northern Hemisphere cooling. Geophys. Res. Lett. 33 (1), 2005GL024546. http://dx.doi.org/10.1029/2005GL024546, URL: https://agupubs.onlinelibrary.wiley.com/doi/10.1029/2005GL024546.

Brogli, R., Kröner, N., Sørland, S.L., Lüthi, D., Schär, C., 2019. The role of hadley circulation and lapse-rate changes for the future European summer climate. J. Clim. 32 (2), 385–404. http://dx.doi.org/10.1175/JCLI-D-18-0431.1, URL: https://journals.ametsoc.org/view/journals/clim/32/2/jcli-d-18-0431.1.xml.

Bronk Ramsey, C., Albert, P.G., Blockley, S.P.E., Hardiman, M., Housley, R.A., Lane, C.S., Lee, S., Matthews, I.P., Smith, V.C., Lowe, J.J., 2015. Improved age estimates for key late quaternary European tephra horizons in the RESET lattice. Quat. Sci. Rev. 118, 18–32. http://dx.doi.org/10.1016/j.quascirev.2014.11.007.

Cacho, I., Grimalt, J.O., Canals, M., Sbaffi, L., Shackleton, N.J., Schönfeld, J., Zahn, R., 2001. Alkenone-derived Holocene sea-surface temperature records of sediment core BS79-38. http://dx.doi.org/10.1594/PANGAEA.438379, Type: dataset.

Calanchi, N., Dinelli, E., 2008. Tephrostratigraphy of the last 170 ka in sedimentary successions from the Adriatic Sea. J. Volcanol. Geotherm. Res. 177 (1), 81–95. http://dx.doi.org/10.1016/j.jvolgeores.2008.06.008.

Camuera, J., Jiménez-Espejo, F.J., Soto-Chica, J., Jiménez-Moreno, G., García-Alix, A., Ramos-Román, M.J., Ruha, L., Castro-Priego, M., 2023. Drought as a possible contributor to the Visigothic Kingdom crisis and Islamic expansion in the Iberian Peninsula. Nat. Commun. 14 (1), 5733. http://dx.doi.org/10.1038/s41467-023-41367-7.

Carcaillet, C., Almquist, H., Asnong, H., Bradshaw, R.H.W., Carrión, J.S., Gaillard, M.J., Gajewski, K., Haas, J.N., Haberle, S.G., Hadorn, P., Müller, S.D., Richard, P.J.H., Richoz, I., Rösch, M., Sánchez Goñi, M.F., von Stedingk, H., Stevenson, A.C., Talon, B., Tardy, C., Tinner, W., Tryterud, E., Wick, L., Willis, K.J., 2002. Holocene biomass burning and global dynamics of the carbon cycle. Chemosphere 49 (8), 845–863. http://dx.doi.org/10.1016/S0045-6535(02)00385-5, URL: https://www.sciencedirect.com/science/article/pii/S0045653502003855.

Carcaillet, C., Bergeron, Y., Richard, P.J.H., Fréchette, B., Gauthier, S., Prairie, Y.T., 2001. Change of fire frequency in the eastern Canadian boreal forests during the Holocene: does vegetation composition or climate trigger the fire regime? J. Ecol. 89 (6), 930–946. http://dx.doi.org/10.1111/j.1365-2745.2001.00614.x.

Carcaillet, C., Perroux, A.S., Genries, A., Perrette, Y., 2007. Sedimentary charcoal pattern in a karstic underground lake, vercors massif, French Alps: implications for palaeo-fire history. Holocene 17 (6), 845–850. http://dx.doi.org/10.1177/0959683607080526, Publisher: SAGE Publications Ltd.

Caroli, I., Caldara, M., 2007. Vegetation history of lago battaglia (eastern gargano coast, apulia, Italy) during the middle-late holocene. Veg. Hist. Archaeobotany 16 (4), 317–327. http://dx.doi.org/10.1007/s00334-006-0045-y, URL: http://link.springer.com/10.1007/s00334-006-0045-y.

Chen, T.C., 2005. Maintenance of the midtropospheric north African summer circulation: Saharan high and african easterly jet. J. Clim. 18 (15), 2943–2962. http://dx.doi.org/10.1175/JCLI3446.1, Publisher: American Meteorological Society Section: Journal of Climate, URL: https://journals.ametsoc.org/view/journals/clim/18/15/jcli3446.1.xml.

Chevalier, M., Davis, B., Heiri, O., Seppä, H., Chase, B.M., Gajewski, K., Lacourse, T., Telford, R.J., Finsinger, W., Guiot, J., Kühl, N., Maezumi, S.Y., Tipton, J.R., Carter, V.A., Brussel, T., Phelps, L.N., Dawson, A., Zanon, M., Vallé, F., Nolan, C., Mauri, A., de Vernal, A., Izumi, K., Holmström, L., Marsicek, J., Goring, S., Sommer, P.S., Chaput, M., Kupriyanov, D., 2020. Pollen-based climate reconstruction techniques for late quaternary studies. Earth-Sci. Rev. 210 (103384), 33.

Cioni, R., Bertagnini, A., Santacroce, R., Andronico, D., 2008. Explosive activity and eruption scenarios at somma-vesuvius (Italy): Towards a new classification scheme. J. Volcanol. Geotherm. Res. 178 (3), 331–346. http://dx.doi.org/10.1016/j.jvolgeores.2008.04.024.

Cipolloni Sampo, M., Ronchitelli, A., Sarti, L., Borgognini Tarli, S., Follieri, M., 1977. Gli scavi nel villaggio neolitico di rendina (1970–1976). Relazione preliminare. Orig. Preist. Protoistoria Della Civiltà Antiche Roma 11, 183–354.

Colcord, D.E., Cadieux, S.B., Brassell, S.C., Castañeda, I.S., Pratt, L.M., White, J.R., 2015. Assessment of branched GDGTs as temperature proxies in sedimentary records from several small lakes in southwestern Greenland. Org. Geochem. 82, 33–41. http://dx.doi.org/10.1016/j.orggeochem.2015.02.005, URL: https://linkinghub.elsevier.com/retrieve/pii/S0146638015000388.

Columbu, A., Spötl, C., Fohlmeister, J., Hu, H.M., Chiarini, V., Hellstrom, J., Cheng, H., Shen, C.C., De Waele, J., 2022. Central Mediterranean rainfall varied with high northern latitude temperatures during the last deglaciation. Commun. Earth Environ. 3 (1), 181. http://dx.doi.org/10.1038/s43247-022-00509-3.

Courtney Mustaphi, C.J., Davis, E.L., Perreault, J.T., Pisaric, M.F.J., 2015. Spatial variability of recent macroscopic charcoal deposition in a small montane lake and implications for reconstruction of watershed-scale fire regimes. J. Paleolimnol. 54 (1), 71–86. http://dx.doi.org/10.1007/s10933-015-9838-2.

Creer, K.M., Morris, A., 1996. Proxy-climate and geomagnetic palaeointensity records extending back to Ca. 75,000 BP derived from sediments cored from Lago Grande di Monticchio, Southern Italy. Quat. Sci. Rev. 15 (2), 167–188. http://dx.doi.org/10.1016/0277-3791(95)00080-1.

Cruz-Silva, E., Harrison, S.P., Prentice, I.C., Marinova, E., Bartlein, P.J., Renssen, H., Zhang, Y., 2023. Pollen-based reconstructions of holocene climate trends in the eastern Mediterranean region. Clim. Past 19 (11), 2093–2108. http://dx.doi.org/10.5194/cp-19-2093-2023.

Dallmeyer, A., Claussen, M., Lorenz, S.J., Shanahan, T., 2020. The end of the African humid period as seen by a transient comprehensive Earth system model simulation of the last 8000 years. Clim. Past 16 (1), 117–140. http://dx.doi.org/10.5194/cp-16-117-2020, URL: https://cp.copernicus.org/articles/16/117/2020/.

Damaschke, M., Sulpizio, R., Zanchetta, G., Wagner, B., Böhm, A., Nowaczyk, N., Rethemeyer, J., Hilgers, A., 2013. Tephrostratigraphic studies on a sediment core from Lake Prespa in the Balkans. Clim. the Past 9 (1), 267–287. http://dx.doi.org/10.5194/cp-9-267-2013, Publisher: Copernicus GmbH.

Dang, X., Xue, J., Yang, H., Xie, S., 2016. Environmental impacts on the distribution of microbial tetraether lipids in Chinese lakes with contrasting pH: Implications for lacustrine paleoenvironmental reconstructions. Sci. China Earth Sci. 59 (5), 939–950. http://dx.doi.org/10.1007/s11430-015-5234-z, URL: http://link.springer.com/10.1007/s11430-015-5234-z.

Davis, B., Brewer, S., Stevenson, A., Guiot, J., 2003. The temperature of Europe during the Holocene reconstructed from pollen data. Quat. Sci. Rev. 22 (15–17), 1701–1716. http://dx.doi.org/10.1016/S0277-3791(03)00173-2.

De Jonge, C., Hopmans, E.C., Zell, C.I., Kim, J.H., Schouten, S., Sinninghe Damsté, J.S., 2014. Occurrence and abundance of 6-methyl branched glycerol dialkyl glycerol tetraethers in soils: Implications for palaeoclimate reconstruction. Geochim. Cosmochim. Acta 141, 97–112. http://dx.doi.org/10.1016/j.gca.2014.06.013.

de Vita, S., Orsi, G., Civetta, L., Carandente, A., D'Antonio, M., Deino, A., di Cesare, T., Di Vito, M.A., Fisher, R.V., Isaia, R., Marotta, E., Necco, A., Ort, M., Pappalardo, L., Piochi, M., Southon, J., 1999. The agnano–Monte spina eruption (4100 years BP) in the restless campi flegrei caldera (Italy). J. Volcanol. Geotherm. Res. 91 (2), 269–301. http://dx.doi.org/10.1016/S0377-0273(99)00039-6.

Dearing Crampton-Flood, E., Tierney, J.E., Peterse, F., Kirkels, F.M., Sinninghe Damsté, J.S., 2020. BayMBT: A Bayesian calibration model for branched glycerol dialkyl glycerol tetraethers in soils and peats. Geochim. Cosmochim. Acta 268, 142–159. http://dx.doi.org/10.1016/j.gca.2019.09.043.

Deino, A.L., Orsi, G., De Vita, S., Piochi, M., 2004. The age of the neapolitan yellow tuff caldera-forming eruption (campi flegrei caldera – Italy) assessed by 40Ar/39Ar dating method. J. Volcanol. Geotherm. Res. 133 (1–4), 157–170. http://dx.doi.org/10.1016/S0377-0273(03)00396-2, URL: https://linkinghub.elsevier.com/retrieve/pii/S0377027303003962.

Delibrias, G., Di Paola, G., Rosi, M., Santacroce, R., 1979. La storia eruttiva del complesso vulcanico somma vesuvio ricostruita dalle successioni piroclastiche del Monte somma. Rend. Della Soc. Ital. Miner. E Pet. 35, 411–438.

Delworth, T.L., Zeng, F., 2016. The impact of the north Atlantic oscillation on climate through its influence on the atlantic meridional overturning circulation. J. Clim. 29 (3), 941–962. http://dx.doi.org/10.1175/JCLI-D-15-0396.1, Publisher: American Meteorological Society Section: Journal of Climate, URL: https://journals.ametsoc.org/view/journals/clim/29/3/jcli-d-15-0396.1.xml.

Desprat, S., Combourieu-Nebout, N., Essallami, L., Sicre, M.A., Dormoy, I., Peyron, O., Siani, G., Bout Roumazeilles, V., Turon, J.L., 2013. Deglacial and Holocene vegetation and climatic changes in the southern Central Mediterranean from a direct land–sea correlation. Clim. Past 9 (2), 767–787. http://dx.doi.org/10.5194/cp-9-767-2013, URL: https://cp.copernicus.org/articles/9/767/2013/.

Di Rita, F., Fletcher, W.J., Aranbarri, J., Margaritelli, G., Lirer, F., Magri, D., 2018a. Holocene forest dynamics in central and western Mediterranean: periodicity, spatio-temporal patterns and climate influence. Sci. Rep. 8 (1), 8929. http://dx.doi.org/10.1038/s41598-018-27056-2, URL: https://www.nature.com/articles/s41598-018-27056-2.

Di Rita, F., Lirer, F., Bonomo, S., Cascella, A., Ferraro, L., Florindo, F., Insinga, D.D., Lurcock, P.C., Margaritelli, G., Petrosino, P., Rettori, R., Vallefuoco, M., Magri, D., 2018b. Late holocene forest dynamics in the Gulf of Gaeta (central Mediterranean) in relation to NAO variability and human impact. Quat. Sci. Rev. 179, 137–152. http://dx.doi.org/10.1016/j.quascirev.2017.11.012.

Di Rita, F., Magri, D., 2009. Holocene drought, deforestation and evergreen vegetation development in the central Mediterranean: a 5500 year record from Lago Alimini Piccolo, Apulia, southeast Italy. Holocene 19 (2), 295–306. http://dx.doi.org/10.1177/0959683608100574, Publisher: SAGE Publications, URL: https://journals.sagepub.com/doi/10.1177/0959683608100574.

Di Vito, M.A., Isaia, R., Orsi, G., Southon, J., de Vita, S., D'Antonio, M., Pappalardo, L., Piochi, M., 1999. Volcanism and deformation since 12,000 years at the Campi Flegrei caldera (Italy). J. Volcanol. Geotherm. Res. 91 (2), 221–246. http://dx.doi.org/10.1016/S0377-0273(99)00037-2.

Ding, S., Xu, Y., Wang, Y., He, Y., Hou, J., Chen, L., He, J.S., 2015. Distribution of branched glycerol dialkyl glycerol tetraethers in surface soils of the Qinghai–Tibetan Plateau: implications of brGDGTs-based proxies in cold and dry regions. Biogeosciences 12 (11), 3141–3151. http://dx.doi.org/10.5194/bg-12-3141-2015, URL: https://bg.copernicus.org/articles/12/3141/2015/.

Djebbar, A., Goosse, H., Klein, F., 2020. Robustness of the link between precipitation in North Africa and standard modes of atmospheric variability during the last millennium. Climate 8 (5), 62. http://dx.doi.org/10.3390/cli8050062, Publisher: Multidisciplinary Digital Publishing Institute, URL: https://www.mdpi.com/2225-1154/8/5/62.

d'Oliveira, L., Dugerdil, L., Ménot, G., Evin, A., Muller, S.D., Ansanay-Alex, S., Azuara, J., Bonnet, C., Bremond, L., Shah, M., Peyron, O., 2023. Reconstructing 15 000 years of southern France temperatures from coupled pollen and molecular (branched glycerol dialkyl glycerol tetraether) markers (Canroute, Massif Central). Clim. Past 19 (11), 2127–2156. http://dx.doi.org/10.5194/cp-19-2127-2023.

d'Oliveira, L., Joannin, S., Ménot, G., Combourieu-Nebout, N., Dugerdil, L., Blache, M., Robles, M., Florenzano, A., Masi, A., Mercuri, A.M., Sadori, L., Balasse, M., Peyron, O., 2025. Holocene climate dynamics in the central Mediterranean inferred from pollen data. Clim. Past 21 (11), 2331–2359. http://dx.doi.org/10.5194/cp-21-2331-2025, URL: https://cp.copernicus.org/articles/21/2331/2025/.

Doose, H., 2001. (Table 2c) alkenones, stable isotopes and sea surface temperature from sediment core KC01. http://dx.doi.org/10.1594/PANGAEA.59762, Type: dataset.

Drysdale, R., Zanchetta, G., Hellstrom, J., Maas, R., Fallick, A., Pickett, M., Cartwright, I., Piccini, L., 2006. Late Holocene drought responsible for the collapse of Old World civilizations is recorded in an Italian cave flowstone. Geology 34 (2), 101. http://dx.doi.org/10.1130/G22103.1, URL: https://pubs.geoscienceworld.org/geology/article/34/2/101-104/129423.

Dubrovský, M., Hayes, M., Duce, P., Trnka, M., Svoboda, M., Zara, P., 2014. Multi-GCM projections of future drought and climate variability indicators for the Mediterranean region. Reg. Environ. Chang. 14 (5), 1907–1919. http://dx.doi.org/10.1007/s10113-013-0562-z, URL: http://link.springer.com/10.1007/s10113-013-0562-z.

Dugerdil, L., Ménot, G., Peyron, O., Jouffroy-Bapicot, I., Ansanay-Alex, S., Antheaume, I., Behling, H., Boldgiv, B., Develle, A.L., Grossi, V., Magail, J., Makou, M., Robles, M., Unkelbach, J., Vannière, B., Joannin, S., 2021. Late holocene mongolian climate and environment reconstructions from brGDGTs, NPPs and pollen transfer functions for Lake Ayrag: Paleoclimate implications for arid central Asia. Quat. Sci. Rev. 273, 107235. http://dx.doi.org/10.1016/j.quascirev.2021.107235, URL: https://linkinghub.elsevier.com/retrieve/pii/S027737912100442X.

Dugerdil, L., Peyron, O., Ménot, G., Egamberdieva, D., Alimov, J., Leroy, S.A., Garnier, E., Nowak, A., Joannin, S., 2025. First paleoenvironmental calibrations for modern pollen rain of Tajikistan and Uzbekistan: A case study of pollen - vegetation functional biogeography of Arid Central Asia. Glob. Planet. Change 252, 104857. http://dx.doi.org/10.1016/j.gloplacha.2025.104857, URL: https://linkinghub.elsevier.com/retrieve/pii/S0921818125001663.

Elith, J., Leathwick, J.R., Hastie, T., 2008. A working guide to boosted regression trees. J. Anim. Ecol. 77 (4), 802–813. http://dx.doi.org/10.1111/j.1365-2656.2008.01390.x, URL: https://onlinelibrary.wiley.com/doi/abs/10.1111/j.1365-2656.2008.01390.x.

Emeis, K.C., Dawson, A.G., 2003. Age and alkenone-derived holocene sea-surface temperature records of sediment core M40-4-SL78. http://dx.doi.org/10.1594/PANGAEA.438795, Type: dataset.

Emeis, K.C., Struck, U., Schulz, H.M., Rosenberg, M., Bernasconi, S.M., Erlenkeuser, H., Sakamoto, T., Martinez-Ruiz, F.C., 2000. Age and alkenone-derived holocene sea-surface temperature records of sediment core m25/4-KL11. http://dx.doi.org/10.1594/PANGAEA.438794, Type: dataset.

Enache, M.D., Cumming, B.F., 2007. Charcoal morphotypes in lake sediments from British Columbia (Canada): an assessment of their utility for the reconstruction of past fire and precipitation. J. Paleolimnol. 38 (3), 347–363. http://dx.doi.org/10.1007/s10933-006-9084-8, URL: http://link.springer.com/10.1007/s10933-006-9084-8.

Fernandez, G., Giaccio, B., Monaco, L., Tomatis, M., Pacella, A., Palladino, D.M., Sulpizio, R., Turci, F., Zanchetta, G., Ballirano, P., Sottili, G., 2023. Physical and chemical characterization of the Pomici di Avellino ashes (3.9 ka) from Somma-Vesuvius volcano for future health hazard assessment. J. Volcanol. Geotherm. Res. 438, 107826. http://dx.doi.org/10.1016/j.jvolgeores.2023.107826, URL: https://www.sciencedirect.com/science/article/pii/S0377027323000835.

Fick, S.E., Hijmans, R.J., 2017. WorldClim 2: new 1-km spatial resolution climate surfaces for global land areas. Int. J. Climatol. 37 (12), 4302–4315. http://dx.doi.org/10.1002/joc.5086, URL: https://onlinelibrary.wiley.com/doi/abs/10.1002/joc.5086.

Finné, M., Woodbridge, J., Labuhn, I., Roberts, C.N., 2019. Holocene hydro-climatic variability in the Mediterranean: A synthetic multi-proxy reconstruction. Holocene 29 (5), 847–863. http://dx.doi.org/10.1177/0959683619826634, URL: http://journals.sagepub.com/doi/10.1177/0959683619826634.

Fletcher, W.J., Debret, M., Goñi, M.F.S., 2013. Mid-Holocene emergence of a low-frequency millennial oscillation in western Mediterranean climate: Implications for past dynamics of the North Atlantic atmospheric westerlies. Holocene 23 (2), 153–166. http://dx.doi.org/10.1177/0959683612460783, URL: http://journals.sagepub.com/doi/10.1177/0959683612460783.

Fratianni, S., Acquaotta, F., 2017. The climate of Italy. In: Soldati, M., Marchetti, M. (Eds.), Landscapes and Landforms of Italy. Springer International Publishing, Cham, pp. 29–38. http://dx.doi.org/10.1007/978-3-319-26194-2_4, Series Title: World Geomorphological Landscapes, URL: http://link.springer.com/10.1007/978-3-319-26194-2_4.

Gaetani, M., Baldi, M., Dalu, G.A., Maracchi, G., 2011. Jetstream and rainfall distribution in the Mediterranean region. Nat. Hazards Earth Syst. Sci. 11 (9), 2469–2481. http://dx.doi.org/10.5194/nhess-11-2469-2011, URL: https://nhess.copernicus.org/articles/11/2469/2011/.

Geng, R., Weinelt, M., Zhang, W., 2025. Syntheses of pollen-based temperature reconstructions with respect to seasonal and spatiotemporal change in Europe. Quat. Sci. Rev. 353, 109228. http://dx.doi.org/10.1016/j.quascirev.2025.109228, URL: https://linkinghub.elsevier.com/retrieve/pii/S0277379125000484.

Giaccio, B., Hajdas, I., Isaia, R., Deino, A., Nomade, S., 2017a. High-precision 14C and 40Ar/39Ar dating of the Campanian Ignimbrite (Y-5) reconciles the time-scales of climatic-cultural processes at 40 ka. Sci. Rep. 7 (1), 45940. http://dx.doi.org/10.1038/srep45940, Publisher: Nature Publishing Group, URL: https://www.nature.com/articles/srep45940.

Giaccio, B., Niespolo, E.M., Pereira, A., Nomade, S., Renne, P.R., Albert, P.G., Arienzo, I., Regattieri, E., Wagner, B., Zanchetta, G., Gaeta, M., Galli, P., Mannella, G., Peronace, E., Sottili, G., Florindo, F., Leicher, N., Marra, F., Tomlinson, E.L., 2017b. First integrated tephrochronological record for the last 190 kyr from the Fucino Quaternary lacustrine succession, central Italy. Quat. Sci. Rev. 158, 211–234. http://dx.doi.org/10.1016/j.quascirev.2017.01.004, URL: https://www.sciencedirect.com/science/article/pii/S027737911730015X.

Giorgi, F., Lionello, P., 2008. Climate change projections for the mediterranean region. Glob. Planet. Change 63 (2), 90–104. http://dx.doi.org/10.1016/j.gloplacha.2007.09.005, URL: https://linkinghub.elsevier.com/retrieve/pii/S0921818107001750.

Giraudi, C., Magny, M., Zanchetta, G., Drysdale, R., 2011. The Holocene climatic evolution of Mediterranean Italy: A review of the continental geological data. Holocene 21 (1), 105–115. http://dx.doi.org/10.1177/0959683610377529, URL: http://journals.sagepub.com/doi/10.1177/0959683610377529.

Giunta, S., Emeis, K.C., 2006. Age and alkenone-derived holocene sea-surface temperature records of sediment core AD91-17. http://dx.doi.org/10.1594/PANGAEA.438366, Type: dataset.

Grimm, E.C., 1987. CONISS: a FORTRAN 77 program for stratigraphically constrained cluster analysis by the method of incremental sum of squares. Comput. Geosci. 13 (1), 13–35. http://dx.doi.org/10.1016/0098-3004(87)90022-7, URL: https://www.sciencedirect.com/science/article/pii/0098300487900227.

Guilaine, J., Radi, G., Angeli, L., 2019. La Néolithisation de l'Italie du Sud-Est. Eurasian Prehistory 15 (1–2), 101, URL: https://univ-tlse2.hal.science/hal-03542655.

Guiot, J., 1990. Methodology of the last climatic cycle reconstruction in France from pollen data. Palaeogeogr. Palaeoclimatol. Palaeoecol. 80 (1), 49–69. http://dx.doi.org/10.1016/0031-0182(90)90033-4, URL: https://www.sciencedirect.com/science/article/pii/0031018290900334.

Guiot, J., Cramer, W., 2016. Climate change: The 2015 Paris agreement thresholds and Mediterranean basin ecosystems. Science 354 (6311), 465–468. http://dx.doi.org/10.1126/science.aah5015, URL: https://www.science.org/doi/10.1126/science.aah5015.

Harning, D.J., Sacco, S., Raberg, J.H., Ardenghi, N., Sepúlveda, J., Shapiro, B., Miller, G.H., Geirsdóttir, Á., 2025. Both redox potential and climate control molecular proxies in Icelandic Holocene lake sediments. Commun. Earth Environ. 6 (1), 763. http://dx.doi.org/10.1038/s43247-025-02701-7, URL: https://www.nature.com/articles/s43247-025-02701-7.

Haug, G.H., Hughen, K.A., Sigman, D.M., Peterson, L.C., Röhl, U., 2001. Southward migration of the intertropical convergence zone through the holocene. Science 293 (5533), 1304–1308. http://dx.doi.org/10.1126/science.1059725, URL: https://www.science.org/doi/10.1126/science.1059725.

Heaton, T.J., Köhler, P., Butzin, M., Bard, E., Reimer, R.W., Austin, W.E.N., Bronk Ramsey, C., Grootes, P.M., Hughen, K.A., Kromer, B., Reimer, P.J., Adkins, J., Burke, A., Cook, M.S., Olsen, J., Skinner, L.C., 2020. Marine20—The marine radiocarbon age calibration curve (0–55,000 cal BP). Radiocarbon 62 (4), 779–820. http://dx.doi.org/10.1017/RDC.2020.68, URL: https://www.cambridge.org/core/product/identifier/S0033822220000685/type/journal_article.

Herzschuh, U., Böhmer, T., Chevalier, M., Hébert, R., Dallmeyer, A., Li, C., Cao, X., Peyron, O., Nazarova, L., Novenko, E.Y., Park, J., Rudaya, N.A., Schlütz, F., Shumilovskikh, L.S., Tarasov, P.E., Wang, Y., Wen, R., Xu, Q., Zheng, Z., 2023. Regional pollen-based Holocene temperature and precipitation patterns depart from the Northern Hemisphere mean trends. Clim. Past 19 (7), 1481–1506. http://dx.doi.org/10.5194/cp-19-1481-2023, URL: https://cp.copernicus.org/articles/19/1481/2023/.

Higuera, P.E., Brubaker, L.B., Anderson, P.M., Hu, F.S., Brown, T.A., 2009. Vegetation mediated the impacts of postglacial climate change on fire regimes in the south-central Brooks Range, Alaska. Ecol. Monograph. 79 (2), 201–219. http://dx.doi.org/10.1890/07-2019.1, URL: https://onlinelibrary.wiley.com/doi/abs/10.1890/07-2019.1, _eprint: https://onlinelibrary.wiley.com/doi/pdf/10.1890/07-2019.1.

Hijmans, R.J., Phillips, S., Leathwick, J., Elith, J., 2024. Dismo: Species distribution modeling. http://dx.doi.org/10.32614/CRAN.package.dismo, R package version 1.3-16, URL: https://CRAN.R-project.org/package=dismo.

Hopmans, E.C., Schouten, S., Sinninghe Damsté, J.S., 2016. The effect of improved chromatography on GDGT-based palaeoproxies. Org. Geochem. 93, 1–6. http://dx.doi.org/10.1016/j.orggeochem.2015.12.006.

Huguet, C., Hopmans, E.C., Febo-Ayala, W., Thompson, D.H., Sinninghe Damsté, J.S., Schouten, S., 2006. An improved method to determine the absolute abundance of glycerol dibiphytanyl glycerol tetraether lipids. Org. Geochem. 37 (9), 1036–1041. http://dx.doi.org/10.1016/j.orggeochem.2006.05.008, URL: https://linkinghub.elsevier.com/retrieve/pii/S0146638006001094.

Huntley, B., Allen, J.R.M., Watts, W.A., 1996. Weichselian late-glacial palaeoecology and palaeoenvironment at Lago Grande di Monticchio (Basilicata, s Italy). Alp. Mediterr. Quat. 9 (2), 605–616, Number: 2, URL: https://amq.aiqua.it/index.php/amq/article/view/1059.

Huntley, B., Watts, W., Allen, J., Zolitschka, B., 1999. Palaeoclimate, chronology and vegetation history of the Weichselian Lateglacial: comparative analysis of data from three cores at Lago Grande di Monticchio, southern Italy. Quat. Sci. Rev. 18 (7), 945–960. http://dx.doi.org/10.1016/S0277-3791(99)00007-4, URL: https://linkinghub.elsevier.com/retrieve/pii/S0277379199000074.

Hurrell, J.W., 1995. Decadal trends in the north atlantic oscillation: Regional temperatures and precipitation. Science 269 (5224), 676–679. http://dx.doi.org/10.1126/science.269.5224.676, Publisher: American Association for the Advancement of Science, URL: https://www.science.org/doi/abs/10.1126/science.269.5224.676.

Hurrell, J.W., Kushnir, Y., Ottersen, G., Visbeck, M., 2003. An overview of the north atlantic oscillation. In: Hurrell, J.W., Kushnir, Y., Ottersen, G., Visbeck, M. (Eds.), In: Geophysical Monograph Series, vol. 134, American Geophysical Union, Washington, D. C., pp. 1–35. http://dx.doi.org/10.1029/134GM01, URL: https://onlinelibrary.wiley.com/doi/10.1029/134GM01.

Incarbona, A., Martrat, B., Mortyn, P.G., Sprovieri, M., Ziveri, P., Gogou, A., Jordà, G., Xoplaki, E., Luterbacher, J., Langone, L., Marino, G., Rodriguez-Sanz, L., Triantaphyllou, M., Stefano, E.D., Grimalt, J.O., Tranchida, G., Sprovieri, R., Mazzola, S., 2016. Stable isotopes, radionuclides, and calculated sea surface temperature of sediment core ANSIC-03_342. http://dx.doi.org/10.1594/PANGAEA.861972, Type: dataset.

IPCC, 2023. Climate Change 2022 – Impacts, Adaptation and Vulnerability: Working Group II Contribution to the Sixth Assessment Report of the Intergovernmental Panel on Climate Change, first ed. Cambridge University Press, http://dx.doi.org/10.1017/9781009325844, URL: https://www.cambridge.org/core/product/identifier/9781009325844/type/book.

Isaia, R., Marianelli, P., Sbrana, A., 2009. Caldera unrest prior to intense volcanism in Campi Flegrei (Italy) at 4.0 ka B.P.: Implications for caldera dynamics and future eruptive scenarios. Geophys. Res. Lett. 36 (21), http://dx.doi.org/10.1029/2009GL040513.

ISPRA, 2023. SCIA – sistema nazionale per l'elaborazione e diffusione di dati climatici. https://scia.isprambiente.it/servertsutm/serietemporali400.php. (Accessed June 2025).

Jackson, L.C., Kahana, R., Graham, T., Ringer, M.A., Woollings, T., Mecking, J.V., Wood, R.A., 2015. Global and European climate impacts of a slowdown of the AMOC in a high resolution GCM. Clim. Dyn. 45 (11–12), 3299–3316. http://dx.doi.org/10.1007/s00382-015-2540-2, URL: http://link.springer.com/10.1007/s00382-015-2540-2.

Jacob, D., Goettel, H., Jungclaus, J., Muskulus, M., Podzun, R., Marotzke, J., 2005. Slowdown of the thermohaline circulation causes enhanced maritime climate influence and snow cover over Europe. Geophys. Res. Lett. 32 (21), http://dx.doi.org/10.1029/2005GL023286, URL: https://onlinelibrary.wiley.com/doi/abs/10.1029/2005GL023286, _eprint: https://agupubs.onlinelibrary.wiley.com/doi/pdf/10.1029/2005GL023286.

Joannin, S., Ali, A.A., Ollivier, V., Roiron, P., Peyron, O., Chevaux, S., Nahapetyan, S., Tozalakyan, P., Karakhanyan, A., Chataigner, C., 2014. Vegetation, fire and climate history of the Lesser Caucasus: a new Holocene record from Zarishat fen. J. Quat. Sci. 29 (1), 70–82. http://dx.doi.org/10.1002/jqs.2679, Publisher: Wiley, URL: https://onlinelibrary.wiley.com/doi/10.1002/jqs.2679.

Joannin, S., Brugiapaglia, E., de Beaulieu, J.L., Bernardo, L., Magny, M., Peyron, O., Goring, S., Vannière, B., 2012. Pollen-based reconstruction of Holocene vegetation and climate in southern Italy: the case of Lago Trifoglietti. Clim. Past 8 (6), 1973–1996. http://dx.doi.org/10.5194/cp-8-1973-2012, URL: https://cp.copernicus.org/articles/8/1973/2012/.

Jochum, K.P., Stoll, B., Herwig, K., Willbold, M., Hofmann, A.W., Amini, M., Aarburg, S., Abouchami, W., Hellebrand, E., Mocek, B., Raczek, I., Stracke, A., Alard, O., Bouman, C., Becker, S., Dücking, M., Brätz, H., Klemd, R., de Bruin, D., Canil, D., Cornell, D., de Hoog, C.-J., Dalpé, C., Danyushevsky, L., Eisenhauer, A., Gao, Y., Snow, J.E., Groschopf, N., Günther, D., Latkoczy, C., Guillong, M., Hauri, E.H., Höfer, H.E., Lahaye, Y., Horz, K., Jacob, D.E., Kasemann, S.A., Kent, A.J.R., Ludwig, T., Zack, T., Mason, P.R.D., Meixner, A., Rosner, M., Misawa, K., Nash, B.P., Pfänder, J., Premo, W.R., Sun, W.D., Tiepolo, M., Vannucci, R., Vennemann, T., Wayne, D., Woodhead, J.D., 2006. MPI-DING reference glasses for in situ microanalysis: New reference values for element concentrations and isotope ratios. Geochem. Geophys. Geosystems 7 (2), http://dx.doi.org/10.1029/2005GC001060.

Juggins, S., 2024. Rioja: Analysis of quaternary science data. R package version 1.0-7, URL: https://cran.r-project.org/package=rioja.

Lane, C.S., Andrič, M., Cullen, V.L., Blockley, S.P., 2011. The occurrence of distal icelandic and Italian tephra in the Lateglacial of Lake Bled, Slovenia. Quat. Sci. Rev. 30 (9–10), 1013–1018. http://dx.doi.org/10.1016/j.quascirev.2011.02.014, URL: https://linkinghub.elsevier.com/retrieve/pii/S0277379111000734.

Lanos, P., Dufresne, P., 2019. Chronomodel version2.0: Software for chronological modelling of archaeological data using Bayesian statistics. URL: http://www.chronomodel.com.

Laskar, J., Robutel, P., Joutel, F., Gastineau, M., Correia, A.C.M., Levrard, B., 2004. A long-term numerical solution for the insolation quantities of the Earth. Astron. Astrophys. 428 (1), 261–285. http://dx.doi.org/10.1051/0004-6361:20041335, URL: http://www.aanda.org/10.1051/0004-6361:20041335.

Le Maitre, R.W., Streckeisen, A., Zanettin, B., Le Bas, M.J., Bonin, B., Bateman, P. (Eds.), 2002. Igneous Rocks: A Classification and Glossary of Terms: Recommendations of the International Union of Geological Sciences Subcommission on the Systematics of Igneous Rocks, second ed. Cambridge University Press, Cambridge, http://dx.doi.org/10.1017/CBO9780511535581, URL: https://www.cambridge.org/core/books/igneous-rocks-a-classification-and-glossary-of-terms/7F458E82BF81BF6A011CEA0D41DE9311.

Lefèvre, D., Raynal, J.P., Vernet, G., Pilleyre, T., Piperno, M., Sanzelle, S., Fain, J., Miallier, D., Montret, M., 1994. Sédimentation, volcanisme et présence humaine dans le bassin de venosa (basilicata, italie) au pléistocène moyen : exemple du site de notarchirico. Bull. Société Préhistorique Française 91 (2), 103–112. http://dx.doi.org/10.3406/bspf.1994.9721, URL: https://www.persee.fr/doc/bspf_0249-7638_1994_num_91_2_9721.

Lehmann, J., Coumou, D., 2015. The influence of mid-latitude storm tracks on hot, cold, dry and wet extremes. Sci. Rep. 5 (1), 17491. http://dx.doi.org/10.1038/srep17491, URL: https://www.nature.com/articles/srep17491.

Lestienne, M., Jouffroy-Bapicot, I., Leyssenne, D., Sabatier, P., Debret, M., Albertini, P.J., Colombaroli, D., Didier, J., Hély, C., Vannière, B., 2020. Fires and human activities as key factors in the high diversity of Corsican vegetation. Holocene 30 (2), 244–257. http://dx.doi.org/10.1177/0959683619883025, URL: https://journals.sagepub.com/doi/10.1177/0959683619883025.

Leys, B., Carcaillet, C., Dezileau, L., Ali, A.A., Bradshaw, R.H.W., 2013. A comparison of charcoal measurements for reconstruction of Mediterranean paleo-fire frequency in the mountains of Corsica. Quat. Res. 79 (3), 337–349. http://dx.doi.org/10.1016/j.yqres.2013.01.003, URL: https://www.cambridge.org/core/journals/quaternary-research/article/abs/comparison-of-charcoal-measurements-for-reconstruction-of-mediterranean-paleofire-frequency-in-the-mountains-of-corsica/010D1A2AD56F506A86797551D1822C36.

Leys, B., Finsinger, W., Carcaillet, C., 2014. Historical range of fire frequency is not the Achilles' heel of the Corsican black pine ecosystem. J. Ecol. 102 (2), 381–395. http://dx.doi.org/10.1111/1365-2745.12207, URL: https://onlinelibrary.wiley.com/doi/abs/10.1111/1365-2745.12207, _eprint: https://besjournals.onlinelibrary.wiley.com/doi/pdf/10.1111/1365-2745.12207.

Lézine, A.M., Ivory, S.J., Braconnot, P., Marti, O., 2017. Timing of the southward retreat of the ITCZ at the end of the Holocene humid period in Southern Arabia: Data-model comparison. Quat. Sci. Rev. 164, 68–76. http://dx.doi.org/10.1016/j.quascirev.2017.03.019, URL: https://linkinghub.elsevier.com/retrieve/pii/S027737911730255X.

Li, K.Y., Liu, W., 2025. Weakened atlantic meridional overturning circulation causes the historical north atlantic warming hole. Commun. Earth Environ. 6 (1), 416. http://dx.doi.org/10.1038/s43247-025-02403-0, URL: https://www.nature.com/articles/s43247-025-02403-0.

Li, J., Sun, C., Jin, F.F., 2013. NAO implicated as a predictor of Northern Hemisphere mean temperature multidecadal variability. Geophys. Res. Lett. 40 (20), 5497–5502. http://dx.doi.org/10.1002/2013GL057877, URL: https://agupubs.onlinelibrary.wiley.com/doi/10.1002/2013GL057877.

Lionello, P., Abrantes, F., Congedi, L., Dulac, F., Gacic, M., Gomis, D., Goodess, C., Hoff, H., Kutiel, H., Luterbacher, J., Planton, S., Reale, M., Schröder, K., Vittoria Struglia, M., Toreti, A., Tsimplis, M., Ulbrich, U., Xoplaki, E., 2012. Introduction: Mediterranean climate—Background information. In: The Climate of the Mediterranean Region. Elsevier, pp. xxxv–xc. http://dx.doi.org/10.1016/B978-0-12-416042-2.00012-4, URL: https://linkinghub.elsevier.com/retrieve/pii/B9780124160422000124.

Lionello, P., D'Agostino, R., Ferreira, D., Nguyen, H., Singh, M.S., 2024. The Hadley circulation in a changing climate. Ann. New York Acad. Sci. 1534 (1), 69–93. http://dx.doi.org/10.1111/nyas.15114, URL: https://nyaspubs.onlinelibrary.wiley.com/doi/10.1111/nyas.15114.

Lionello, P., Malanotte-Rizzoli, P., Boscolo, R., Alpert, P., Artale, V., Li, L., Luterbacher, J., May, W., Trigo, R., Tsimplis, M., Ulbrich, U., Xoplaki, E., 2006. The mediterranean climate: An overview of the main characteristics and issues. In: Developments in Earth and Environmental Sciences, vol. 4, Elsevier, pp. 1–26. http://dx.doi.org/10.1016/S1571-9197(06)80003-0, URL: https://linkinghub.elsevier.com/retrieve/pii/S1571919706800030.

Liu, M., Shen, Y., González-Sampériz, P., Gil-Romera, G., Ter Braak, C.J.F., Prentice, I.C., Harrison, S.P., 2023. Holocene climates of the Iberian Peninsula: pollen-based reconstructions of changes in the west–east gradient of temperature and moisture. Clim. Past 19 (4), 803–834. http://dx.doi.org/10.5194/cp-19-803-2023, URL: https://cp.copernicus.org/articles/19/803/2023/.

López-Moreno, J., Vicente-Serrano, S., Morán-Tejeda, E., Lorenzo-Lacruz, J., Kenawy, A., Beniston, M., 2011. Effects of the north Atlantic oscillation (NAO) on combined temperature and precipitation winter modes in the mediterranean mountains: Observed relationships and projections for the 21st century. Glob. Planet. Change 77 (1–2), 62–76. http://dx.doi.org/10.1016/j.gloplacha.2011.03.003, URL: https://linkinghub.elsevier.com/retrieve/pii/S0921818111000385.

Magny, M., Combourieu-Nebout, N., de Beaulieu, J.L., Bout-Roumazeilles, V., Colombaroli, D., Desprat, S., Francke, A., Joannin, S., Ortu, E., Peyron, O., Revel, M., Sadori, L., Siani, G., Sicre, M.A., Samartin, S., Simonneau, A., Tinner, W., Vannière, B., Wagner, B., Zanchetta, G., Anselmetti, F., Brugiapaglia, E., Chapron, E., Debret, M., Desmet, M., Didier, J., Essallami, L., Galop, D., Gilli, A., Haas, J.N., Kallel, N., Millet, L., Stock, A., Turon, J.L., Wirth, S., 2013. North–south palaeohydrological contrasts in the central Mediterranean during the Holocene: tentative synthesis and working hypotheses. Clim. Past 9 (5), 2043–2071. http://dx.doi.org/10.5194/cp-9-2043-2013, URL: https://cp.copernicus.org/articles/9/2043/2013/.

Magny, M., De Beaulieu, J.L., Drescher-Schneider, R., Vannière, B., Walter-Simonnet, A.-V., Miras, Y., Millet, L., Bossuet, G., Peyron, O., Brugiapaglia, E., Leroux, A., 2007. Holocene climate changes in the central Mediterranean as recorded by lake-level fluctuations at Lake Accesa (Tuscany, Italy). Quat. Sci. Rev. 26 (13–14), 1736–1758. http://dx.doi.org/10.1016/j.quascirev.2007.04.014, URL: https://linkinghub.elsevier.com/retrieve/pii/S0277379107001114.

Magny, M., Peyron, O., Sadori, L., Ortu, E., Zanchetta, G., Vannière, B., Tinner, W., 2012. Contrasting patterns of precipitation seasonality during the Holocene in the south- and north-central Mediterranean. J. Quat. Sci. 27 (3), 290–296. http://dx.doi.org/10.1002/jqs.1543, URL: https://onlinelibrary.wiley.com/doi/10.1002/jqs.1543.

Magny, M., Vannière, B., Calo, C., Millet, L., Leroux, A., Peyron, O., Zanchetta, G., La Mantia, T., Tinner, W., 2011. Holocene hydrological changes in south-western Mediterranean as recorded by lake-level fluctuations at Lago Preola, a coastal lake in southern Sicily, Italy. Quat. Sci. Rev. 30 (19–20), 2459–2475. http://dx.doi.org/10.1016/j.quascirev.2011.05.018, URL: https://linkinghub.elsevier.com/retrieve/pii/S0277379111001648.

Manen, C., Perrin, T., Guilaine, J., Bouby, L., Bréhard, S., Briois, F., Durand, F., Marinval, P., Vigne, J.D., 2019. The neolithic transition in the western mediterranean: a complex and non-linear diffusion process—The radiocarbon record revisited. Radiocarbon 61 (2), 531–571. http://dx.doi.org/10.1017/RDC.2018.98, URL: https://www.cambridge.org/core/product/identifier/S003382221800098X/type/journal_article.

Marriner, N., Kaniewski, D., Pourkerman, M., Devillers, B., 2022. Anthropocene tipping point reverses long-term Holocene cooling of the mediterranean sea: A meta-analysis of the basin's sea surface temperature records. Earth-Sci. Rev. 227, 103986. http://dx.doi.org/10.1016/j.earscirev.2022.103986, URL: https://linkinghub.elsevier.com/retrieve/pii/S0012825222000708.

Martin, C., Ménot, G., Thouveny, N., Peyron, O., Andrieu-Ponel, V., Montade, V., Davtian, N., Reille, M., Bard, E., 2020. Early holocene thermal maximum recorded by branched tetraethers and pollen in Western Europe (massif central, France). Quat. Sci. Rev. 228, 106109. http://dx.doi.org/10.1016/j.quascirev.2019.106109, URL: https://linkinghub.elsevier.com/retrieve/pii/S0277379119307905.

Martínez-Sosa, P., Tierney, J.E., 2019. Lacustrine brGDGT response to microcosm and mesocosm incubations. Org. Geochem. 127, 12–22. http://dx.doi.org/10.1016/j.orggeochem.2018.10.011, URL: https://linkinghub.elsevier.com/retrieve/pii/S0146638018302468.

Martínez-Sosa, P., Tierney, J.E., Pérez-Angel, L.C., Stefanescu, I.C., Guo, J., Kirkels, F., Sepúlveda, J., Peterse, F., Shuman, B.N., Reyes, A.V., 2023. Development and application of the branched and isoprenoid GDGT machine learning classification algorithm (BIGMaC) for paleoenvironmental reconstruction. Paleoceanogr. Paleoclimatology 38 (7), e2023PA004611. http://dx.doi.org/10.1029/2023PA004611, URL: https://agupubs.onlinelibrary.wiley.com/doi/10.1029/2023PA004611.

Martínez-Sosa, P., Tierney, J.E., Stefanescu, I.C., Dearing Crampton-Flood, E., Shuman, B.N., Routson, C., 2021. A global Bayesian temperature calibration for lacustrine brGDGTs. Geochim. Cosmochim. Acta 305, 87–105. http://dx.doi.org/10.1016/j.gca.2021.04.038, URL: https://linkinghub.elsevier.com/retrieve/pii/S0016703721002635.

Marzocchella, A., Calderoni, G., Nisbet, R., 1994. Sarno e frattaminore: evidenze degli abitati. In: L'eruzione vesuviana delle "Pomici di Avellino" e la facies di Palma Campania (Bronzo Antico). Atti del seminario internazionale di Ravello, Bari, Edipuglia, pp. 15–17.

Mauri, A., Davis, B., Collins, P., Kaplan, J., 2015. The climate of Europe during the Holocene: a gridded pollen-based reconstruction and its multi-proxy evaluation. Quat. Sci. Rev. 112, 109–127. http://dx.doi.org/10.1016/j.quascirev.2015.01.013, URL: https://linkinghub.elsevier.com/retrieve/pii/S0277379115000372.

Menviel, L., Govin, A., Avenas, A., Meissner, K.J., Grant, K.M., Tzedakis, P.C., 2021. Drivers of the evolution and amplitude of African humid periods. Commun. Earth Environ. 2 (1), 237. http://dx.doi.org/10.1038/s43247-021-00309-1, URL: https://www.nature.com/articles/s43247-021-00309-1.

Moncel, M.H., Santagata, C., Pereira, A., Nomade, S., Voinchet, P., Bahain, J.J., Daujeard, C., Curci, A., Lemorini, C., Hardy, B., Eramo, G., Berto, C., Raynal, J.P., Arzarello, M., Mecozzi, B., Iannucci, A., Sardella, R., Allegretta, I., Delluniversità, E., Terzano, R., Dugas, P., Jouanic, G., Queffelec, A., d'Andrea, A., Valentini, R., Minucci, E., Carpentiero, L., Piperno, M., 2020. The origin of early acheulean expansion in Europe 700 ka ago: new findings at notarchirico (Italy). Sci. Rep. 10 (1), 13802. http://dx.doi.org/10.1038/s41598-020-68617-8, URL: https://www.nature.com/articles/s41598-020-68617-8.

Moore, P.D., Webb, J.A., Collison, M.E., 1991. Pollen Analysis. Blackwell Scientific Publications, Oxford, viii + 216 pp.

Mustaphi, C.J.C., Pisaric, M.F., 2014. A classification for macroscopic charcoal morphologies found in Holocene lacustrine sediments. Prog. Phys. Geogr.: Earth Environ. 38 (6), 734–754. http://dx.doi.org/10.1177/0309133314548886, URL: https://journals.sagepub.com/doi/10.1177/0309133314548886.

Naafs, B., Gallego-Sala, A., Inglis, G., Pancost, R., 2017a. Refining the global branched glycerol dialkyl glycerol tetraether (brGDGT) soil temperature calibration. Org. Geochem. 106, 48–56. http://dx.doi.org/10.1016/j.orggeochem.2017.01.009, URL: https://linkinghub.elsevier.com/retrieve/pii/S0146638016301930.

Naafs, B., Inglis, G., Zheng, Y., Amesbury, M., Biester, H., Bindler, R., Blewett, J., Burrows, M., del Castillo Torres, D., Chambers, F., Cohen, A., Evershed, R., Feakins, S., Gałka, M., Gallego-Sala, A., Gandois, L., Gray, D., Hatcher, P., Honorio Coronado, E., Hughes, P., Huguet, A., Könönen, M., Laggoun-Défarge, F., Lähteenoja, O., Lamentowicz, M., Marchant, R., McClymont, E., Pontevedra-Pombal, X., Ponton, C., Pourmand, A., Rizzuti, A., Rochefort, L., Schellekens, J., De Vleeschouwer, F., Pancost, R., 2017b. Introducing global peat-specific temperature and pH calibrations based on brGDGT bacterial lipids. Geochim. Cosmochim. Acta 208, 285–301. http://dx.doi.org/10.1016/j.gca.2017.01.038, URL: https://linkinghub.elsevier.com/retrieve/pii/S0016703717300522.

Narcisi, B., 1996. Tephrochronology of a late quaternary lacustrine record from the Monticchio maar (Vulture volcano, southern Italy). Quat. Sci. Rev. 15 (2), 155–165. http://dx.doi.org/10.1016/0277-3791(95)00045-3, URL: https://www.sciencedirect.com/science/article/pii/0277379195000453.

Newton, A.J., Dugmore, A.J., 1993. Tephrochronology of core C from lago grande di Monticchio. In: Negendank, J.F.W., Zolitschka, B. (Eds.), Paleolimnology of European Maar Lakes. Springer, Berlin, Heidelberg, pp. 333–348. http://dx.doi.org/10.1007/BFb0117605.

Nimmergut, A.P., Allen, J.R.M., Jones, V.J., Huntley, B., Battarbee, R.W., 1999. Submillennial environmental fluctuations during marine oxygen isotope stage 2: a comparative analysis of diatom and pollen evidence from lago grande di monticchio, south Italy. J. Quat. Sci. 14 (2), 111–123. http://dx.doi.org/10.1002/(SICI)1099-1417(199903)14:2<111::AID-JQS427>3.0.CO;2-A, URL: https://onlinelibrary.wiley.com/doi/10.1002/(SICI)1099-1417(199903)14:2<111::AID-JQS427>3.0.CO;2-A.

NOAA National Centers for Environmental Information, 2022. ETOPO 2022 15 arc-second global relief model. http://dx.doi.org/10.25921/fd45-gt74, NOAA National Centers for Environmental Information, (Accessed September 2023).

Novak, J.B., Russell, J.M., Lindemuth, E.R., Prokopenko, A.A., Pérez-Angel, L., Zhao, B., Swann, G.E.A., Polissar, P.J., 2025. The branched GDGT isomer ratio refines lacustrine paleotemperature estimates. Geochem. Geophys. Geosystems 26 (3), e2024GC012069. http://dx.doi.org/10.1029/2024GC012069, URL: https://agupubs.onlinelibrary.wiley.com/doi/10.1029/2024GC012069.

Olsen, J., Anderson, N.J., Knudsen, M.F., 2012. Variability of the north atlantic oscillation over the past 5,200 years. Nat. Geosci. 5 (11), 808–812. http://dx.doi.org/10.1038/ngeo1589, URL: https://www.nature.com/articles/ngeo1589.

Oris, F., Ali, A.A., Asselin, H., Paradis, L., Bergeron, Y., Finsinger, W., 2014. Charcoal dispersion and deposition in boreal lakes from 3 years of monitoring: Differences between local and regional fires. Geophys. Res. Lett. 41 (19), 6743–6752. http://dx.doi.org/10.1002/2014GL060984, URL: https://onlinelibrary.wiley.com/doi/abs/10.1002/2014GL060984.

Otiniano, G.A., Porter, T.J., Phillips, M.A., Juutinen, S., Weckström, J.B., Heikkilä, M.P., 2024. Reconstructing warm-season temperatures using brGDGTs and assessing biases in holocene temperature records in northern Fennoscandia. Quat. Sci. Rev. 329, 108555. http://dx.doi.org/10.1016/j.quascirev.2024.108555, URL: https://www.sciencedirect.com/science/article/pii/S0277379124000568.

Passariello, I., Lubritto, C., D'Onofrio, A., Guan, Y., Terrasi, F., 2010. The somma–vesuvius complex and the phlaegrean fields caldera: New chronological data of several eruptions of the copper–middle bronze age period. Nucl. Instruments Methods Phys. Res. Sect. B: Beam Interactions Mater. Atoms 268 (7–8), 1008–1012. http://dx.doi.org/10.1016/j.nimb.2009.10.085.

Paterne, M., Guichard, F., Labeyrie, J., 1988. Explosive activity of the south Italian volcanoes during the past 80,000 years as determined by marine tephrochronology. J. Volcanol. Geotherm. Res. 34 (3), 153–172. http://dx.doi.org/10.1016/0377-0273(88)90030-3, URL: https://www.sciencedirect.com/science/article/pii/0377027388900303.

Pedrotta, T., Gobet, E., Schwörer, C., Beffa, G., Butz, C., Henne, P.D., Morales-Molino, C., Pasta, S., Van Leeuwen, J.F.N., Vogel, H., Zwimpfer, E., Anselmetti, F.S., Grosjean, M., Tinner, W., 2021. 8,000 years of climate, vegetation, fire and land-use dynamics in the thermo-mediterranean vegetation belt of northern Sardinia (Italy). Veg. Hist. Archaeobotany 30 (6), 789–813. http://dx.doi.org/10.1007/s00334-021-00832-3, URL: https://link.springer.com/10.1007/s00334-021-00832-3.

Pereira, A., Moncel, M.H., Nomade, S., Voinchet, P., Shao, Q., Falguères, C., Lefèvre, D., Raynal, J.P., Scao, V., Piperno, M., Simone, S., Bahain, J.J., 2024. Update and synthesis of the available archaeological and geochronological data for the lower paleolithic site of loreto at venosa (Basilicata, Italy). Quat. Res. 119, 12–27. http://dx.doi.org/10.1017/qua.2023.71, URL: https://www.cambridge.org/core/product/identifier/S0033589423000716/type/journal_article.

Perrin, T., Binder, D., 2011. Le mésolithique à trapèzes et la néolithisation de l'europe sud-occidentale. In: Manen, C., Perrin, T., Guilaine, J. (Eds.), la Transition NÉolithique En MÉditerranÉe. Actes Du Colloque Transitions En MÉditerranÉe, Ou Comment Des Chasseurs Devinrent Agriculteurs, MusÉum de Toulouse. Errance et Archives d'Ecologie Préhistorique, Toulouse, France, pp. 271–281, URL: https://hal.science/hal-01009471.

Peterse, F., van der Meer, J., Schouten, S., Weijers, J.W., Fierer, N., Jackson, R.B., Kim, J.H., Sinninghe Damsté, J.S., 2012. Revised calibration of the MBT–CBT paleotemperature proxy based on branched tetraether membrane lipids in surface soils. Geochim. Cosmochim. Acta 96, 215–229. http://dx.doi.org/10.1016/j.gca.2012.08.011, URL: https://linkinghub.elsevier.com/retrieve/pii/S0016703712004589.

Petrosino, P., Arienzo, I., Mazzeo, F.C., Natale, J., Petrelli, M., Milia, A., Perugini, D., D'Antonio, M., 2019. The San Gregorio Magno lacustrine basin (Campania, southern Italy): improved characterization of the tephrostratigraphic markers based on trace elements and isotopic data. J. Quat. Sci. 34 (6), 393–404. http://dx.doi.org/10.1002/jqs.3107, URL: https://onlinelibrary.wiley.com/doi/abs/10.1002/jqs.3107, _eprint: https://onlinelibrary.wiley.com/doi/pdf/10.1002/jqs.3107.

Peyron, O., Bégeot, C., Brewer, S., Heiri, O., Magny, M., Millet, L., Ruffaldi, P., Van Campo, E., Yu, G., 2005. Late-glacial climatic changes in eastern France (Lake Lautrey) from pollen, lake-levels, and chironomids. Quat. Res. 64 (2), 197–211. http://dx.doi.org/10.1016/j.yqres.2005.01.006, URL: https://www.cambridge.org/core/product/identifier/S0033589400027198/type/journal_article.

Peyron, O., Combourieu-Nebout, N., Brayshaw, D., Goring, S., Andrieu-Ponel, V., Desprat, S., Fletcher, W., Gambin, B., Ioakim, C., Joannin, S., Kotthoff, U., Kouli, K., Montade, V., Pross, J., Sadori, L., Magny, M., 2017. Precipitation changes in the Mediterranean basin during the Holocene from terrestrial and marine pollen records: a model–data comparison. Clim. Past 13 (3), 249–265. http://dx.doi.org/10.5194/cp-13-249-2017, URL: https://cp.copernicus.org/articles/13/249/2017/.

Peyron, O., Goring, S., Dormoy, I., Kotthoff, U., Pross, J., de Beaulieu, J.L., Drescher-Schneider, R., Vannière, B., Magny, M., 2011. Holocene seasonality changes in the central Mediterranean region reconstructed from the pollen sequences of lake Accesa (Italy) and Tenaghi Philippon (Greece). Holocene 21 (1), 131–146. http://dx.doi.org/10.1177/0959683610384162, URL: http://journals.sagepub.com/doi/10.1177/0959683610384162.

Peyron, O., Magny, M., Goring, S., Joannin, S., de Beaulieu, J.L., Brugiapaglia, E., Sadori, L., Garfi, G., Kouli, K., Ioakim, C., Combourieu-Nebout, N., 2013. Contrasting patterns of climatic changes during the Holocene across the Italian Peninsula reconstructed from pollen data. Clim. Past 9 (3), 1233–1252. http://dx.doi.org/10.5194/cp-9-1233-2013, URL: https://cp.copernicus.org/articles/9/1233/2013/.

Raberg, J.H., De Wet, G.A., Geirsdóttir, Á., Sepúlveda, J., Miller, G.H., 2025. Oxygen depletion in lake waters may skew brGDGT-inferred temperatures by more than 10°C. Geophys. Res. Lett. 52 (15), e2024GL113562. http://dx.doi.org/10.1029/2024GL113562, URL: https://agupubs.onlinelibrary.wiley.com/doi/10.1029/2024GL113562.

Raberg, J.H., Harning, D.J., Crump, S.E., de Wet, G., Blumm, A., Kopf, S., Geirsdóttir, Á., Miller, G.H., Sepúlveda, J., 2021. Revised fractional abundances and warm-season temperatures substantially improve brGDGT calibrations in lake sediments. Biogeosciences 18 (12), 3579–3603. http://dx.doi.org/10.5194/bg-18-3579-2021, URL: https://bg.copernicus.org/articles/18/3579/2021/.

Radić, D., 2007. Napuljski žuti tuf (NYT) iz pleistocenskih naslaga u Veloj spili na Korčuli: dragocjeni marker prijelaza iz paleolitika u mezolitik. Opvscvla Archaeol. 31 (1), 7–26.

Ramrath, A., Zolitschka, B., Wulf, S., Negendank, J.F., 1999. Late Pleistocene climatic variations as recorded in two Italian maar lakes (Lago di mezzano, lago grande di monticchio). Quat. Sci. Rev. 18 (7), 977–992. http://dx.doi.org/10.1016/S0277-3791(99)00009-8, URL: https://linkinghub.elsevier.com/retrieve/pii/S0277379199000098.

Regattieri, E., Giaccio, B., Zanchetta, G., Drysdale, R.N., Galli, P., Nomade, S., Peronace, E., Wulf, S., 2015. Hydrological variability over the apennines during the early last glacial precession minimum, as revealed by a stable isotope record from sulmona basin, central Italy. J. Quat. Sci. 30 (1), 19–31. http://dx.doi.org/10.1002/jqs.2755, URL: https://onlinelibrary.wiley.com/doi/abs/10.1002/jqs.2755, _eprint: https://onlinelibrary.wiley.com/doi/pdf/10.1002/jqs.2755.

Regattieri, E., Zanchetta, G., Drysdale, R.N., Isola, I., Hellstrom, J.C., Dallai, L., 2014. Lateglacial to holocene trace element record (Ba, Mg, Sr) from corchia cave (apuan alps, central Italy): paleoenvironmental implications: Trace element record from corchia cave, central Italy. J. Quat. Sci. 29 (4), 381–392. http://dx.doi.org/10.1002/jqs.2712, URL: https://onlinelibrary.wiley.com/doi/10.1002/jqs.2712.

Reille, M., 1992. Pollen et spores d'Europe et d'Afrique du Nord, second ed. Laboratoire de Botanique historique et Palynologie.

Reimer, P.J., Austin, W.E.N., Bard, E., Bayliss, A., Blackwell, P.G., Bronk Ramsey, C., Butzin, M., Cheng, H., Edwards, R.L., Friedrich, M., Grootes, P.M., Guilderson, T.P., Hajdas, I., Heaton, T.J., Hogg, A.G., Hughen, K.A., Kromer, B., Manning, S.W., Muscheler, R., Palmer, J.G., Pearson, C., van der Plicht, J., Reimer, R.W., Richards, D.A., Scott, E.M., Southon, J.R., Turney, C.S.M., Wacker, L., Adolphi, F., Büntgen, U., Capano, M., Fahrni, S.M., Fogtmann-Schulz, A., Friedrich, R., Köhler, P., Kudsk, S., Miyake, F., Olsen, J., Reinig, F., Sakamoto, M., Sookdeo, A., Talamo, S., 2020. The IntCal20 northern hemisphere radiocarbon age calibration curve (0–55 cal kBP). Radiocarbon 62 (4), 725–757. http://dx.doi.org/10.1017/RDC.2020.41, URL: https://www.cambridge.org/core/product/identifier/S0033822220000417/type/journal_article.

Reschke, M., Kunz, T., Laepple, T., 2019. Comparing methods for analysing time scale dependent correlations in irregularly sampled time series data. Comput. Geosci. 123, 65–72. http://dx.doi.org/10.1016/j.cageo.2018.11.009, URL: https://linkinghub.elsevier.com/retrieve/pii/S0098300418304308.

Reschke, M., Laepple, T., 2024. corit: time scale dependent correlation of irregular time series. R package version 0.0.0.9000, commit adb0d55bcbdda52ba1691ac44971c36901c936fc, URL: https://github.com/EarthSystemDiagnostics/corit.

Roberts, N., Brayshaw, D., Kuzucuoğlu, C., Perez, R., Sadori, L., 2011. The mid-holocene climatic transition in the mediterranean: Causes and consequences. Holocene 21 (1), 3–13. http://dx.doi.org/10.1177/0959683610388058, URL: http://journals.sagepub.com/doi/10.1177/0959683610388058.

Robinson, C., 1994. Lago Grande di Monticchio, southern Italy: a long record of environmental change illustrated by sediment geochemistry. Chem. Geol. 118 (1–4), 235–254. http://dx.doi.org/10.1016/0009-2541(94)90179-1, URL: https://linkinghub.elsevier.com/retrieve/pii/0009254194901791.

Robles, M., Peyron, O., Brugiapaglia, E., Ménot, G., Dugerdil, L., Ollivier, V., Ansanay-Alex, S., Develle, A.-L., Tozalakyan, P., Meliksetian, K., Sahakyan, K., Sahakyan, L., Perello, B., Badalyan, R., Colombié, C., Joannin, S., 2022. Impact of climate changes on vegetation and human societies during the Holocene in the south caucasus (vanevan, armenia): A multiproxy approach including pollen, NPPs and brGDGTs. Quat. Sci. Rev. 277, 107297. http://dx.doi.org/10.1016/j.quascirev.2021.107297, URL: https://linkinghub.elsevier.com/retrieve/pii/S0277379121005047.

Robles, M., Peyron, O., Ménot, G., Brugiapaglia, E., Wulf, S., Appelt, O., Blache, M., Vannière, B., Dugerdil, L., Paura, B., Ansanay-Alex, S., Cromartie, A., Charlet, L., Guédron, S., De Beaulieu, J.-L., Joannin, S., 2023. Climate changes during the late glacial in southern Europe: new insights based on pollen and brGDGTs of lake matese in Italy. Clim. Past 19 (2), 493–515. http://dx.doi.org/10.5194/cp-19-493-2023, URL: https://cp.copernicus.org/articles/19/493/2023/.

Rocca, R., Giannandrea, P., Pereira, A., Bahain, J.J., Boschin, F., Da Costa, A., Di Rita, F., Fouriaux, F., Iannucci, A., Germond, L., Gioia, D., Magri, D., Mecozzi, B., Nomade, S., Sardella, R., Schiattarella, M., Voinchet, P., Aureli, D., 2023. Multidisciplinary study of the lower palaeolithic site of cimitero di atella (Basilicata), Italy. Quat. Int. 676, 1–26. http://dx.doi.org/10.1016/j.quaint.2023.09.004, URL: https://linkinghub.elsevier.com/retrieve/pii/S104061822300277X.

Rodrigo-Gámiz, M., García-Alix, A., Jiménez-Moreno, G., Ramos-Román, M.J., Camuera, J., Toney, J.L., Sachse, D., Anderson, R.S., Sinninghe Damsté, J.S., 2022. Paleoclimate reconstruction of the last 36 kyr based on branched glycerol dialkyl glycerol tetraethers in the Padul palaeolake record (Sierra Nevada, southern Iberian Peninsula). Quat. Sci. Rev. 281, 107434. http://dx.doi.org/10.1016/j.quascirev.2022.107434, URL: https://linkinghub.elsevier.com/retrieve/pii/S0277379122000658.

Rolandi, G., Petrosino, P., Mc Geehin, J., 1998. The interplinian activity at Somma–Vesuvius in the last 3500 years. J. Volcanol. Geotherm. Res. 82 (1–4), 19–52. http://dx.doi.org/10.1016/S0377-0273(97)00056-5.

RStudio Team, 2020. RStudio: Integrated Development Environment for R. RStudio, PBC, Boston, MA, URL: http://www.rstudio.com/.

Russell, J.M., Hopmans, E.C., Loomis, S.E., Liang, J., Sinninghe Damsté, J.S., 2018. Distributions of 5- and 6-methyl branched glycerol dialkyl glycerol tetraethers (brGDGTs) in east African lake sediment: Effects of temperature, pH, and new lacustrine paleotemperature calibrations. Org. Geochem. 117, 56–69. http://dx.doi.org/10.1016/j.orggeochem.2017.12.003, URL: https://linkinghub.elsevier.com/retrieve/pii/S0146638017304394.

Russo Ermolli, E., Di Lorenzo, H., Santangelo, N., Santo, A., Comegna, C., Petrosino, P., 2024. Unravelling 6000 years of interplay among environmental changes, anthropogenic activities, and vesuvius eruptions in the upper Sarno plain (Campania, Italy). Quat. Res. 122, 18–39. http://dx.doi.org/10.1017/qua.2024.30.

Sadori, L., Jahns, S., Peyron, O., 2011. Mid-holocene vegetation history of the central Mediterranean. Holocene 21 (1), 117–129. http://dx.doi.org/10.1177/0959683610377530, URL: http://journals.sagepub.com/doi/10.1177/0959683610377530.

Salonen, J.S., Korpela, M., Williams, J.W., Luoto, M., 2019. Machine-learning based reconstructions of primary and secondary climate variables from north American and European fossil pollen data. Sci. Rep. 9 (1), 15805. http://dx.doi.org/10.1038/s41598-019-52293-4, URL: http://www.nature.com/articles/s41598-019-52293-4.

Salonen, J.S., Seppä, H., Luoto, M., Bjune, A.E., Birks, H.J.B., 2012. A north European pollen–climate calibration set: analysing the climatic responses of a biological proxy using novel regression tree methods. Quat. Sci. Rev. 45, 95–110. http://dx.doi.org/10.1016/j.quascirev.2012.05.003, URL: https://linkinghub.elsevier.com/retrieve/pii/S0277379112001849.

Samartin, S., Heiri, O., Joos, F., Renssen, H., Franke, J., Brönnimann, S., Tinner, W., 2017. Warm Mediterranean mid-Holocene summers inferred from fossil midge assemblages. Nat. Geosci. 10 (3), 207–212. http://dx.doi.org/10.1038/ngeo2891, URL: http://www.nature.com/articles/ngeo2891.

Sanchi, L., Ménot, G., Bard, E., 2015. Environmental controls on paleo-pH at mid-latitudes: A case study from central and eastern Europe. Palaeogeogr. Palaeoclimatol. Palaeoecol. 417, 458–466. http://dx.doi.org/10.1016/j.palaeo.2014.10.007, URL: https://linkinghub.elsevier.com/retrieve/pii/S0031018214004945.

Santacroce, R., Cioni, R., Marianelli, P., Sbrana, A., Sulpizio, R., Zanchetta, G., Donahue, D.J., Joron, J.L., 2008. Age and whole rock–glass compositions of proximal pyroclastics from the major explosive eruptions of Somma-Vesuvius: A review as a tool for distal tephrostratigraphy. J. Volcanol. Geotherm. Res. 177 (1), 1–18. http://dx.doi.org/10.1016/j.jvolgeores.2008.06.009.

Sassoon, D., Combourieu-Nebout, N., Peyron, O., Bertini, A., Toti, F., Lebreton, V., Moncel, M.H., 2025. Pollen-based climatic reconstructions for the interglacial analogues of MIS 1 (MIS 19, 11, and 5) in the southwestern mediterranean: insights from ODP site 976. Clim. Past 21 (2), 489–515. http://dx.doi.org/10.5194/cp-21-489-2025, URL: https://cp.copernicus.org/articles/21/489/2025/.

Schmidt, R., Van Den Bogaard, C., Merkt, J., Müller, J., 2002. A new lateglacial chronostratigraphic tephra marker for the south-eastern alps: The neapolitan yellow tuff (NYT) in Längsee (Austria) in the context of a regional biostratigraphy and palaeoclimate. Quat. Int. 88 (1), 45–56. http://dx.doi.org/10.1016/S1040-6182(01)00072-6, URL: https://linkinghub.elsevier.com/retrieve/pii/S1040618201000726.

Schneider, C.A., Rasband, W.S., Eliceiri, K.W., 2012. NIH image to ImageJ: 25 years of image analysis. Nature Methods 9 (7), 671–675. http://dx.doi.org/10.1038/nmeth.2089, Publisher: Nature Publishing Group, URL: https://www.nature.com/articles/nmeth.2089.

Schouten, S., Hopmans, E.C., Sinninghe Damsté, J.S., 2013. The organic geochemistry of glycerol dialkyl glycerol tetraether lipids: A review. Org. Geochem. 54, 19–61. http://dx.doi.org/10.1016/j.orggeochem.2012.09.006, URL: https://www.sciencedirect.com/science/article/pii/S0146638012001982.

Schulz, M., Prange, M., Klocker, A., 2007. Low-frequency oscillations of the Atlantic Ocean meridional overturning circulation in a coupled climate model. Clim. Past 3, 97–107. http://dx.doi.org/10.5194/cp-3-97-2007.

Seo, K.H., Yoon, S.P., Lu, J., Hu, Y., Staten, P.W., Frierson, D.M.W., 2023. What controls the interannual variation of hadley cell extent in the northern Hemisphere: physical mechanism and empirical model for edge variation. Npj Clim. Atmospheric Sci. 6 (1), 204. http://dx.doi.org/10.1038/s41612-023-00533-w, URL: https://www.nature.com/articles/s41612-023-00533-w.

Sevink, J., Bakels, C., Van Hall, R., Dee, M., 2021. Radiocarbon dating distal tephra from the early bronze age avellino eruption (EU-5) in the coastal basins of southern lazio (Italy): Uncertainties, results, and implications for dating distal tephra. Quat. Geochronol. 63, 101154. http://dx.doi.org/10.1016/j.quageo.2021.101154.

Shanahan, T.M., McKay, N.P., Hughen, K.A., Overpeck, J.T., Otto-Bliesner, B., Heil, C.W., King, J., Scholz, C.A., Peck, J., 2015. The time-transgressive termination of the African humid period. Nat. Geosci. 8 (2), 140–144. http://dx.doi.org/10.1038/ngeo2329, URL: https://www.nature.com/articles/ngeo2329.

Siani, G., Sulpizio, R., Paterne, M., Sbrana, A., 2004. Tephrostratigraphy study for the last 18,000 14C years in a deep-sea sediment sequence for the south Adriatic. Quat. Sci. Rev. 23 (23), 2485–2500. http://dx.doi.org/10.1016/j.quascirev.2004.06.004.

Silvestri, L., Saraceni, M., Bongioannini Cerlini, P., 2022. Links between precipitation, circulation weather types and orography in central Italy. Int. J. Climatol. 42 (11), 5807–5825. http://dx.doi.org/10.1002/joc.7563, URL: https://rmets.onlinelibrary.wiley.com/doi/10.1002/joc.7563.

Smith, V.C., Isaia, R., Pearce, N.J.G., 2011. Tephrostratigraphy and glass compositions of post-15 kyr Campi Flegrei eruptions: implications for eruption history and chronostratigraphic markers. Quat. Sci. Rev. 30 (25), 3638–3660. http://dx.doi.org/10.1016/j.quascirev.2011.07.012.

Smith, A.C., Wynn, P.M., Barker, P.A., Leng, M.J., Noble, S.R., Tych, W., 2016. North Atlantic forcing of moisture delivery to Europe throughout the Holocene. Sci. Rep. 6 (1), 24745. http://dx.doi.org/10.1038/srep24745, URL: http://www.nature.com/articles/srep24745.

Sulpizio, R., Bonasia, R., Dellino, P., Di Vito, M.A., La Volpe, L., Mele, D., Zanchetta, G., Sadori, L., 2008. Discriminating the long distance dispersal of fine ash from sustained columns or near ground ash clouds: The example of the pomici di Avellino eruption (Somma-Vesuvius, Italy). J. Volcanol. Geotherm. Res. 177 (1), 263–276. http://dx.doi.org/10.1016/j.jvolgeores.2007.11.012.

Sulpizio, R., Cioni, R., Di Vito, M.A., Mele, D., Bonasia, R., Dellino, P., 2010. The pomici di avellino eruption of Somma-Vesuvius (3.9 ka bp). Part I: stratigraphy, compositional variability and eruptive dynamics. Bull. Volcanol. 72 (5), 539–558. http://dx.doi.org/10.1007/s00445-009-0339-x.

Sun, C., Li, J., Jin, F.F., 2015. A delayed oscillator model for the quasi-periodic multidecadal variability of the NAO. Clim. Dyn. 45 (7–8), 2083–2099. http://dx.doi.org/10.1007/s00382-014-2459-z, URL: https://link.springer.com/10.1007/s00382-014-2459-z.

Thornalley, D.J.R., Barker, S., Broecker, W.S., Elderfield, H., McCave, I.N., 2011. The deglacial evolution of north atlantic deep convection. Science 331 (6014), 202–205. http://dx.doi.org/10.1126/science.1196812, URL: https://www.science.org/doi/10.1126/science.1196812.

Tierney, J.E., Russell, J.M., 2009. Distributions of branched GDGTs in a tropical lake system: Implications for lacustrine application of the MBT/CBT paleoproxy. Org. Geochem. 40 (9), 1032–1036. http://dx.doi.org/10.1016/j.orggeochem.2009.04.014, URL: https://linkinghub.elsevier.com/retrieve/pii/S0146638009000989.

Tierney, J.E., Russell, J.M., Eggermont, H., Hopmans, E., Verschuren, D., Sinninghe Damste, J., 2010. Environmental controls on branched tetraether lipid distributions in tropical east African lake sediments. Geochim. Cosmochim. Acta 74, 4902–4918. http://dx.doi.org/10.1016/j.gca.2010.06.002.

Tinner, W., Hu, F.S., Beer, R., Kaltenrieder, P., Scheurer, B., Krähenbühl, U., 2006. Postglacial vegetational and fire history: pollen, plant macrofossil and charcoal records from two Alaskan lakes. Veg. Hist. Archaeobotany 15 (4), 279–293. http://dx.doi.org/10.1007/s00334-006-0052-z.

Tomlinson, E.L., Smith, V.C., Albert, P.G., Aydar, E., Civetta, L., Cioni, R., Çubukçu, E., Gertisser, R., Isaia, R., Menzies, M.A., Orsi, G., Rosi, M., Zanchetta, G., 2015. The major and trace element glass compositions of the productive Mediterranean volcanic sources: tools for correlating distal tephra layers in and around Europe. Quat. Sci. Rev. 118, 48–66. http://dx.doi.org/10.1016/j.quascirev.2014.10.028.

Totaro, F., Insinga, D.D., Lirer, F., Margaritelli, G., Caparrós, A.C.i., de la Fuente, M., Petrosino, P., 2022. The late pleistocene to holocene tephra record of ND14Q site (southern adriatic sea): Traceability and preservation of neapolitan explosive products in the marine realm. J. Volcanol. Geotherm. Res. 423, 107461. http://dx.doi.org/10.1016/j.jvolgeores.2021.107461.

Tramblay, Y., Koutroulis, A., Samaniego, L., Vicente-Serrano, S.M., Volaire, F., Boone, A., Le Page, M., Llasat, M.C., Albergel, C., Burak, S., Cailleret, M., Kalin, K.C., Davi, H., Dupuy, J.L., Greve, P., Grillakis, M., Hanich, L., Jarlan, L., Martin-StPaul, N., Martínez-Vilalta, J., Mouillot, F., Pulido-Velazquez, D., Quintana-Seguí, P., Renard, D., Turco, M., Türkeş, M., Trigo, R., Vidal, J.P., Vilagrosa, A., Zribi, M., Polcher, J., 2020. Challenges for drought assessment in the mediterranean region under future climate scenarios. Earth-Sci. Rev. 210, 103348. http://dx.doi.org/10.1016/j.earscirev.2020.103348, URL: https://linkinghub.elsevier.com/retrieve/pii/S0012825220303949.

Turton, I., 1993. Palaeomagnetic investigations of lago grande di monticchio, southern Italy. In: Negendank, J.F.W., Zolitschka, B. (Eds.), Paleolimnology of European Maar Lakes. Springer, Berlin, Heidelberg, pp. 377–392. http://dx.doi.org/10.1007/BFb0117608.

Tyler, J.J., Nederbragt, A.J., Jones, V.J., Thurow, J.W., 2010. Assessing past temperature and soil pH estimates from bacterial tetraether membrane lipids: Evidence from the recent lake sediments of Lochnagar, Scotland. J. Geophys. Res. 115, http://dx.doi.org/10.1029/2009JG001109.

Umbanhowar, C.E., Mcgrath, M.J., 1998. Experimental production and analysis of microscopic charcoal from wood, leaves and grasses. Holocene 8 (3), 341–346. http://dx.doi.org/10.1191/095968398666496051, URL: https://journals.sagepub.com/doi/10.1191/095968398666496051.

Vannière, B., Bossuet, G., Walter-Simonnet, A.V., Gauthier, E., Barral, P., Petit, C., Buatier, M., Daubigney, A., 2003. Land use change, soil erosion and alluvial dynamic in the lower doubs valley over the 1st millenium AD (Neublans, Jura, France). J. Archaeol. Sci. 30 (10), 1283–1299. http://dx.doi.org/10.1016/S0305-4403(03)00017-7, URL: https://linkinghub.elsevier.com/retrieve/pii/S0305440303000177.

Vannière, B., Colombaroli, D., Chapron, E., Leroux, A., Tinner, W., Magny, M., 2008. Climate versus human-driven fire regimes in mediterranean landscapes: the holocene record of lago dell'accesa (tuscany, Italy). Quat. Sci. Rev. 27 (11–12), 1181–1196. http://dx.doi.org/10.1016/j.quascirev.2008.02.011, URL: https://linkinghub.elsevier.com/retrieve/pii/S0277379108000620.

Vannière, B., Power, M., Roberts, N., Tinner, W., Carrión, J., Magny, M., Bartlein, P., Colombaroli, D., Daniau, A., Finsinger, W., Gil-Romera, G., Kaltenrieder, P., Pini, R., Sadori, L., Turner, R., Valsecchi, V., Vescovi, E., 2011. Circum-mediterranean fire activity and climate changes during the mid-holocene environmental transition (8500-2500 cal. BP). Holocene 21 (1), 53–73. http://dx.doi.org/10.1177/0959683610384164, URL: https://journals.sagepub.com/doi/10.1177/0959683610384164.

Versteegh, G.J.M., Leeuw, J.W.d., Taricco, C., Romero, A., 2007. Alkenone-derived UK'37 data and sea surface temperatures (SST) of a combined sediment core. http://dx.doi.org/10.1594/PANGAEA.789691, Type: dataset.

Villa, I.M., Buettner, A., 2009. Chronostratigraphy of Monte Vulture volcano (southern Italy): secondary mineral microtextures and 39Ar-40Ar systematics. Bull. Volcanol. 71 (10), 1195–1208. http://dx.doi.org/10.1007/s00445-009-0294-6.

Wang, X., Li, J., Sun, C., Liu, T., 2017. NAO and its relationship with the northern hemisphere mean surface temperature in CMIP5 simulations. J. Geophys. Res.: Atmospheres 122 (8), 4202–4227. http://dx.doi.org/10.1002/2016JD025979, URL: https://agupubs.onlinelibrary.wiley.com/doi/10.1002/2016JD025979.

Wang, H., Liu, W., He, Y., Zhou, A., Zhao, H., Liu, H., Cao, Y., Hu, J., Meng, B., Jiang, J., Kolpakova, M., Krivonogov, S., Liu, Z., 2021. Salinity-controlled isomerization of lacustrine brGDGTs impacts the associated MBT'5ME terrestrial temperature index. Geochim. Cosmochim. Acta 305, 33–48. http://dx.doi.org/10.1016/j.gca.2021.05.004, URL: https://www.sciencedirect.com/science/article/pii/S0016703721002672.

Wanner, H., Beer, J., Bütikofer, J., Crowley, T.J., Cubasch, U., Flückiger, J., Goosse, H., Grosjean, M., Joos, F., Kaplan, J.O., Küttel, M., Müller, S.A., Prentice, I.C., Solomina, O., Stocker, T.F., Tarasov, P., Wagner, M., Widmann, M., 2008. Mid- to late holocene climate change: an overview. Quat. Sci. Rev. 27 (19–20), 1791–1828. http://dx.doi.org/10.1016/j.quascirev.2008.06.013, URL: https://linkinghub.elsevier.com/retrieve/pii/S0277379108001479.

Wanner, H., Solomina, O., Grosjean, M., Ritz, S.P., Jetel, M., 2011. Structure and origin of Holocene cold events. Quat. Sci. Rev. 30 (21–22), 3109–3123. http://dx.doi.org/10.1016/j.quascirev.2011.07.010, URL: https://linkinghub.elsevier.com/retrieve/pii/S0277379111002149.

Watts, W.A., 1985. A long pollen record from Laghi di Monticchio, southern Italy: a preiminary account. J. Geol. Soc. 142 (3), 491–499. http://dx.doi.org/10.1144/gsjgs.142.3.0491.

Watts, W.A., Allen, J.R.M., Huntley, B., 1996a. Vegetation history and palaeoclimate of the last glacial period at Lago Grande di Monticchio, Southern Italy. Quat. Sci. Rev. 15 (2–3), 133–153. http://dx.doi.org/10.1016/0277-3791(95)00093-3.

Watts, W., Allen, J., Huntley, B., 2000. Palaeoecology of three interstadial events during oxygen-isotope stages 3 and 4: a lacustrine record from Lago Grande di Monticchio, southern Italy. Palaeogeogr. Palaeoclimatol. Palaeoecol. 155 (1–2), 83–93. http://dx.doi.org/10.1016/S0031-0182(99)00096-6, URL: https://linkinghub.elsevier.com/retrieve/pii/S0031018299000966.

Watts, W., Allen, J.R.M., Huntley, B., Fritz, S.C., 1996b. Vegetation history and climate of the last 15,000 years at Laghi Di Monticchio, southern Italy. Quat. Sci. Rev. 15 (2–3), 113–132. http://dx.doi.org/10.1016/0277-3791(95)00038-0, URL: https://linkinghub.elsevier.com/retrieve/pii/0277379195000380.

Weber, Y., Sinninghe Damsté, J.S., Zopfi, J., De Jonge, C., Gilli, A., Schubert, C.J., Lepori, F., Lehmann, M.F., Niemann, H., 2018. Redox-dependent niche differentiation provides evidence for multiple bacterial sources of glycerol tetraether lipids in lakes. Proc. Natl. Acad. Sci. 115 (43), 10926–10931. http://dx.doi.org/10.1073/pnas.1805186115, URL: https://pnas.org/doi/full/10.1073/pnas.1805186115.

Wei, T., Simko, V., 2024. R package 'corrplot': Visualization of a correlation matrix. (Version 0.95), URL: https://github.com/taiyun/corrplot.

Weijers, J.W., Schouten, S., van den Donker, J.C., Hopmans, E.C., Sinninghe Damsté, J.S., 2007. Environmental controls on bacterial tetraether membrane lipid distribution in soils. Geochim. Cosmochim. Acta 71 (3), 703–713. http://dx.doi.org/10.1016/j.gca.2006.10.003, URL: https://linkinghub.elsevier.com/retrieve/pii/S0016703706021090.

Weijers, J.W., Schouten, S., Linden, M., Geel, B., Sinninghe Damsté, J.S., 2004. Water table related variations in the abundance of intact archaeal membrane lipids in a Swedish peat bog. FEMS Microbiol. Lett. 239 (1), 51–56. http://dx.doi.org/10.1016/j.femsle.2004.08.012, URL: https://academic.oup.com/femsle/article-lookup/doi/10.1016/j.femsle.2004.08.012.

Wu, J., Yang, H., Pancost, R.D., Naafs, B.D.A., Qian, S., Dang, X., Sun, H., Pei, H., Wang, R., Zhao, S., Xie, S., 2021. Variations in dissolved O2 in a Chinese lake drive changes in microbial communities and impact sedimentary GDGT distributions. Chem. Geol. 579, 120348. http://dx.doi.org/10.1016/j.chemgeo.2021.120348, URL: https://linkinghub.elsevier.com/retrieve/pii/S0009254121002928.

Wulf, S., Brauer, A., Mingram, J., Zolitschka, B., Negendank, J., 2006. Distal tephras in the sediments of monticchio maar lakes. In: La Geologia Del Monte Vulture. Bollettino della Società Geologica Italiana, pp. 105–122.

Wulf, S., Keller, J., Paterne, M., Mingram, J., Lauterbach, S., Opitz, S., Sottili, G., Giaccio, B., Albert, P.G., Satow, C., Tomlinson, E.L., Viccaro, M., Brauer, A., 2012. The 100–133 ka record of Italian explosive volcanism and revised tephrochronology of Lago Grande di Monticchio. Quat. Sci. Rev. 58, 104–123. http://dx.doi.org/10.1016/j.quascirev.2012.10.020, URL: https://linkinghub.elsevier.com/retrieve/pii/S0277379112004167.

Wulf, S., Kraml, M., Brauer, A., Keller, J., Negendank, J.F., 2004. Tephrochronology of the 100ka lacustrine sediment record of Lago Grande di Monticchio (southern Italy). Quat. Int. 122 (1), 7–30. http://dx.doi.org/10.1016/j.quaint.2004.01.028, URL: https://linkinghub.elsevier.com/retrieve/pii/S1040618204000382.

Wulf, S., Kraml, M., Keller, J., 2008. Towards a detailed distal tephrostratigraphy in the central Mediterranean: The last 20,000 yrs record of Lago Grande di Monticchio. J. Volcanol. Geotherm. Res. 177 (1), 118–132. http://dx.doi.org/10.1016/j.jvolgeores.2007.10.009, URL: https://linkinghub.elsevier.com/retrieve/pii/S0377027307003484.

Xian, T., Xia, J., Wei, W., Zhang, Z., Wang, R., Wang, L.P., Ma, Y.F., 2021. Is hadley cell expanding? Atmosphere 12 (12), 1699. http://dx.doi.org/10.3390/atmos12121699, URL: https://www.mdpi.com/2073-4433/12/12/1699.

Xu, X., Chassignet, E.P., Wang, F., 2019. On the variability of the Atlantic meridional overturning circulation transports in coupled CMIP5 simulations. Clim. Dyn. 52 (11), 6511–6531. http://dx.doi.org/10.1007/s00382-018-4529-0, URL: http://link.springer.com/10.1007/s00382-018-4529-0.

Yang, H., Lü, X., Ding, W., Lei, Y., Dang, X., Xie, S., 2015. The 6-methyl branched tetraethers significantly affect the performance of the methylation index (MBT') in soils from an altitudinal transect at Mount Shennongjia. Org. Geochem. 82, 42–53. http://dx.doi.org/10.1016/j.orggeochem.2015.02.003, URL: https://linkinghub.elsevier.com/retrieve/pii/S0146638015000285.

Yang, H., Pancost, R.D., Dang, X., Zhou, X., Evershed, R.P., Xiao, G., Tang, C., Gao, L., Guo, Z., Xie, S., 2014. Correlations between microbial tetraether lipids and environmental variables in Chinese soils: Optimizing the paleo-reconstructions in semi-arid and arid regions. Geochim. Cosmochim. Acta 126, 49–69. http://dx.doi.org/10.1016/j.gca.2013.10.041, URL: https://linkinghub.elsevier.com/retrieve/pii/S0016703713006133.

Yuan, S., Chiang, H.W., Liu, G., Bijaksana, S., He, S., Jiang, X., Imran, A.M., Wicaksono, S.A., Wang, X., 2023. The strength, position, and width changes of the intertropical convergence zone since the last glacial maximum. Proc. Natl. Acad. Sci. 120 (47), e2217064120. http://dx.doi.org/10.1073/pnas.2217064120, URL: https://pnas.org/doi/10.1073/pnas.2217064120.

Zanchetta, G., Regattieri, E., Isola, I., Drysdale, R.N., Baneschi, I., Hellstrom, J.C., 2016. The so-called "4.2 event" in the Central Mediterranean and its climatic teleconnections. Alp. Mediterr. Quat. 29 (1), 5–17.

Zander, P.D., Böhl, D., Sirocko, F., Auderset, A., Haug, G.H., Martínez-García, A., 2024. Reconstruction of warm-season temperatures in central Europe during the past 60 000 years from lacustrine branched glycerol dialkyl glycerol tetraethers (brGDGTs). Clim. Past 20 (4), 841–864. http://dx.doi.org/10.5194/cp-20-841-2024, URL: https://cp.copernicus.org/articles/20/841/2024/.

Zeileis, A., Grothendieck, G., 2005. Zoo: S3 infrastructure for regular and irregular time series. J. Stat. Softw. 14 (6), 1–27. http://dx.doi.org/10.18637/jss.v014.i06.

Zhao, B., Russell, J.M., Tsai, V.C., Blaus, A., Parish, M.C., Liang, J., Wilk, A., Du, X., Bush, M.B., 2023. Evaluating global temperature calibrations for lacustrine branched GDGTs: Seasonal variability, paleoclimate implications, and future directions. Quat. Sci. Rev. 310, 108124. http://dx.doi.org/10.1016/j.quascirev.2023.108124, URL: https://linkinghub.elsevier.com/retrieve/pii/S0277379123001725.

Zheng, Y., Li, Q., Wang, Z., Naafs, B.D.A., Yu, X., Pancost, R.D., 2015. Peatland GDGT records of holocene climatic and biogeochemical responses to the Asian Monsoon. Org. Geochem. 87, 86–95. http://dx.doi.org/10.1016/j.orggeochem.2015.07.012, URL: https://linkinghub.elsevier.com/retrieve/pii/S0146638015001540.

Zheng, Y., Pancost, R.D., Naafs, B.D.A., Li, Q., Liu, Z., Yang, H., 2018. Transition from a warm and dry to a cold and wet climate in NE China across the Holocene. Earth Planet. Sci. Lett. 493, 36–46. http://dx.doi.org/10.1016/j.epsl.2018.04.019, URL: https://linkinghub.elsevier.com/retrieve/pii/S0012821X1830222X.

Zielhofer, C., Köhler, A., Mischke, S., Benkaddour, A., Mikdad, A., Fletcher, W.J., 2019. Western Mediterranean hydro-climatic consequences of Holocene ice-rafted debris (bond) events. Clim. Past 15 (2), 463–475. http://dx.doi.org/10.5194/cp-15-463-2019, URL: https://cp.copernicus.org/articles/15/463/2019/.

Zolitschka, B., 1996. Sedimentology, dating and palaeoclimatic interpretation of a 76.3 ka record from Lago Grande di Monticchio, Southern Italy. Quat. Sci. Rev. 15, 101–112. http://dx.doi.org/10.1016/0277-3791(95)00022-4.

Zolitschka, B., Negendank, J.F.W., 1993. Lago grande di monticchio (southern Italy) a high resolution sedimentary record of the last 70,000 years. In: Negendank, J.F.W., Zolitschka, B. (Eds.), In: Paleolimnology of European Maar Lakes, vol. 49, Springer Berlin Heidelberg, Berlin, Heidelberg, pp. 277–288. http://dx.doi.org/10.1007/BFb0117601, Series Title: Lecture Notes in Earth Sciences, URL: http://link.springer.com/10.1007/BFb0117601.